BRNO UNIVERSITY OF TECHNOLOGY

Faculty of Information Technology

PHD THESIS

Brno, 2023   Ing. Marek Žák

BRNO UNIVERSITY OF TECHNOLOGY
VYSOKÉ UČENÍ TECHNICKÉ V BRNĚ

FACULTY OF INFORMATION TECHNOLOGY
FAKULTA INFORMAČNÍCH TECHNOLOGIÍ

DEPARTMENT OF INTELLIGENT SYSTEMS
ÚSTAV INTELIGENTNÍCH SYSTÉMŮ

BIOLOGY-INSPIRED CONTROL OF A WALKING ROBOT
BIOLOGIÍ INSPIROVANÉ ŘÍZENÍ KRÁČIVÉHO ROBOTA

PHD THESIS
DISERTAČNÍ PRÁCE

AUTHOR   **Ing. MAREK ŽÁK**
AUTOR PRÁCE

SUPERVISOR   **doc. Ing. FRANTIŠEK V. ZBOŘIL, CSc.**
ŠKOLITEL

SUPERVISOR SPECIALIST   **Ing. JAROSLAV ROZMAN, PhD.**
ŠKOLITEL SPECIALISTA

BRNO 2023

Abstract

Mobile robots have become part of everyday life. Various robots can perform a wide range of different tasks or go to places humans cannot. Their use can be found in rescue operations or in the exploration of remote or hard to reach places on Earth or in space. Walking robots form a separate category of mobile robots due to their unique features. They can negotiate rough terrain, can overcome various obstacles or use their legs to manipulate objects. Although walking robots are well suited to navigate rugged terrain, a number of factors have so far prevented their mass deployment. Their movement is relatively slow and energetically demanding, they have a limited payload and their design is significantly more complex compared to wheeled or tracked robots. Walking robots often have dozens of joints and their control is therefore very complicated.

This thesis describes a new bio-inspired hexapod robot WHexaR (Wheeled Hexapod Robot) and its controller that I designed and implemented as part of this work. The resulting robot is capable of energy-efficient movement in rugged terrain. The leg structure of the robot is inspired by the structure of an insect limb. The robot adapts its movement to the surrounding terrain. A special trochanter joint allows the entire leg of the robot to rotate parallel to gravitational acceleration, which reduces the energy consumption, increases the robot's stability and allows the robot to overcome steep hills. For movement on flat terrain, the robot is equipped with steerable wheels that allow the robot to achieve higher speeds with lower energy consumption than when using gait. The innovative biology-inspired robot controller is equipped with reflexes observed in insects that make the robot more efficient when travelling in rough terrain and improve its ability to overcome obstacles. A series of experiments were conducted to demonstrate the robot's ability to navigate rugged and sloping terrain.

Keywords

Biology-inspired hexapod robot, inspiration in the nature, design and control of a walking robot, energy efficiency.

Reference

Abstrakt

Mobilní roboti se stávají součástí každodenního života. Jsou konstruováni nejrůznější roboti, kteří dokáží provádět celou řadů různých úkolů nebo se pohybovat i v místech, kam lidé nemohou. Jejich využití lze najít při záchranných operacích nebo při průzkumu těžko dostupných míst na Zemi nebo ve vesmíru. Kráčiví roboti tvoří speciální kategorii mobilních robotů, protože se svými vlastnostmi výrazně odlišují od jiných typů robotů. Dokáží se pohybovat v členitém terénu, překonávat různé překážky a mohou využívat svoje končetiny k manipulaci s okolními předměty. Přestože jsou kráčiví roboti skvěle vybaveni pro pohyb v náročném terénu, jejich běžnějšímu užívání zatím brání řada faktorů. Jejich pohyb je relativně pomalý a energeticky náročný, unesou poměrně málo nákladu a jejich konstrukce je mnohem složitější v porovnání s kolovými nebo pásovými roboty. Kráčiví roboti často disponují desítkami kloubů, a jejich řízení je proto velmi složité.

Tato dizertační práce popisuje návrh, konstrukci a řízením nového biologií inspirovaného šestinohého robota WHexaR (z anglického Wheeled Hexapod Robot, kolový šestinohý robot), kterého jsem postavil. Tento robot je schopen energeticky úsporného pohybu ve členitém terénu. Struktura jeho končetin je inspirována stavbou končetiny hmyzu. Robot dokáže přizpůsobit svůj pohyb okolnímu terénu. Speciální trochanterový kloub umožňuje natočení celé končetiny robota rovnoběžně s gravitačním zrychlením, což vede ke snížení spotřeby energie, zvýšení stability robota a schopnosti překonávat strmější svahy. Pro pohyb na rovné terénu je robot vybaven natočitelnými koly, díky kterým se robot může pohybovat vyšší rychlostí s nižší energetickou spotřebou než při pohybu pomocí chůze. Navržený kontrolér robota disponuje řadou reflexů, které byly pozorovány u hmyzu. Tyto reflexy zvyšují efektivitu pohybu robota ve členitém terénu a umožňují mu překonávat různé překážky. Robot byl podroben řadě experimentů, které prokázaly jeho schopnosti pohybu ve členitém a svažitém terénu.

Klíčová slova

Biologií inspirovaný šestinohý robot, inspirace v přírodě, konstrukce a řízení kráčivého robota, energetická úspornost.

Citace

Rozšířený abstrakt

Mobilní roboti se stávají součástí každodenního života. Jsou konstruováni nejrůznější roboti, kteří dokáží provádět celou řadů různých úkolů nebo se pohybovat i v místech, kam lidé nemohou. Jejich využití lze najít při záchranných operacích nebo při průzkumu těžko dostupných míst na Zemi nebo ve vesmíru. Kráčiví roboti tvoří speciální kategorii mobilních robotů, protože se svými vlastnostmi výrazně odlišují od jiných typů robotů. Dokáží se pohybovat v členitém terénu, překonávat různé překážky a mohou využívat svoje končetiny k manipulaci s okolními předměty. Přestože jsou kráčiví roboti skvěle vybaveni pro pohyb v náročném terénu, jejich běžnějšímu užívání zatím brání řada faktorů. Jejich pohyb je relativně pomalý a energeticky náročný, unesou poměrně málo nákladu a jejich konstrukce je mnohem složitější v porovnání s kolovými nebo pásovými roboty. Kráčiví roboti často disponují desítkami kloubů, a jejich řízení je proto velmi složité.

Cílem této práce bylo navrhnout a zkonstruovat šestinohého robota, jehož konstrukce by vycházela ze stavby těla hmyzu. Dále navrhnout a implementovat řídicí kontrolér tohoto robota, který by napodoboval pohyb a chování hmyzu a byl by schopen přizpůsobit pohyb robota aktuálním terénním podmínkám. V práci jsem se také zaměřil na možnosti zvýšení rychlosti pohybu kráčivých robotů na rovném, nečlenitém terénu, jejich schopnost překonávat svažité terény a energetickou spotřebu při pohybu v různých terénních podmínkách.

Text této práce se skládá ze sedmi kapitol. Kapitola 1 uvozuje problematiku kráčivých robotů a stanovuje cíle práce. Kapitola 2 se zabývá studiem hmyzu, strukturou jejich těla, nervovou soustavou, vnímáním a pohybem. V Kapitole 3 jsou popsány charakteristiky kráčivých robotů se zaměřením na šestinohé roboty. Jsou zde prezentovány různé konstrukce těla a končetin těchto robotů, jejich pohybové vlastnosti a řídicí kontroléry. V kapitole jsou také uvedeny příklady některých kráčivých robotů. Kapitola 4 popisuje návrh nového biologií inspirovaného šestinohého robota WHexaR (z anglického Wheeled Hexapod Robot, kolový šestinohý robot) a jeho adaptivního kontroléru. Kapitola 5 následně ukazuje postup při implementaci tohoto robota. Výsledný robot, kterého jsem navrhl a postavil, je schopen energeticky úsporného pohybu ve členitém terénu. Struktura jeho končetin je inspirována stavbou končetiny hmyzu. Robot dokáže přizpůsobit svůj pohyb okolnímu terénu. Speciální trochanterový kloub umožňuje natočení celé končetiny robota rovnoběžně s gravitačním zrychlením, což vede ke snížení spotřeby energie, zvýšení stability robota a schopnosti překonávat strmější svahy. Pro pohyb na rovném terénu je robot vybaven natočitelnými koly, díky kterým se robot může pohybovat vyšší rychlostí s nižší energetickou spotřebou než při pohybu pomocí chůze. Navržený kontrolér robota disponuje řadou reflexů, které byly pozorovány u hmyzu. Tyto reflexy zvyšují efektivitu pohybu robota ve členitém terénu a umožňují mu překonávat různé překážky.

Robot byl podroben řadě experimentů, které jsou uvedené v Kapitole 6. Tyto experimenty potvrdily, že kombinace trochanterového kloubu a pohybového kontroléru umožňuje mému robotu chodit až do sklonu 32°, jezdit po svažitých terénech až do sklonu 40° a zůstat staticky stabilní ve svazích do sklonu 50°. Tyto výsledky ukazují zlepšení oproti jiným srovnatelným robotům, jako je LAURON [148], který je schopen chodit ve svahu o sklonu až 25° a stabilně stát až do sklonu 42°, a Weaver [24], který je schopen chodit ve svahu o sklonu až 30° a zůstat stabilní ve svahu o sklonu až 50°. Zlepšení jsem dosáhl také z hlediska energetické účinnosti. Naměřená hodnota energetického ukazatele cost of transport (lze přeložit jako cena přesunu) mého robota při chůzi po rovném terénu byla 6,05. Při použití kolového podvozku bylo dosaženo hodnoty 2,41. Pro srovnání, hexapod Weaver má při chůzi na rovném terénu cost of transport 15,2. V Kapitole 7 jsou shrnuty dosažené výsledky.

Šestinohými roboty jsem se zabýval již během bakalářského a magisterského studia. Zúčastnil jsem se také několika přehlídek a konferencí. Se svým prvním robotem jsem získal první místo na studentské konferenci EEICT. Později jsem tohoto robota vylepšil a získal několik ocenění na studentské konferenci Excel@FIT, včetně prvního místa v kategorii Technologická úroveň a cenu zlatého sponzora.

O robotovi vytvořeném v rámci této práce jsem publikoval článek v časopise Open Computer Science (Q2), který byl již několikrát citován. Moje nejnovější publikace vyšla v časopise Robotics (IF 3.7, Q1) a zabývá se energetickou účinností zkonstruovaného robota.

Biology-Inspired Control of a Walking Robot

Declaration

I hereby declare that this PhD Thesis was prepared as an original work by the author under the supervision of doc. Ing. Fratišek V. Zbořil, CSc. and Ing. Jaroslav Rozman, PhD. I have listed all the literary sources, publications and other sources which were used during the preparation of this thesis.

<div align="right">

. . . .
Marek Žák
August 31, 2023

</div>

Acknowledgements

I would like to thank everyone who helped me to solve all the challenges related to this Thesis. I especially thank my supervisor doc. Ing. František V. Zbořil, CSc. and supervisor specialist Ing. Jaroslav Rozman, PhD. for their expertise, valuable feedback and constant support. I also thank my current and former colleagues in the Intelligent Systems Research Group for their valuable advice and long discussions. Special thanks also to my beloved wife for her endless encouragement. Finally, my gratitude goes to my family and friends for their support during my studies.

Contents

List of Figures

List of Tables

List of Equations

List of abbreviations

A/D	Analogue to digital
AC	Alternating current
AEP	Anterior extreme position
API	Application programming interface
CAD	Computer-aided design
CNN	Cellular nonlinear networks
CNS	Central nervous system
CoG	Center of gravity
CoT	Cost of transport
CPG	Central pattern generator
CRC	Cyclic redundancy check
D-H	Denavit-Hartenberg
DC	Direct current
DOF	Degree of freedom
FK	Forward kinematics
FPGA	Field Programmable Gate Arrays
FSR	Force-sensitive resistor
I2C	Inter-integrated circuit
IK	Inverse kinematics
IMU	Inertial measurement uni
IR	Infrared
IRR	Infrared rangefinders
Li-Po	Lithium polymer
PEP	Posterior extreme position
PID	Proportional-integral-derivative
PWM	Pulse width modulation
RC	Remote control
RX	Receive
SDK	Software development kit
SPI	Serial peripheral interface
SSM	Static stability margin
TTL	Transistor–transistor logic
TX	Transmit
UART	Universal asynchronous receiver-transmitter
USART	Universal synchronous and asynchronous receiver-transmitter
WHexaR	Wheeled hexapod robot

Chapter 1

Introduction

In this era of technological advances and enhancements, many tasks are being automated by robots. The use of robots has spread to many different areas. It is very common to use robots in manufacturing productions as well as in industrial fields. Robots can perform repetitive tasks or work in hazardous environments. One type of robots are mobile robots. Their use can be found for example in rescue operations [50], transporting goods in warehouses [97] or delivering parcels [32]. At the same time, people use robots to sweep floors or clean swimming pools. Furthermore, robots are being sent to remote places on Earth [12] or to the far reaches of space [161] where they must navigate reliably and deal with the various hazards and obstacles that unfamiliar places can bring. For navigating in isolated places or difficult terrain conditions, walking robots can be used. Unlike wheeled or tracked chassis, walking robots can negotiate uneven terrain, steep slopes, deep craters and large boulders.

Walking robots are most often distinguished by the number of legs. One-legged robots move by jumping. If they stop, they will fall, therefore they have to keep jumping even if they stay in place to keep their balance. Although they are very efficient when moving in the field, their design and control is very complex. An example is one-legged jumping robot KEN-2 [174].

Bipedal robots (humanoids) have similar body structure to humans and are able to move with relatively low energy consumption. That is due to the fact that most of their weight does not load the actuators of the leg directly but rather uses the design of the leg itself. In this case the actuators are only used to compensate for small fluctuations in stability or to change the position of the leg. However, bipedal robots are not capable of static stability and must maintain balance through the dynamics of their movement. This makes them difficult to control. An example is robot Atlas [177].

Three-legged robots are statically stable because they have three points on the ground. They also excel in low power consumption, as only three legs need to be powered. However, they are not capable of statically stable motion. An example of a three-legged robot is THALeR. [181].

Quadruped robots mimic four-legged animals like horses or dogs. The number of legs already allows statically stable movement, even at the cost of lower speed, because only one leg can move at a time. To reach higher speeds, quadruped robots can also use dynamically stable movements such as trotting, galloping or pacing. They have a lower center of gravity compared to bipedal robots and therefore higher stability. Representatives of four-legged robots are MIT Cheetah [160] or BigDog [129].

Six-legged robots offer greater stability than bipedal and quadrupedal robots and are capable of statically stable motion that mimics the movement of insects. Due to their higher number of legs, hexapods are able to continue moving even if one of their legs is damaged or use their extra legs to manipulate objects. Their tripod gait allows for fast movement while maintaining static stability. In contrast, the wave gait provides exceptional stability because the robot always rests on at least five legs. Hexapods are extremely versatile walking robots and are well suited for challenging terrain. Representatives of hexapods are Weaver [24] or HAntR [199].

In addition, one can find eight-legged robots, crawling robots or hybrid robots that combine legs and wheels. Although walking robots in most cases excel in their ability to navigate rough terrain, their mechanical design is much more complex and their control is more complicated compared to wheeled or tracked robots. Movement by gait is also far more energy demanding than movement on wheels. The design of walking robots also severely limits the load that the robot can carry.

1.1 Objectives of the Thesis

I dealt with walking robots during my bachelor and master studies. As part of my bachelor thesis I have designed and built a prototype of my own hexapod robot that is capable of moving in rugged terrain (see Figure 1.1). Furthermore, I continued working on the robot for my master thesis, implementing major improvements in robot's control system, mechanical design and overall effectiveness [194]. However, the design and components used limited its speed and ability to move in sloping terrain. Therefore, I decided to use the acquired experience and design a new hexapod robot that would be able to move faster on flat surfaces and be able to move on sloping terrains. This robot will be inspired by the body structure of insects and will be able to mimic their movement and behaviour.

As this work brings together research from various different fields, it will be necessary to study all the areas involved. The objectives of this dissertation are as follows:

- Study insects with a focus on the nervous system, body and limb structure, behaviour and movement.

- Study walking robots with a focus on hexapods, their design, construction and control.

- Design a six-legged walking robot whose body and leg structure is inspired by the body and limb structure of insects.

- Design a biology-inspired control system for a walking robot that will be able to adapt the robot's motion in regard to the complexity of the surrounding terrain and mimic insect behavior.

- Focus on the speed of walking robots on flat surfaces and the ability to move stably in sloping terrain, with an emphasis on energy-efficient movement.

1.2 Organization of the Thesis

The Thesis is organized into seven chapters. Chapter 2 deals with the study of insects, their body structure, nervous system, perception and movement. In Chapter 3, the characteristics of walking robots with a focus on hexapods are discussed. The body and leg structure,

locomotion and control methods are described. A number of existing walking robots are presented. Chapter 4 deals with the design of the mechanical structure, electronic system and movement controller of the WHexaR hexapod robot. Chapter 5 describes the design of the body and legs of the proposed robot and its electronic system and movement controller. The proposed design is verified and the properties and skills of the resulting robot are analyzed through various experiments in Chapter 6. The last Chapter 7 summarizes the important points of the presented research.
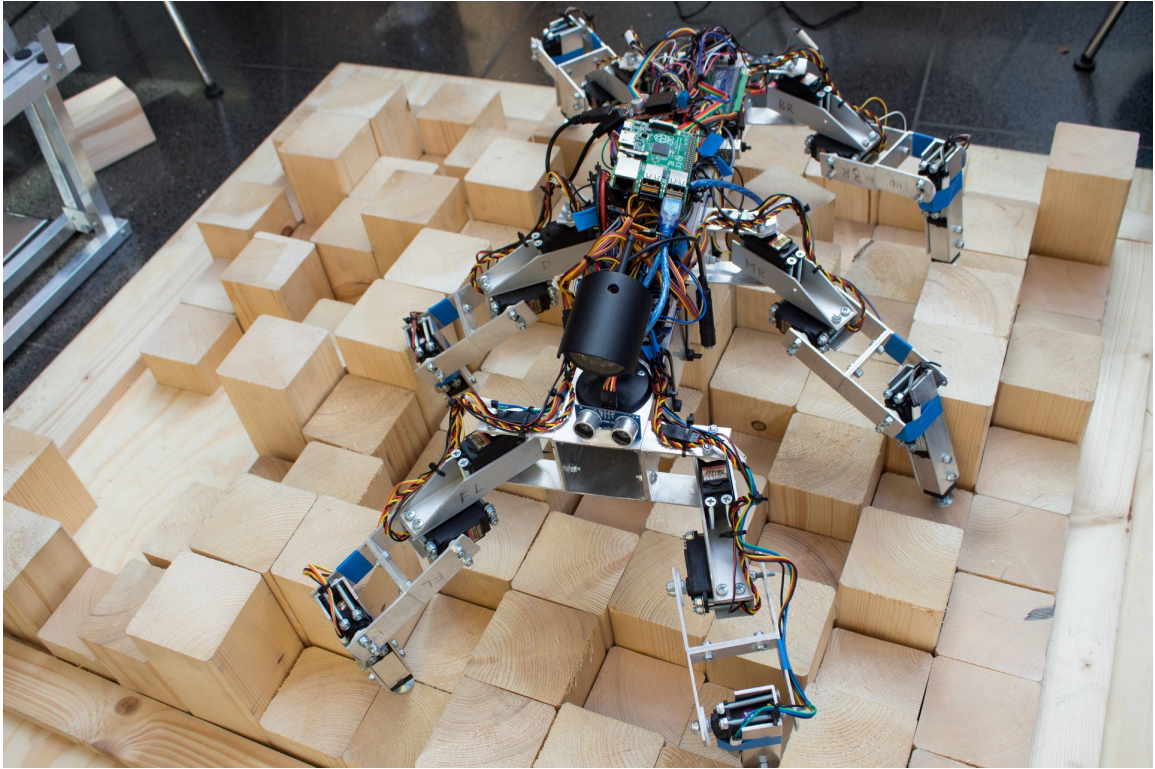
Figure 1.1: Hexapod, which I designed and implemented as part of my bachelor and master thesis.

Chapter 2

Insect – Inspiration in the Nature

Nature has been a profound source of inspiration for humans throughout history. Its beauty, complexity and diversity stimulate creativity and influence various aspects of human life. The complex structures and mechanisms of nature have inspired scientific discoveries and technological advances. Examples include Velcro inspired by burrs [176], airplane wings and fuselage inspired by the wings and body of birds [113] (see Figure 2.1) or self-cleaning surfaces inspired by lotus leaves [196]. Other inspirations do not refer to the shape or appearance of natural objects, but use their internal mechanisms. Bats in flight emit sound waves that bounce off obstacles in the environment. The subsequent detection of these sound waves is used by bats to orient themselves in the environment. Sonar is based on a similar principle. The study of the structure and function of biologically engineered materials and biological processes and mechanisms in order to create similar designs that mimic the properties of natural ones is called biomimetics [9, 10]. The term biomimetics is often associated with two other terms – bionics and biomimicry. Although researchers do not agree on a clear distinction between these terms, some similarities can be found in the definitions. Bionics is a combination of the words biology and technics or electronics usually refers to the use of biological systems or methods found in nature in artificially engineered products. Biomimicry (imitation of the living) does not only imitate or take inspiration from nature, but it also uses an ecological standard to judge the appropriateness of the innovation. According to the study, almost half of the experts interviewed perceive biomimetics and biomimicry as identical. However, only a third of experts believe that bionics corresponds to the meaning of biomimetics [82].

Inspiration in nature can not only be found in Velcro or airplanes, but also in robotics. The appearance of many robots resembles an animal. These include legged robots that, depending on their size and number of legs, resemble a spider [175], beetle [110], dog [28] or horse [135, 27]. Some legged robots have only two legs and thus resemble humans [26]. In addition to legged robots, similarities can also be found, for example, in aquatic robots that resemble fish [55] or crawling robots that resemble snakes [42] or worms [87]. Even some flying robots resemble flying animals such as birds [78] or flying insects [99].

Arthropoda (arthropods) is the largest phylum in the animal kingdom. It includes familiar forms such as spiders, crabs, lobsters and centipedes. About 84 percent of all known animal species on Earth are members of this phylum [74, 13]. In the case of hexapod robots, inspiration is most often taken from hexapoda (hexapods) that comprises most species of

Figure 2.1: Fuselage shape inspired by the shape of a bird in flight. The figure shows that the fuselage of the fighter aircraft is similar to the shape of a bird of prey in flight.[1]

arthropoda including insecta (insects), which are best suited to inspiring walking robots due to their body structure [91, 172].

Insects and other arthropods are built on a segmental structure and their characteristic feature is a hard, jointed exoskeleton [37]. The cuticle, which forms the exoskeleton, is continuous throughout the outer side of the body and consists of a series of hard plates connected to the skin by elastic membranes. The individual segments are grouped into three main parts – head, thorax and abdomen. The legs used for walking are usually attached to the three thoracic segments. In the head, the appendages are adapted for sensory and feeding purposes, and in the abdomen they are lost. The information in the following text is taken from [37].

2.1   Leg Structure

Insects usually have three pairs of legs. Therefore, the insect is sometimes referred to as the hexapods, although not all hexapods are now considered insects. Each insect leg usually consists of six parts, that are connected to each other by joints. The six basic parts are coxa, trochanter, femur, tibia, tarsus and pretarsus (see Figure 2.2).

The coxa is often in the form of a truncated cone and is attached to the body of the insect. If the coxa has only one articulation, its movement is very free. In most cases, however, the coxa has a second articulation that restricts movement to some extent.

The trochanter is a small segment with a dicondylar articulation with the coxa. Therefore, the trochanter can only move in the vertical plane.

The femur is the largest and strongest part of the leg in most adults. It is often more or less fixed to the trochanter and moves with it. Usually there are no muscles that move the femur with respect to the trochanter.

---

[1]Figure taken from https://miro.medium.com/v2/resize:fit:4800/format:webp/0*3nVsBS9LQsnA1hbG.png, 15.7.2023.
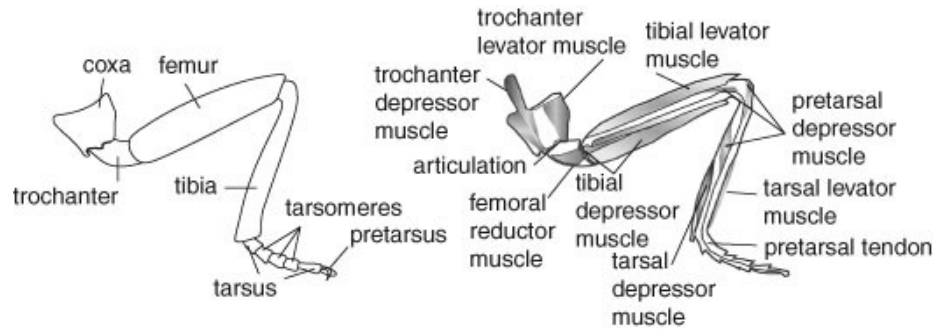
Figure 2.2: Insect leg structure. The figure on the left shows the structure of the insect limb, which consists of five main segments, the coxa, trochanter, femur, tibia and tarsus. The figure on the right shows the individual muscles that are attached in pairs to the segments of the limb.[2]

The tibia is usually a long segment of the leg that is connected to the femur by a di-condylic joint and therefore it can only move in the vertical plane. In most insects, the head of the tibia is bent so that the shank can flex directly against the femur.

The tarsus is divided into two to five tarsomeres in most insects. Unlike the other segments of the leg, the tarsus has no muscles. The individual tarsomeres are connected only by a flexible membrane, so they can move freely.

The pretarsus in most insects consists of a membranous base and a pair of claws.

The legs of insects are usually used for walking. Some insects also use their legs to climb on smooth surfaces. Many insects use adhesive setae, sometimes called tenent hairs, to move along a vertical surface. These setae are clustered into adhesive pads. Their flexibility and quantity create contact with the irregular surface much more efficiently than would be true of a single, larger structure. Except for adhesive setae, hairless adhesive pads can also be found in insects. Adhesion in both cases is the result of the surface tension of the liquid at the tips of the hairs or on the pads [58].

In some insects, the structure of the leg has been modified in various ways to perform other functions such as jumping (e.g. locust), swimming (e.g. whirligig beetles), digging (e.g. mole cricket), grasping (e.g. mantids), grooming (e.g. cockroaches) and stridulation (producing sound [116], e.g. crickets).

2.2 Leg Muscles

Muscles allow the movement of the different segments and parts of the body of the insect. The muscles that move the leg are of two types. Extrinsic muscles protrude out of the leg. Intrinsic muscles are inside the leg and run from one segment to another and are much simpler than extrinsic muscles. The innervation of the leg muscles is complex. Most muscles are innervated by fast, slow and inhibitory axons.

Each muscle consists of a number of fibres. Each fibre is connected to many nerve endings that come from the corresponding innervating axon. The action potential arriving from the nerves stimulates muscle contraction. The skeletal muscles are attached to the skin at both ends and bridge the joint in the skeleton, so that contraction of the muscle moves

---

[2]Figure taken from https://media.springernature.com/lw685/springer-static/image/prt%3A978-1-4020-6359-6%2F12/MediaObjects/978-1-4020-6359-6_12_Part_Fig45-2006_HTML.jpg, 14.8.2023.

14

one part of the skeleton relative to the other. The tension exerted by insect muscles ranges from about 3–9 g/cm^2. For comparison, human muscles exert a tension of 6–10 g/cm^2.

2.3   Leg Sensory System

Insect legs have an extensive sensory system. Some of the sensory elements are proprioceptors that monitor the position of the leg segments and the posture of the insect. Other sensory elements are mechanoreceptors and chemoreceptors, which sense the environment.

The proprioceptors include hair plates (a cluster of hairs terminated by neurons that detect extreme leg positions [190, 14]), campaniform sensilla (respond to stress and torsion of the cuticle [34]) and chordotonal organs (are found only in Insecta and Crustacea in almost every exoskeletal joint and between joints within legs and body segments [60]).

Campaniform sensilla measure forces and loads acting in different directions on the leg, and the femoral chordotonal organ provides information about movement of the femur-tibia joint. These signals are used by local motor networks to control the timing and strength of motor activity by activating motor neurons that target leg muscles to maintain stability of the body. Although the topology of the neural pathways that process signals from proprioceptors is known in detail, little is known about how these proprioceptive feedbacks are connected to the local neural network that controls leg movement [65]. The structure of these connections is only investigated using experiments that examine responses to certain stimuli. Unfortunately, these experiments provide an understanding of the behavior of individual local networks, but not their exact structure. Therefore, it is not possible to replicate the structure of these networks into artificial neural networks. However, it is possible to replicate their behaviour.

Except proprioceptors there are also many exteroreceptive sensilla on the legs of insects. Mechanosensitive trichoid sensilla (hair-like structure protruding beyond the cuticle structure, its neurons are connected by axons to the central nervous system [88]) and chemoreceptors are distributed all over the leg.

2.4   Movement

The possibility of mobility is very important for insects. They have to move to find food or a mate, or to avoid predators. Despite the fact that insects mostly use flying for their movement, they also use running or walking for local movements. The movement of each leg varies according to different speeds of movement to maintain stability. Coordination of movements is controlled centrally, but local reflexes are also used.

Each leg can serve either as a strut or as a lever. In the case of struts, the leg only supports the body with the forces acting down it depend on the angle of inclination relative to the body and the weight of the insect. The force acting down the leg can be resolved into two components, horizontal and vertical. If the opposing forces of the fore, and middle and hind legs are in balance, no movement occurs. If this balance is disturbed, the body moves.

If the leg is used as a lever, the force of the muscles on the leg leads to movement. However, comparing a leg to a lever is an extreme simplification of the situation, because a leg, unlike a lever, has a number of muscles and joints that can direct the applied force and shape the direction of body movement.

Each step comprises a period of protraction – movement of the leg forward over the ground, and a period of retraction – movement of the leg, which is on the ground, backward relative to the body. The pattern of walking is usually dependent on the speed of movement. At lower speeds, most of the legs are in contact with the ground most of the time. The legs are protracted individually in the order right hind, right middle, right fore, left hind, left middle and left fore. At higher speeds, the left middle leg and the fore and hind right legs are lifted and swung simultaneously, with the remaining three legs providing support for the body. This tripod-based pattern of locomotion is found in all insects examined so far. Higher movement speed is achieved by increasing the frequency with which the legs move and increasing the length of each stride. As the frequency of leg movement increases, the retraction period shortens significantly. The period of protraction is also shortened, but less significantly. Some insects do not touch the ground with any leg for a short time at high speed or run only on their hind legs. It is believed that each movement of each leg is controlled by its own pattern generator, which are interconnected in the central nervous system.

2.5   Nervous System

The nervous system processes information from the sensory system and ensures rapid function, coordination and response of effectors. The basic elements of the nervous system are neurons (nerve cells). Neurons are conducting cells that transduce, transmit or process nerve impulses. They are similar to other cells, but have specialized extensions – dendrites and axons. Dendrites bring information to the soma and axons take information away from the soma. Communication between neurons is achieved through synapses and chemicals (neurotransmitters) [45]. Depending on the connection between soma, axon and dendrite, three types of synapses can be distinguished. The axosomatic synapse is formed by the connection of the soma and the axon. When the axon and dendrites are connected, an axodendritic synapse is formed. When two axons are connected, an axoaxonic synapse is created [71]. Neurons communicate with each other mostly chemically. However, some neurons are so close that they can communicate directly using electrical signals.

Neurons can be classified according to their function. Sensory (afferent) neurons have dendrites attached to sense organs and transmit information to the central nervous system (CNS). Motor (efferent) neurons conduct signals from the CNS and stimulate responses in muscles and glands. Association (interneuron) neurons form connections between sensory and motor neurons and conduct signals within the CNS.

Most neurons in insects are monopolar. They have only one projection (neurite) from the soma. It then branches into axon and dendrite. The peripheral sense cells are bipolar with a short dendrite and a proximal axon. They receive stimuli from the environment and transmit them to the central ganglia. Multipolar neurons occurring at stretch receptors have several branched dendrites and a single axon projecting from the soma.

Cells are connected together by a large number of synapses. A single retinula cell in the eye of a fly has about 200 output synapses. Some association neurons of the locust can have up to one million output synapses.

Signal transmission through the nervous system involves three different processes. The first is transduction, which is the conversion of a visual, mechanical or chemical signal into an electrical signal. The second process is the transmission of an electrical signal across the axon in the form of an action potential. The third process is the conversion of the electrical signal into a chemical signal, which is then transmitted to the cell at the synapse.

Larger clusters of neurons are called ganglia. It is composed of association neurons and motor neurons. Inside the ganglion, the axons and dendrites of individual neurons are interwoven to form synapses. Except for connections to muscles, there are no synapses outside the CNS.

The central nervous system of insects usually consists of a brain located in the head, which is followed by a series of segmental ganglia. Adjacent ganglia are connected by a pair of interganglionic junctions that contain only axons and glia (non-neuronal cells). These connections do not contain any somata or synapses. In most cases, the muscles of one segment are innervated from the ganglion of the same segment. Each segmental ganglion contains somata of motorneurons that control the muscles of that segment. The number of motorneurons is usually relatively small, corresponding to the relatively small number of muscles found in insects. Although there are cases where motor neurons and sensory neurons are connected directly to each other, in most cases the interneurons provide the interconnection. The various structures of the insect CNS are shown in Figure 2.3.

The main task of the central nervous system is to integrate individual body parts and their activities so that appropriate behavioural responses and internal regulating changes are made. In some cases this is only achieved by interneurons that receive appropriate input from elsewhere. In other cases, the signal is modulated at the synapses.

Some activities such as walking, flying or breathing involve muscle activity that is repeated frequently. These routine movements are controlled by basic sequences of motor neuron activity that are generated in the CNS. Some essential functions are generated even when the CNS is isolated (e.g., in an experiment) and receives no input signals from peripheral receptors. These signals are generated by clusters of interneurons forming a central pattern generator (CPG). Each activity such as walking or breathing has its own independent CPG.

2.6   Perception and Communication

Perception of the environment is an important function that most animals possess. It enables orientation in space or can be used for communication. Perception can be divided into three groups – optical, mechanical and chemical.

Optical perception is based on the perception of light, its intensity or colour. Insects have several types of light-sensitive receptors. Adult insects usually have a pair of compound eyes and often three single-lens eyes (ocelli) can also be found. Some insects have epidermal light receptors and in some insects light has a direct effect on brain cells.

The insect eye is composed of many small similar units called ommatidia. Their number varies from species to species. For example, a dragonfly has an eye composed of 10,000 ommatidia and a worker honeybee has 5,500 ommatidia. In contrast, workers of the ant has only two ommatidia, one on each side of the head. Sensory elements are elongated neurons known as retinula cells. In one ommatidium there are usually eight retinula cells, although some species have seven or nine.

Mechanical perception or mechanoreception is the perception of a mechanical change in the body. It may be caused by a vibration in the environment or the touch of an object. Mechonoperception also includes hearing. There are three broad categories of mechanoreceptors in insects: cuticular structures with bipolar neurons; subcuticular structures with bipolar neurons, known as chordotonal organs; internal multipolar neurons which function
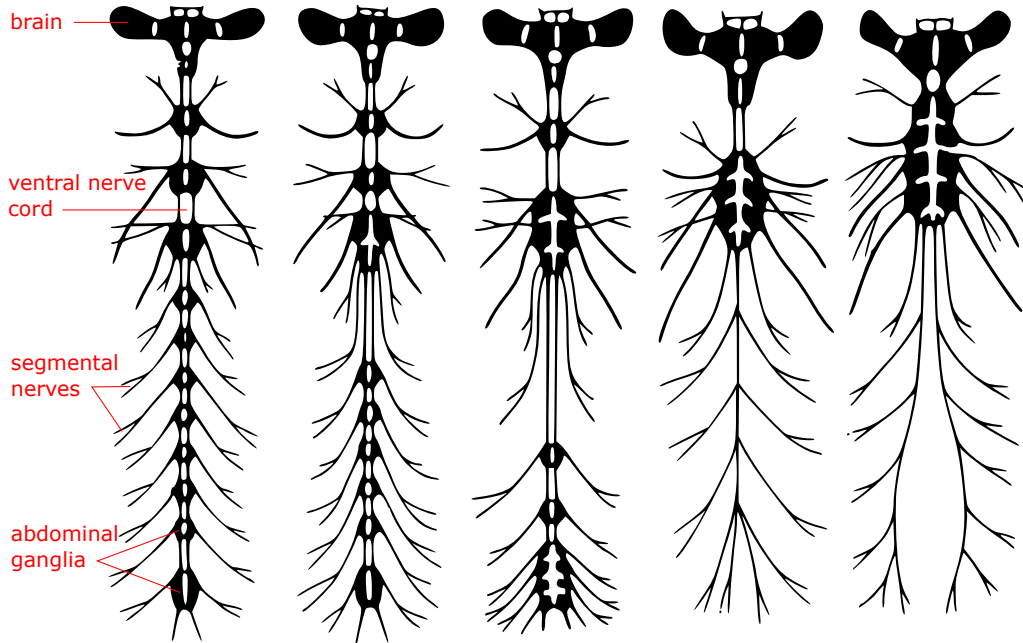
Figure 2.3: Insect central nervous system structure. The insect central nervous system consists of the brain, which is located in the head, and the ventral nervous cord, which connects the ganglia in each segment of the body. From these ganglia, nerve endings lead to the muscles of that segment. The structure of the central nervous system varies between species. The examples shown can be found from left in dictyopterus and pulex; blatta and chironomus; crabro and eucera; musca, calliphora and lucilia; hydrometra and rhizotrogus. The figure is inspired by [45].

as stretch receptors. Cuticular mechanoreceptors are divided into two types: hair-like and dome-like. Both types have a similar arrangement of neurons and sheath cells and they respond to touch.

All insects possess a pair of antennae located on the head. Antennae are moved by muscles and their main purpose is to detect obstacles. Research shows that the antennae measure the distance to obstacles, which is important for proper leg placement and obstacle overcoming [72, 156].

For sound perception, the insect is equipped with tympanal organs [77]. They are composed of tympanal membrane, are backed by an air-filled space and are innervated by a chordotonal sensory organ. The tympanal membrane is vibrated by the incoming sound. Depending on the intensity and frequency of the sound wave, the corresponding neurons are activated. The frequency of sound that an insect is able to perceive varies by species. For example, tettigoniids (katydids) can perceive sound from 1 to 100 kHz. Cicadas can perceive sound as low as 100 Hz.

Chemoreception is defined as the ability to perceive certain chemicals. This includes in particular the sense of taste and smell. While in humans taste is mainly associated with the detection of compounds in solution or in a liquid state by receptors in the oral cavity, insects have similar receptors throughout the body and their use is not directly related to feeding. Moreover, insects are able to detect chemicals even on dry surfaces. For these reasons, the term contact chemoreception is used in insects rather than taste. While the

axons of neurons associated with smell receptors lead to the brain, the axons of contact chemoreceptors are terminated in the ganglion of the corresponding body segment.

Perception is not only used to explore the environment, but also to communicate. In addition to sight, one way of visual communication is colour. Bold colours can serve as a warning or can attract attention. Some insects can change their colour. This change can be short-term reversible or permanent. Short-term colour change is rather rare in insects. It is usually associated with a change in cuticle condition or pigment movement. On the other hand, permanent discolouration is relatively common. The larval stages of insects are often colour camouflaged whereas the adults are coloured.

Another way to communicate is by vibration. These can be created by a sound radiator, which is often part of the wings, rubbing a body part against the ground (percussion) or by moving a cuticular ridge on one of the body over a toothed ridge on another (stridulation). The vibrations can be transmitted through the air, water or the substrate on which the insect is standing. Vibration production is controlled by central pattern generators in the central nervous system.

The last but not least way of communication is chemical communication. Pheromones are used for intraspecific communication, allelochemicals are used for interspecific communication. Pheromones, when given to an individual of the same species, cause particular behaviours. Pheromones have a wide range of uses, from marking territory, to signalling the direction of a food source, to reproduction. Allelochemicals usually have the function of a defense mechanism.

2.7 Reflexes

In most animals that have a nervous system, certain patterns of behaviour can be found in response to a particular situation. These actions triggered by some stimulus (typically change in the environment or in the body) are called reflexes [133, 40]. Their activation is usually unplanned and involuntary and they are used to maintain homeostasis (maintenance of vital internal variables in a state of relative constancy [8]). Some reflexes are temporary and eventually disappear, others work for the entire life of the individual. For example, in newborns we observe a number of reflexes such as the palmar grasp reflex or the sucking reflex [154], which disappear as they grow.

A number of reflexes can also be found in insects. Some involve maintaining a posture when the insect stands still. The postural position reflex is activated if an external force (e.g. a gust of wind) causes the angles between the leg segments to change.

Further reflexes relate to the movement of the legs. The depressor reflex increases the frequency of muscle activity when the leg comes into contact with an obstacle [132]. The levator reflex is activated when a leg is touched and leads to a momentary lifting of the leg in an attempt to place the leg on the stimulating object. Other reflexes relate, for example, to orientation, speed of movement or reaction to light.

Chapter 3

Six-Legged Walking Robots

Legged robots come in many different sizes and shapes. They differ in the structure of the legs, their number or their distribution and position on the body of the robot. They are driven by various systems such as electric motors or servomotors or hydraulic devices. Compared to wheeled or tracked chassis, they are capable of overcoming larger obstacles and are therefore more suitable for challenging rugged and sloping terrain [36]. They also have less influence on the terrain because they are only in contact with it at a few small points. On the other hand, due to their more complex design, they are more expensive, relatively slow, more demanding to control and usually have higher energy requirements because they require control and they consume energy even when they are standing still.

Many legged robots resemble an animal. Two-legged robots look like humans, four-legged robots look like dogs or horses, six-legged robots look like bugs, and eight-legged robots look like spiders. Mimicking evolution-tested structures, body shapes or gaits is very common in the design and control of walking robots. As the number of legs increases, the number of gaits of the robot and its stability also increases. The greatest improvement is observed between four- and six-legged robots [86]. The following text will discuss mainly the characteristics of six-legged walking robots – hexapods.

Hexapods are characterized by six legs, which gives them unique features compared to four-legged or two-legged robots. Thanks to this number of legs, they are able to remain statically stable at any moment of their movement. The greater number of legs also allows the use of a greater number of stances and gaits, which helps hexapods to move over rough terrain. They also have a high fault tolerance and are able to continue moving relatively efficiently when several joints or legs are damaged or even lost. These characteristics determine the hexapod for movement in the most difficult conditions such as space missions [11, 89, 161] or operations in inaccessible terrain [183] and mine detection [68, 122].

The first hexapods were simple robots with few joints. They were incapable of complex movements or gaits, not to mention adaptation to rough terrain. One of the first hexapods was built in 1972 at the University of Rome. This robot was controlled by a computer and was equipped with electric drives [128, 170]. At the Russian Academy of Sciences in Moscow a hexapod robot was built whose control was based on a mathematical model [124]. The robot was equipped with a rangefinder so it was able to overcome obstacles. A „Six-Legged Hydraulic Walker" was built at Carnegie-Mello University in 1983. It was the first robot capable of carrying a human. It was powered by a gasoline engine that produced electricity for the control computer and powered a set of hydraulic pumps. Each leg had three degrees of freedom (DOF) [43].

A six-legged robot „Functionoid" was developed by Odetics Inc. in 1983. Odex I is a hexapod robot with pantographic legs. Its weight is about 170 kg and one limb can lift a load of over 200 kg [149]. Each leg is controlled by its own computer. Another computer receives command from operator and commands leg controllers. The robot is controlled by joystick control unit. It was powered by aircraft battery.

A large scale six-legged robot called Adaptive Suspension Vehicle (ASV) and powered by a two-stage hydraulic system was invented in 1985 [180]. Unlike most recent robots, the ASV is not autonomous, but carries an operator who controls it on the level of path selection and navigation. The robot controller then provides leg coordination and foothold selection. ASV is 5 m long, 2.4 m wide, 3 m high, weighs 2700 kg and reaches a speed of 3.6 m/s. The robot was able to climb an incline of 31°, cross 1.8 m wide ditches and overcame walls of 1.35 m height.

The very common inspiration when designing the body of a hexapod robot is the stick insect. Many robots have been built whose body resembles or is at least partially inspired by this order of tropical insects.

Lauron V is one of the robots whose design is inspired by stick Insect. It is a versatile six-legged robot that has 24 DOF [147]. The robot can traverse slopes with an incline of 25° and remain stable on slopes up to 42.8°. The robot uses modular, behavior-based controller. Lauron V is the fifth generation of legged robot. Its first version had only 18 DOF, its weight was 13 kg, length 50 cm and its maximum velocity was 1.1 m/s [21]. The second version was extended with a head that carries a line laser and two cameras that are used to detect obstacles. The robot uses a hierarchical controller [41]. Lauron III is the third version of hexapod. Its weight is 18 kg, length 70 cm and its maximum velocity is 0.3 m/s. The robot can navigate in sloping terrain up to 30° [64]. Lauron IV features with fault diagnosis and status monitoring system [146].

HECTOR is a hexapod robot [153]. It is bio-inspired in both biomechanical design and neurobiological control and serves as a testbed for cognitive approaches. The body structure of this robot is based on carausius morosus. Each leg acts autonomously and exchanges information with adjacent legs to achieve coordinated movements. Each leg controller is implemented as an neural network. It consists of two main parts – swing module and stance module which inhibit each other and generate gait cycle.

Inspiration for the design of a walking robot can also be taken from other species, such as cockroaches. Nelson et al. [118, 117] designed a cockroach-like hexapod robot to test control principles extracted from the cockroach. The uniqueness of the robot lies in the different number of DOF on the legs. The robot has five, four and three DOF on its front, middle and rear legs, respectively, allowing it to mimic the different functions of the legs of a cockroach. The legs are driven by pneumatic actuator, which are commanded by a pulse width modulation (PWM) controller.

The structure and locomotion control of the hexapod robot Gregor is also inspired by biological observations of cockroaches [127, 7]. Its legs have different numbers of DOF and different sizes. The front and middle legs have three DOF and differ only in their attachment to the body. The rear legs have only two DOF, one of which is prismatic, and are longer than the front legs. The robot weighs approximately 1 kg.

3.1 Hexapod Architecture

The complex structure and control of walking robots requires careful design of the individual robot components. In [198], the author discusses design issues and constraints in

the development of walking robots. It mentions, for example mechanical structure and leg configuration, actuating and drive mechanisms, evaluation of expected power consumption, motion conditions or assumed method of walk. The following section describes existing body and leg configurations of hexapod robots.

There are two basic types of hexapod bodies: rectangular and hexagonal [49]. The rectangular body has two groups of three legs distributed symmetrically on the two longer sides. The hexagonal (or round) body is regular and the individual legs are evenly distributed around the perimeter of the robot body. Both options have their advantages and disadvantages. The symmetrical design of the hexagonal body allows the robot to move in any direction and rotate easily on the spot [131, 167]. The elongated rectangular body design is more suitable for overcoming large obstacles and height differences. Gonzalez de Santos [150] optimized the distribution of the legs of the rectangular hexapod. He found that extending the middle leg reduces the energy consumption of the robot.

The body shape of hexapods and their connection to gaits has motivated a number of studies in an attempt to find the best body shape and gaits for hexapods. Lee et al. [94] formulated a mathematical expression that describes the relationships between the stability margin, the stride length and the duty factor. McGhee and Frank [105] showed that for quadrupedal robots, of the six known gaits in which at least three legs remain on the ground, only three satisfy the static stability condition at all times. Of these three gaits, there is one that maximizes static stability, which corresponds to the normal quadruped crawl favored by most animals for very low-speed locomotion. The optimum stability is at $3/4 < \beta < 1$, where β is the duty factor (see Section 3.2.3). Bessonov and Umnov [22] extended this proof to hexapods. They proved that a hexapodal wave gait has the optimum stability in the range of $1/2 < \beta < 1$, where β is the duty factor. This was later confirmed by several other studies [166, 162].

3.1.1 Leg Design

In addition to the body shape, the kinematic properties of a hexapod are also defined by the structure of its legs. The design of the robot leg must take into account the purpose of the robot, the roughness of the terrain in which it will move and the payload that the robot must carry. A number of legs of different shapes, sizes and purposes were built. Figure 3.1a shows the classification scheme of hexapod leg types.

At the highest level, a distinction can be made between bio-inspired legs and non zoomorfic legs. Bio-inspired legs are based on the leg structure of animals and their structure is suitable for certain gaits observed in reptiles, mammals or arachnids. The legs of mammals are placed under the body, resulting in less body support and the need to maintain stability. At the same time, however, the stance and gait of mammals is less energy demanding (e.g. Cassino Hexapod III [171]). In the mammalian configuration, the legs are placed under the body and the knees can be oriented in different directions according to the application they require. In the arachnid configuration, the legs are positioned evenly on both sides of the body and their knee joints stick out above the robot body (e.g. MAX [53], ASTERISK [168], COMET-IV [122]). This configuration is similar to the configuration of the legs in insects, although in most insects some pairs of legs (typically the hind and often the middle) are rotated backwards at the coxa joints. During locomotion, the insect often switches to the last configuration, reptilian, in which the legs, like in the arachnid configuration, are evenly distributed on both sides of the body, but no longer stick out above the body, but rather are next to the body (e.g. DLR-Crawler [69], ATHLETE [161],
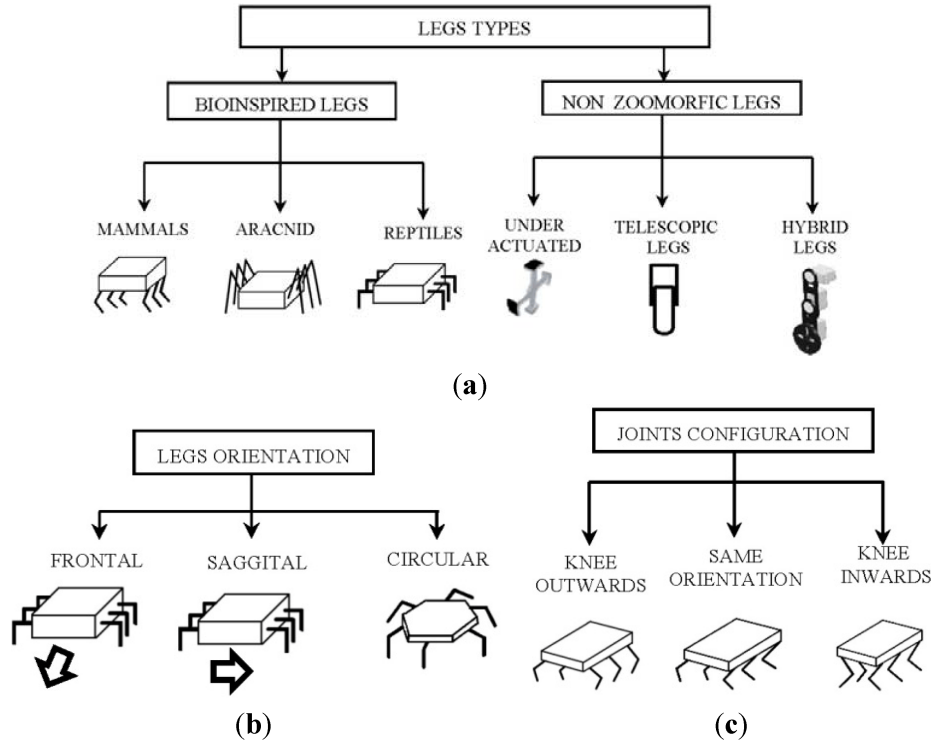
Figure 3.1: Leg types and configurations of hexapod robots. (a) The legs of hexapod robots can be divided on the basis of their shape into bio-inspired legs and non zoomorphic legs. Bio-inspired legs are further divided into mammal type, arachnid type and reptile type. Non zoomorphic can be further divided into under actuated, telescopic and hybrid legs. (b) The orientation of the legs on the robot body is based on the direction of movement. Frontal, sagittal and circular orientation can be distinguished. (c) The configuration of the joints affects the movement characteristics of the leg. The joints can face outwards from the body (knee outwards), in the direction of body movement (same orientation) or inwards (knee inwards). Figure taken with permission of the author from [170].

Weaver [24]). The configuration used for insects also depends on the current stance or gait and speed.

When designing the body shape and leg structure, it is also important to consider the orientation of the legs in relation to the body. There are three possible configurations: frontal, sagittal or circular (see Figure 3.1b). In the case of frontal orientation, the robot primarily moves perpendicular to the leg. In contrast, in the case of sagittal orientation, the direction of movement is parallel to the legs of the robot. In the circular arrangement of the legs, the robot can theoretically move in any direction [90].

Non zoomorphic legs can be under-actuated as THALeR [181] or RHex [151], telescopic as Ambler [93], or hybrid as ASTERISK-H [192] or Cassino Hexapod III [171].

Many researchers take inspiration from nature when designing legs for walking robots. Insects are a very common source of inspiration. The insect leg consists of six segments: coxa, trochanter, femur, tibia, tarsus and pretarsus. The study of insect morphology shows that the size of individual leg segments is not random. With exceptions, which are often due to the adaptation of the leg to a specific purpose, the legs of different insects have similar leg segment sizes. The coxa part is usually less than 10 % of the total leg length

and is free to rotate with three DOF within definite limits. The trochanter is even smaller, in the range of $2 - 8\%$ of the total leg length [61]. Femur and tibia are usually the same size or femur is longer than tibia. Tarsus consists of 3 to 7 segments and its length can vary [202].

If these proportions and sizes are respected in the design of the leg, the resulting robot will be able to better mimic the movement of insects. However, since controlling a leg with a large number of joints is relatively complex, many robots have only three joints, coxa, femur and tibia [66, 153, 197, 178, 179, 75, 20, 53]. These three joints are sufficient to create a smooth, non-slipping movement of the leg. The low number of joints, however, limits the number of stances the robot is capable of, and thus also limits its ability to negotiate complex obstacles and narrow spaces of various shapes and sizes. On the other hand, leg control is easier and fewer actuators should consume less power. Increasing the number of joints in the legs of the robot will enable new stances that can be more energy efficient or better able to overcome rough terrain [161, 147, 24, 199].

3.1.2 Actuator Types

In order for a robot to move, it must move its legs. Therefore, the legs must be equipped with some kind of actuator to move it. The most common type of leg drive for hexapods are electric rotary motors in various forms, which are relatively cheap, easy to control, and provide sufficient power for walking robots of smaller dimensions. These include direct current (DC) and alternating current (AC) motors, servomotors or stepping motors. In addition, electrical power can be easily stored in batteries such as Li-Po batteries, which have a high energy density compared to lead-acid batteries. Electric motors also exist in the form of linear motors. However, their use in hexapods is still rather rare because they have limited movable range to weight ratio. Electric motors are usually equipped with a gearbox because they have relatively small torque.

Pneumatic actuators have low stiffness, are inaccurate and have low power to weight ratio. For their operation, a compressor is needed to pressurize the air. Hydraulic actuators use fluid for their movement, which is pressurized by a hydraulic pump. Due to their high power/weight ratio they are often used in large scale hexapods such as LSHDSL robot [173], HexaTerra [46] or COMET-IV [83], which do not mind having to carry a relatively heavy and large hydraulic pump.

Actuators of individual leg joints can be located in several places. One option is to place all actuators at the beginning of the leg or in the body of the robot. The advantage is that the actuators do not burden the leg at individual joints and the leg is thus light and affects less the center of gravity of the robot when walking. However, the design of the leg is often relatively complex because the force of the actuators must be transmitted to the joints of the leg. For this purpose, various rods, pulley and belt or lead screw can be used. The more joints a leg has, the more complex this solution becomes and is more suitable for larger robots where there is more space in the leg.

Another option is to place the actuators directly into the joint of the leg or somewhere nearby. In the case of placement directly in the joint, the actuator forms part of the leg structure or even protrudes from it. The advantage of this solution is its simplicity, where no mechanisms are needed to transmit the actuator force to the leg joint and the joints can move freely to a relatively large range. The disadvantage is that most actuators are relatively large in size and of considerable weight. This causes the leg to become larger and the higher weight of the leg can play a significant role in keeping the robot stable when

walking. In addition, energy, whether electrical or mechanical, must be supplied to the actuators in the individual joints. The necessary cables or pipes may restrict the movement of the leg at individual joints or may cause frequent damage to them. Some technologies allow chaining of actuators, others require each actuator to be powered separately, which can complicate the leg design.

Leg movement can also be provided by a four-bar linkage structure, which is typical for mammalian legs. The disadvantage of this structure is the high interdependence of the movement of individual joints and thus limited effective workspace. Because the movements are highly coupled, a smaller number of actuators is sufficient. However, their power must be much greater so they can move multiple joints simultaneously.

3.2 Movement

Operating a legged robot is much more difficult than operating a wheeled or tracked robot. This is because a wheeled or tracked robot is able to stand in place due to its design, while the legged robot needs to be controlled even when it is not moving. The forward movement is also considerably more difficult in the case of legged robot. While a wheeled or tracked robot typically has only one motor, a legged robot has several motors on each leg and all the motors need to be synchronously controlled to move the robot in the correct direction. Walking robots use gait to move. There are also hybrid legged robots with wheels attached to the foot tips of their legs so they can move by riding on wheels or walking. In this section, various gait, stability and performance indices of walking robots are discussed.

3.2.1 Gaits

Legged robots use various forms of gait for their locomotion. Gait is a sequence of movements of individual legs. A repeating sequence of the same movements is called a gait cycle and usually corresponds to one step. Each gait cycle consists of a swing phase (also called return stroke) and a stance phase (also called power stroke). There are also two significant positions in the gait cycle for each leg: anterior extreme position (AEP) – the position where the leg is on the ground at the end of the swing phase, and the posterior extreme position (PEP) – the position where the leg is on the ground at the end of its stance phase (see Figure 3.2) [59, 84, 152]. The length of the stance phase trajectory and the swing phase trajectory are important for the movement itself. A gait can be referred to as periodic if similar states of the same leg during successive strokes occur at the same interval in all legs [170].

In insects, several basic gaits have been observed [107, 191, 47]. The most common gait is the tripod. During tripod gait the legs are divided into two groups. The front and rear legs on one side of the body and the middle leg on the other side of the body create one group, the remaining legs form the second group. The legs in the same group move simultaneously. If the first group performs the swing phase, the second group performs the stance phase and vice versa. Thus, at least three legs always remain in contact with the ground. This tends to keep the insect's centre of gravity in the polygon formed by the legs, which are currently providing support, a condition for a statically stable gait. Tripod is the fastest statically stable gait. Although there are faster dynamically stable gaits than the tripod, observations and experiments show that the tripod is strongly favored in upward, downward and sideways climbing using leg adhesion. In most insects gait transitions have
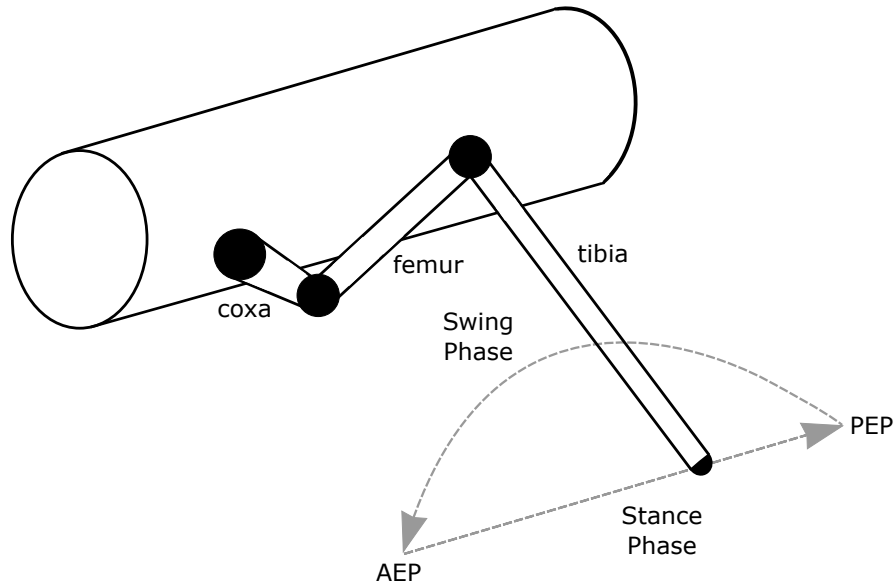
Figure 3.2: Gait cycle phases and significant positions. Each gait cycle consists of a swing phase (return stroke) where the leg is lifted off the ground and travels in the direction of the movement, and a stance phase (power stroke) where the leg is on the ground, providing support to the body and moving against the direction of its movement. There are two significant points in the gait cycle. The anterior extreme position is the point where the swing phase ends and the stance phase begins. The posterior extreme position is the point where the stance phase ends and the swing phase begins. The figure is inspired by [84].

been observed as they gradually increase speed from a slow wave gait to a tetrapod gait and finally reaching a tripod gait [189, 136]. The individual gaits are shown in Figure 3.3.

Metachronal wave is another gait observed in insect [79, 18]. It is the most stable gait because at any given moment only one leg is in swing phase and all other legs are in stance phase.

Ripple is a gait in which the swing phases of the legs overlap and for a short moment the robot rests on only four legs. Once the leg is at the highest point of the swing phase, the swing phase of the next leg begins.

Tetrapod is a medium fast gait. At least four legs always remain in contact with the ground, making the tetrapod gait a more stable but slower gait compared to the tripod gait [107].

In addition to the above-mentioned gaits, it is possible to encounter free movement of the legs, which does not have a clear period. The legs move in an undefined order with the purpose of moving the robot forward. This type of gait is called free gait [106, 56], also described as periodic support state sequences for straight-line locomotion.

3.2.2 Stability

Stability is an important aspect of robot movement. During movement, the robot can be in two different states of stability – static or dynamic. A statically-stable robot is in a stable position at every moment of its movement. The center of gravity (CoG) of the robot must be located in the support polygon – a polygon formed by its legs that are currently providing
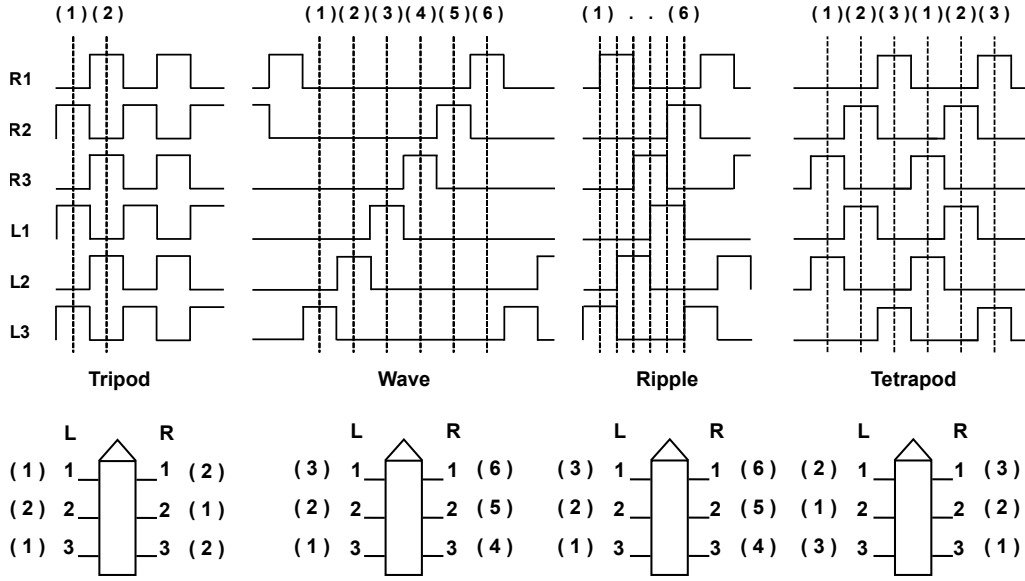
Figure 3.3: The graph shows the movement of each leg in time. A high value represents swing phase of the leg, low value represents stance phase. Tripod, wave, ripple and tetrapod gaits are shown in this figure. The tripod gait has two group of legs, all the legs in the same group move at once. Tripod is the fastest statically stable gait for hexapods, but the least stable. In the wave gait only one leg is moving forward at any time. The other legs support the body. This leads to extremely stable movement, which is good for rough terrain. In the ripple gait all legs move the same way, but their moves are shifted and the swing phases of neighbour legs are overlapped. Once the first leg is being placed on the ground, the second leg is already lifted. In the tetrapod gait, there are always two legs in the swing phase. The other legs support the body. The tetrapod is slower than the tripod, but has greater stability. The figure is inspired by [201].

support (see Figure 3.4a). A statically-unstable robot is not in a stable position at every moment of its movement. CoG of the robot is not located in the support polygon and the robot is basically falling (see Figure 3.4b). Between these two stability states is a critically stable position where the robot is on the limit of stability (see Figure 3.4c). However, a statically-unstable robot can become dynamically stable if additional force is supplied, e.g., by changing the direction of movement or by swinging a leg [19, 195].

The robustness of static stability is measured by the shortest distance from CoG to the edge of the support polygon, which is called the static stability margin (SSM) [134, 115]. The larger the polygon of support, the larger the displacements that can be tolerated. The SSM can be calculated according Equations (3.1)-(3.6) [155]. Consider the tripod gait, where just three legs are in contact with the ground forming a triangle. This situation is illustrated in Figure 3.5.

The Equation (3.1) describes the area (and therefore the stability) of a triangle as a triple of distinct points.

$$S(p_1, p_2, p_3) = \frac{1}{2} \begin{vmatrix} 1 & 1 & 1 \\ x_1 & x_2 & x_3 \\ y_1 & y_2 & y_3 \end{vmatrix} \tag{3.1}$$

(a) Statically stable   (b) Statically unstable   (c) Critically stable
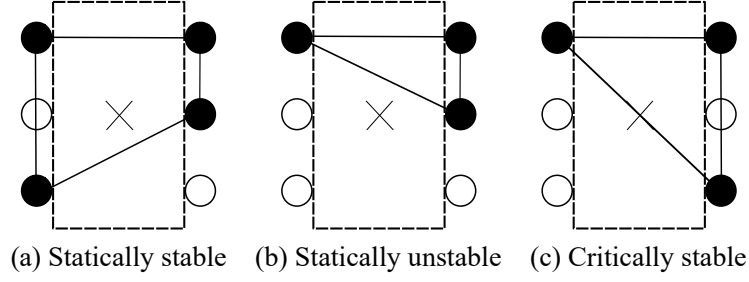
Figure 3.4: Possible stability states of a six-legged robot during its movement. Black dots represent legs on the ground currently supporting the body of the robot and the symbol „x" represents the center of gravity. (a) The robot is statically stable, because the center of gravity is inside the polygon formed by legs supporting the body. (b) The robot is statically unstable, because the center of gravity is outside the polygon formed by the legs supporting the body. (c) The robot is critically stable, balancing at the edge of stability, which is expressed by the centre of gravity at the edge of the polygon formed by the legs supporting the body. The figure is inspired by [114].

where $S(p_1, p_2, p_3)$ is the area of the triangle that is defined by the points p_1, p_2, p_3 with coordinates x_i and y_i. Equation (3.2) is given by expansion of Equation (3.1).

$$S(p_1, p_2, p_3) = \frac{1}{2} \left[(x_2 - x_1)(y_3 - y_1) - (x_3 - x_1)(y_2 - y_1) \right] \tag{3.2}$$

Then S_1 is defined by Equation (3.3).

$$S_1(p_0, p_3, p_{cb}) = \frac{1}{2} \left[(x_3 - x_0)(y_{cb} - y_0) - (x_{cb} - x_0)(y_3 - y_0) \right] \tag{3.3}$$

The distance L_1 between points p_0 and p_3 can be calculated using Equation (3.4).

$$L_1 = \sqrt{(x_0 - x_3)^2 + (y_0 - y_3)^2} \tag{3.4}$$

where x_0, y_0, x_3, y_3 are the coordinates of points p_0 and p_3, respectively. The static stability margin H_1 can be determined using Equation (3.5).

$$H_1 = 2\frac{S_1}{L_1} \tag{3.5}$$

Finally, the static stability margin for the situation shown in Figure 3.5 can be calculated using Equation (3.6).

$$H = min(H_1, H_2, H_3) \tag{3.6}$$
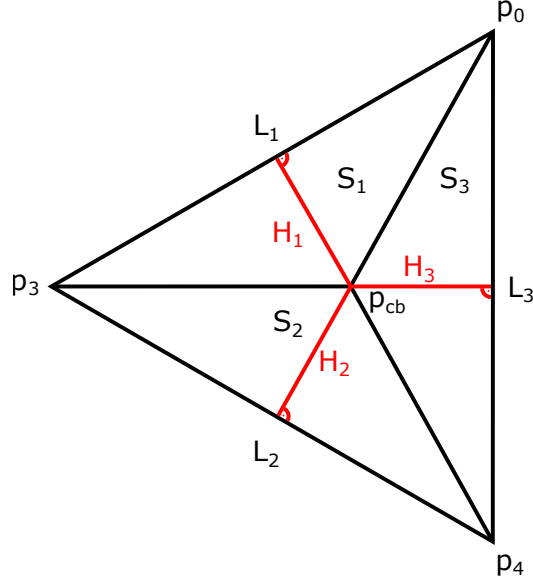
Figure 3.5: Static stability margin in tripod gait. Three legs, the right front (p_0), the left middle (p_3) and the right rear (p_4), are in the contact with the ground at points $p_0[x_0, y_0]$, $p_3[x_3, y_3]$ and $p_4[x_4, y_4]$ respectively, forming a triangle in which the centre of the body is located at point $p_{cb}[x_{cb}, y_{cb}]$. L_1, L_2, L_3 are the distances between the respective legs, H_1, H_2, H_3 are the lengths of the altitudes, S_1, S_2, S_3 are the areas of the triangles.

3.2.3 Performance Indices of Walking Robots

Walking robots are characterized by their diversity in body shape and size or leg structure and length. To compare walking robots with different weight, size and shape, the following indices have been proposed in the literature.

- Duty factor

- Froude number

- Energy cost of transport (specific resistance)

Duty factor β [163] is defined by Equation (3.7).

$$\beta = \frac{support\ period}{cycle\ time} \tag{3.7}$$

where *support time* is time when the leg provides support and *cycle period* is duration of one step. Duty factor can also be used to distinguish between running and walking, where $\beta < 0.5$ is for running and $\beta \geq 0.5$ is for walking [170].

Froude number is another performance index and it is defined by Equation (3.8).

$$Fr = \frac{v^2}{gh} \tag{3.8}$$

where v is the walking or running speed of the robot, g is the the gravitational acceleration and h is the distance of the hip joint from the ground [3].

Since the length h multiplied by the frequency f has the same dimension as the velocity, the characteristic velocity hf can be used to calculate the Froude number Fr according to Equation (3.9) [2].

$$Fr = \frac{(hf)^2}{gh} = \frac{hf^2}{g} \tag{3.9}$$

As shown in [3], animals of different sizes use similar gaits when travelling with the same Froude number. Also, most animals switch between walking and running at a Froude number of around one and change symmetrical gait to asymmetrical gait at Froude numbers between two and three.

The power indicator energetic cost of transport (CoT) is defined as the energy required to move a unit mass over a unit distance (sometimes called specific resistance) [62, 119]. It is defined by Equation (3.10).

$$\epsilon = \frac{E}{mgd} \tag{3.10}$$

where E is the total energy consumption for a travel of distance d, m is the total mass of the vehicle, and g is the acceleration due to gravity. By substituting energy for power [92], the CoT can be written as Equation (3.11).

$$\epsilon = \frac{P}{mgv} \tag{3.11}$$

where P is the electric power consumption of the robot during its motion, m is the mass of the robot and v is the speed of the robot. The electric power P can then be determined by Equation (3.12).

$$P = UI \tag{3.12}$$

where U is the supply voltage of the robot and I is the current drawn from the power supply.

3.3 Controllers

The control system is the brain of the entire walking robot. Its task is to coordinate the movements of the joints of the individual legs so that the robot moves in the desired direction, maintains stability, and eventually overcomes obstacles and terrain irregularities. Due to the complexity of this task, control systems of actual hexapods are often designed as distributed hierarchical systems, where individual subsystems are responsible for a small part of the robot control [170].

These subsystems of a control system may include various levels of navigation, task planning, coordination of leg movement and robot stance, calculation of leg kinematics, actuator control, or reading and processing sensor data. They can be located on different computing devices either directly on the robot or on the controlling computer. The communication between these computing centres can be provided by different buses and protocols. Some robots have a dedicated controller for each leg, other robots have one central controller that controls all legs.

There are many different types of control systems. Some are pre-programmed and generate an unchanging pattern that is translated into the movement of the leg joints. These controllers typically produce only a limited number of gaits and do not take into account uneven terrain. At best, they can stop the leg movement on contact with the ground or an obstacle. Other controllers analyse the data obtained from the sensors of the robot and adjust the movement of the legs accordingly. There are also controllers that have no predefined gait and learn all the movements themselves. These controllers are often based on neural networks.

3.3.1 Control Architectures

The robot control architectures are related to sensing, monitoring and actions of the robot. Different kinds of robot controllers can be distinguished [84].

- Reactive and subsumption / behavior-based control architectures

- Deliberative controllers (hierarchical) or sense-plan-act control architectures

- Hybrid control architectures

The reactive control architecture (scheme based) is a stimulus-response based architecture. The reaction of the robot to a specific sensor input is predefined — each action has a reaction. Although the reactive control architecture response speed is rather high, which can be an advantage when operating in real world where the response time is very important, the reactive architecture is not suitable for predictive planned outcomes. The scheme of the reactive control architecture is shown in Figure 3.6a.

The subsumption architecture (behavior based) is an alternative to the reactive system architecture. It is based on priority behaviors organized into layers. The lower layer behaviors (reflexes) can inhibit higher layer behaviors. The problem of this control architecture is the right order of the layers. The scheme of the subsumption control architecture is shown in Figure 3.6b.

The deliberative control architectures are based on the Sense-Plan-Act principle and for their optimal functioning they usually need full knowledge of the environment. In the deliberative control architecture the robot first senses the environment, then creates a list of possible actions. The robot also considers the results of the plans when choosing appropriate actions. The advantage of this architecture is that the goal can be easily achieved thanks to the goal oriented architecture. On the other hand this architecture is rather slow and it is not suitable for purposes where a quick reaction is needed. Also when the environment changes, the architecture must be changed too. The scheme of the deliberative control architecture is shown in Figure 3.6c.

The limitations seen by the reactive and the deliberative architectures can be solved by combining both approaches into a hybrid architecture. There are many different kinds of hybrid control architecture. In general, the hybrid architecture uses higher level planning in order to guide the lower level of reactive components. The advantage of the hybrid architecture is that it incorporates high-level control and planning in the form of a deliberative layer, while allowing rapid response to unexpected changes in the environment through a reactive layer. The scheme of the hybrid control architecture is shown in Figure 3.6d.
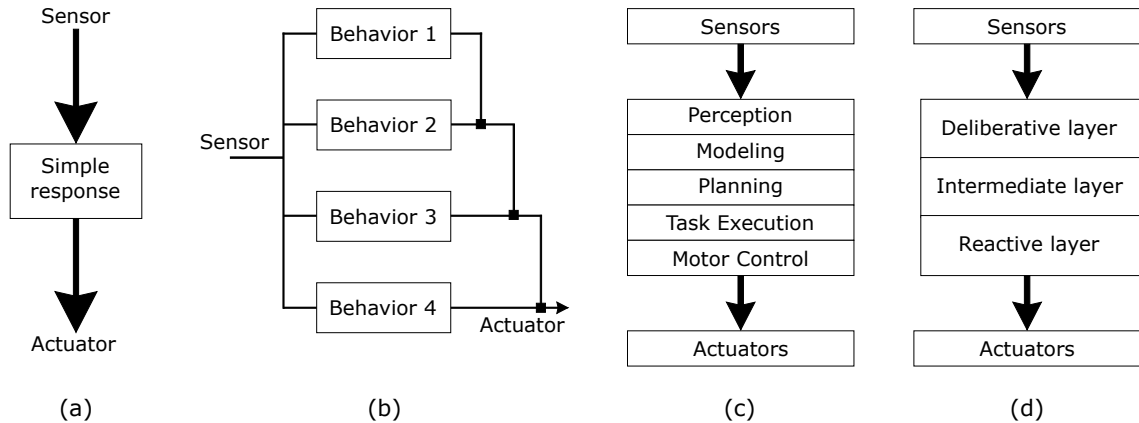
Figure 3.6: Control architecture schemes. (a) Reactive control architecture. The reaction of the robot to a specific sensor input is predefined. A specific perception will trigger a corresponding response. The advantage of the reactive architecture is its rapid response to changes in the environment. The disadvantage is, that the architecture lack any planning. (b) Subsumption architecture. The architecture is based on priority behaviors organized into layers. The disadvantage of the architecture is the necessity to find the most suitable order of the layers. (c) Deliberative control architecture. The architecture is based on Sense-Plan-Act principle and for its optimal functioning it usually need full knowledge of the environment. In the deliberative control architecture the robot first senses the environment, then creates a list of possible actions and then chooses the best suited one. (d) Hybrid control architecture. Hybrid architecture is a combination of reactive and deliberative control architectures. It keeps the advantages of both architectures. The deliberative layer enables planning, the reactive layer enables rapid response to changes in the environment. The figure is inspired by [84].

3.3.2 Neural Network based Controllers

Generating gaits for walking robots is a difficult task because most of these robots have a large number of degrees of freedom. Six-legged robots usually have 18 joints, but robots with 24 or even 30 joints are no exception. Neural networks are one of the options used to generate gaits for walking robots. Beer et al. [15] proposed a heterogeneous neural network that controls the walking of a simulated insect. Beer [16] also developed a recurrent neural network based on studies of the American Cockroach. This neural network was hand tuned to produce the desired outputs. Two years later, Beer et al. introduced a fully distributed neural network architecture designed for hexapod robot control [17]. The design of the neural network is based on research on the neuroethology of insects locomotion and was successfully tested on a real hexapod robot. The reported results were similar to the results observed in simulated insects. The robot was capable of movement using different gaits. The scheme of the controller is shown in the Figure 3.7.

Each leg had its own controller, which operates as follows: Normally, the foot motor neuron is active (supporting the robot body). When the command neuron excites the backward swing motor neuron, the leg is moved backward (stance phase). Periodically, the pacemaker neuron interrupts the stance phase and excites the forward swing motor neuron (swing phase). The frequency of pacemaker bursts and the velocity output of the backward swing motor neuron depend on the level of excitation provided by command neu-
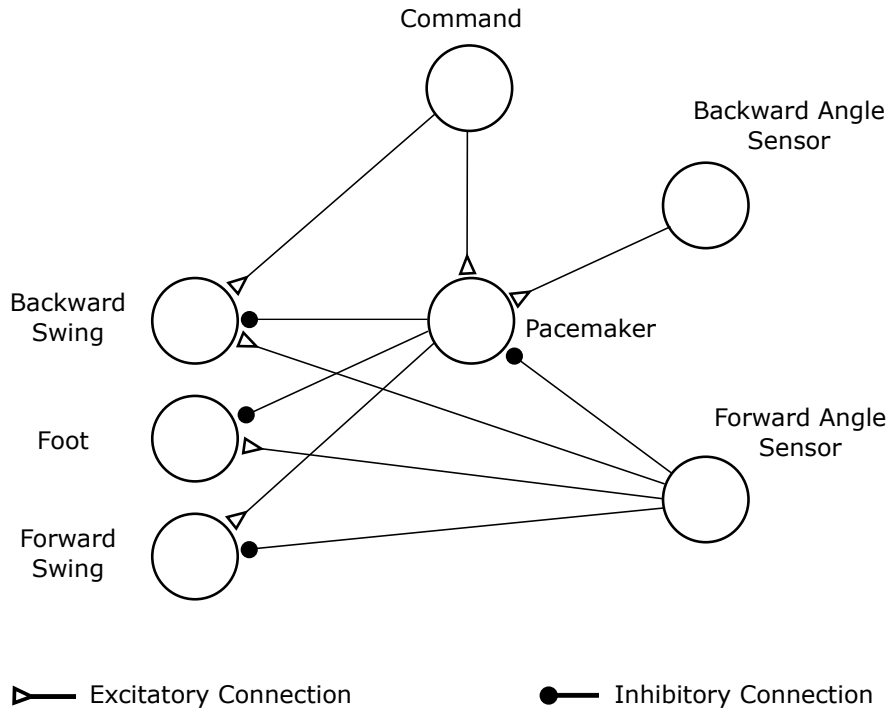
Figure 3.7: Leg controller introduced by Beer et al. Each leg is controlled by three motor neurons, which are driven by the pacemaker neuron whose output rhythmically oscillates. A single command neuron makes the same two connections on every leg controller. The forward angle sensor can inhibit the pacemaker neuron and the backward angle sensor can excite pacemaker neuron and change its rhythm. The figure is inspired by [17].

ron. Additionally, sensors can reset the pacemaker neuron. Adjacent pacemakers mutually inhibit one another to ensure that adjacent legs will not swing at the same time.

The robustness of the controller based on the gait used is discussed in [38]. The robot was capable of stable movement at slow, medium and fast gaits with disconnected forward or backward angle sensor of any leg. Also removing the connections between pacemaker neurons did not prevent the robot from walking stably at any speed. Finally, after disabling the lift motor of the middle leg and retracting the leg so it does not support any load, the robot was ably to walk using slower gaits, but was unable to walk using tripod gait, because tripod gait requires the middle leg. If the leg was disabled but not retracted, the robot was turning towards the disabled leg [200].

Goldschmidt et al. [67] present an adaptive neural control mechanism allowing hexapod robots to negotiate obstacles. In the design of a hexapod robot, they addressed four behaviors necessary for efficient obstacle negotiation observed in insects: a positive change in body angle, center of mass elevation, body flexion, and local leg reflexes. The resulting robot is equipped with an adaptive backbone joint that allows the robot body to bend between the front and middle legs. Each leg implements a searching and elevator reflex. The solution was tested in simulated environment and on a real robot (AMOS II) and the results of testing shows that the robot can efficiently negotiate obstacles with a height up to 85 % of the robot leg length in simulation and 75 % in a real environment.

LAURON is a 18-degrees-of-freedom hexapod robot and it is controlled by a neural control architecture [21]. The first layer of the controller consists of modules for leg control. For each leg, two neural networks were trained. One for the stance phase and one for the swing phase. Parameters for these neural networks are provided by altitude (for stance phase) and foot position (for swing phase) modules.

Parker and Lee [126] used a genetic algorithm to determine the weights of an artificial neural network that would control the leg of a hexapod robot. A neural network consists of six fully connected neurons. Two sensors are connected to two neurons that monitor horizontal and vertical extreme positions. From two other neurons, two outputs lead to the leg servomotors. Once the network topology and individual connections are established, a population of individuals is generated whose genomes carry the weights of individual neurons. Thus prepared neural network is then activated and generates hundreds of control pulses. The generated pulses are then evaluated by a fitness function that has three basic parameters. The first parameter is the forward motion, which corresponds to the movement of the leg at the time of stance phase. The second parameter is the number of leg lifts. This is a penalty parameter because moving the leg up or down does not lead to movement forward and only consumes energy. The third parameter is resistance. This is again a penalty that occurs when the leg is in the most posterior position and is in contact with the surface. Such a leg only slows down the movement of the robot. Parker and Lee also propose to train parts of the controller for each leg individually, and then to make connections between the sub-networks already learned. First, a small network is created and trained. Subsequently, one large network is created from these small networks.

Researches of animal nervous system show that the pattern of locomotion is controlled by neural centers located in the neural systems below the brain stem in the spinal cord known as central pattern generators (CPGs), whose output is an oscillating signal with a certain frequency. CPGs are used to generate most rhythmic or repetitive movements such as walking, swimming, breathing, coughing, panting, chewing or swallowing [100]. They generate a periodic muscle control signal that is independent of the sensory input and is controlled only by the intensity of the excitation electrical signal [103]. The output of most CPGs can be modulated at the level of output frequency and signal phase by changing the synaptic force or by changing the intrinsic properties of the membrane [101].

Central pattern generators are commonly modeled as system of coupled nonlinear oscillators. The term *central* means that they do not need any sensory input to function [80]. Still, sensory feedback is important to maintain proper coordination of movements. Many experiments confirm tight coupling between CPGs and sensory feedback [104, 48, 185]. There are a number of different models of CPGs [80]. The most commonly used are CPGs based on mathematical models of coupled nonlinear oscillators.

CPGs have been widely used to control the motion of walking robots. Ijspeert et al. [81] developed a model of a spinal cord focusing on three main problems related to vertebrate locomotion: changes in the spinal locomotor centre during the evolutionary transition from water to land, the mechanisms necessary for leg coordination, and the mechanisms of transition between gaits. They created a model based on CPG, which is inspired by the movement of the salamander. The model is composed of body CPG and legs CPG. The model generates motion patterns for walking and swimming that are similar to those of a real salamander.

Yu et al. [193] proposed a new control architecture for hexapod robots based on CPG. They split the control into two layers: a motion generation algorithm layer, which is implemented using a ring CPG network based on a modified Van der Pol oscillator, and a layer

coordinating the motion of each joint of a leg, which solves the problem of controlling the coordination of the motion of a single leg with several DOF using phase modulation and changing the amplitude of the neural oscillator. Each leg has its own controller that produces a rhythmic signal. The six controllers are then connected and produce a periodic signal with the same amplitude and frequency, but their signals are phase shifted to generate the desired gait. The transition between gaits is then understood as the ability of the controller to recover from an initial state that occurs outside the expected phase. The controller has been successfully tested on a real robot.

Gregor I. is a hexapod robot whose control architecture is base on CPG, which is composed of nonlinear oscillators [7]. There are six neurons in the CPG made of two cellular nonlinear networks (CNN). Each neuron generates signals for one leg. The CNN outputs do not directly drive the leg actuators, but are first transformed to meet the particular leg kinematics. Single neurons are synchronized by interconnections that ensure coordination of leg movements.

Chung et al. [39] designed a CPG-based controller for a hexapod robot that uses 24 Matsuoka's neural oscillators. One leg controller has four oscillators, one for amplitude regulation and three for phase modulation. Using the mapping function, the oscillator outputs and higher control commands are converted to foot tip positions.

Lele et al. [95] introduced training a legged robot to walk by learning the synchronization patterns of CPGs. The network of the controller consists of six leaky-integrate and fire spiking neurons, each controlling one leg of the robot. The neurons are fully connected to each other. The CPG is driven by an input neuron. Its periodic input causes the CPG to fire. Another neuron connected to a gyroscope sensor only fires when the robot starts to lose its balance while walking. The learning process of the network led to the tripod gait in 70 % of the cases. In the remaining cases, the solution converged to suboptimal gaits that allowed the robot to move.

3.3.3 Central Pattern Generators

Studying animals in order to observe and imitate their behaviour, it was discovered that even very small life forms are capable of very complex movements, despite the fact that their brains are of negligible or no size. In 1914, the English researcher Brown suggested that muscle contraction and relaxation during walking may be controlled by rhythmic centers that control antagonistic muscles by mutually inhibiting neurons [31, 30]. The first experiments that tried to find an answer involved disabling sensory input to the central nervous system. Wilson et al. [188, 187] showed that the locust can generate rhythmic flying pattern in response to non-rhythmic stimulation of the nerve.

The concept of CPG came from experiments, which demonstrated that a group of neurons could produce a rhythmic pattern while isolated from any sensor input [157]. Matsuoka proposed mathematical models for CPG [102, 103] in which the CPG consisted of two neurons. Equation (3.13) gives one of the frequently used CPG models.

$$\left.\begin{array}{l} \tau\dot{x} + x = \sum_{j=1}^{n} c_j s_j \qquad (\dot{} \triangleq d/dt) \\ y = g(x - \theta) \qquad (g(x) \triangleq max(0, x)) \end{array}\right\} \qquad (3.13)$$

35

where x is the membrane potential of the neuron, s_j is the weight of the input signals, θ is the threshold of the neuron, τ is the time constant, c_j are the weights of the neuron (> 0 for exciting connections, < 0 for inhibiting connections), and y is the output of the neuron.

However, this model does not match the behavior of a real neuron – when a neuron receives a spiking input, the value of its output increases monotonically over time and gradually approaches a stationary state.

However, real neurons usually do not show such a dependence on time – their output first increases rapidly and then gradually decreases to a lower level. This reduction in output level is called adaptation [98]. Instead of Equation (3.13), the following neuron model defined by Equation (3.14) can be used, which includes neuron adaptation.

$$\left.\begin{aligned} \tau\dot{x} + x &= \sum_{j=1}^{n} c_j s_j - bx' \\ T\dot{x}' + x' &= y \\ y &= g(x - \theta) \end{aligned}\right\} \tag{3.14}$$

where x' is a variable that represents the adaptation rate of the neuron, and $T(> 0)$ and $b(\geq 0)$ are parameters that specify the time properties of the adaptation. The condition for such parameters is defined by Equation (3.15) as follows.

$$(T - \tau)^2 \geq 4T\tau b \tag{3.15}$$

The model without adaptation according to Equation (3.13) is then a special case of the new model with adaptation for $b = 0$. For n neurons with adaptation that inhibit each other the oscillator model is then defined by Equation (3.16).

$$\left.\begin{aligned} \dot{x}_i + x_i &= -\sum_{j=1}^{n} a_{ij} y_j + s_i - bx'_i \\ T\dot{x}'_i + x'_i &= y_i \\ y_i &= g(x_i) \quad (i = 1, ..., n) \end{aligned}\right\} \tag{3.16}$$

where a_{ij} is the inhibition level of the connection between the two neurons ($a_{ij} \geq 0$ for $i \neq j$ and $a_{ij} = 0$ for $i = j$, assuming that no exciting connection or inhibiting connection to itself is considered). The $\sum a_{ij} y_j$ represents the total input from the neurons in the neural network and s_i represents the total input from the outside of the network. τ and θ can be omitted because by substituting the values $\tau = 1$ and $\theta = 0$ in the Equation (3.14), one can substitute $x_i - \theta$, t/τ, T/τ and $s_i - \theta$ for x_i, t, T and s_i, respectively. Also assume that the inputs s_i are positive and constant in time.

The simplest network producing an oscillating output consists of two mutually inhibiting neurons ($n = 2$); see Figure 3.8a. Other possible connections and their outputs are shown in Figures 3.8b, c, d.
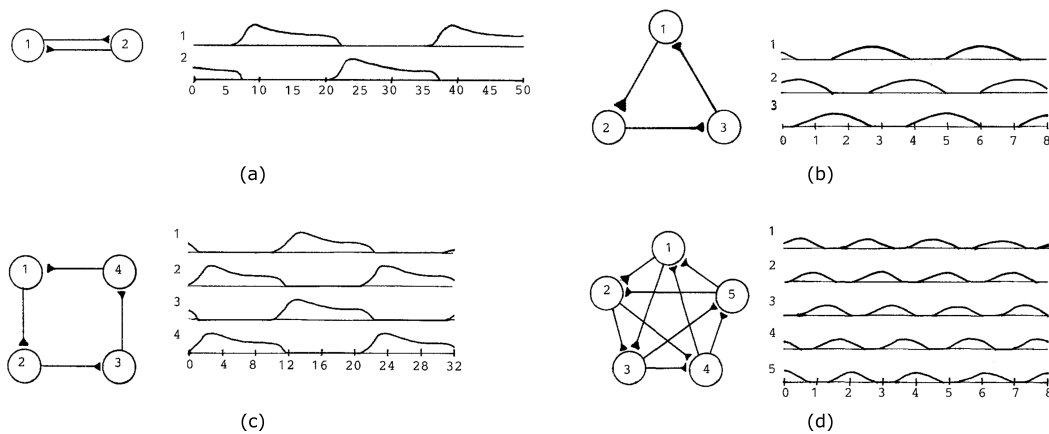
Figure 3.8: CPG configurations with different numbers of neurons and inhibitory edges. When neurons are excited, the network starts to generate an oscillating output signal on individual neurons. The signals are phase-shifted due to the inhibitory edges, but have the same frequency and amplitude. Figure taken from [102].

3.4 Existing Robots

This section contains descriptions of various legged robots. The presented robots differ in body shape and size, number of legs and joints, controller or drive system. At the end of the section, examples of hybrid robots with wheeled legs are presented.

ATHLETE (All-Terrain Hex-Limbed Extra-Terrestrial Explorer) is a vehicle designed for lunar exploration [184]. Its main purpose is to transport cargo across the lunar surface. The vehicle concept is based on six wheeled multi-degree-of-freedom limbs. Each leg has five motors for its movement and additional two motors to drive the wheel movement and its orientation. The wheel motor can also power drilling or gripping tools. The main disadvantage of the robot is its low movement speed. The robot is shown in Figure 3.9a.

RHex is another under-actuated hexapod robot that has only six DOF [151]. It uses a clock excited alternating tripod gait to walk and run. The robot reaches speeds of up to one body length per second in rough terrain. The design of the robot has several modifications, such as Rugged RHex [130], EduBot [182] or AQUA [52]. X-RHex, the latest successor to RHex, has an improved design to offer improvements in power, run-time, payload size, durability, and terrain negotiation [63]. The X-Rhex is shown in Figure 3.9b.

BigDog is four-leg robot designed for rough terrains [129, 135]. The robot is powered by combustion engine that drives hydraulic pump as the robot uses low-friction hydraulic cylinders to move its legs. BigDog is remotely controlled by a human operator. It has about 50 sensors to monitor the environment and the state of the robot. The weight of BigDog is 109 kg and it can reach speeds of up to 3.1 m/s. The successor to BigDog is Legged Squad Support System (LS3) [27] designed mainly for military purposes. The LS3 robot is shown in Figure 3.9c.

MIT Cheetah is a quadruped legged robot equipped with high torque-density motors that uses electric regeneration to increase its energy efficiency [160]. At a speed of 5.95 m/s the robot reaches a minimum CoT of 0.5025 that rival the running animals and is significantly lower in comparison to other running robots. However, due to its design, the Cheetah has reduced maneuverability. The robot is shown in Figure 3.9d.

(a) ATHLETE[1]
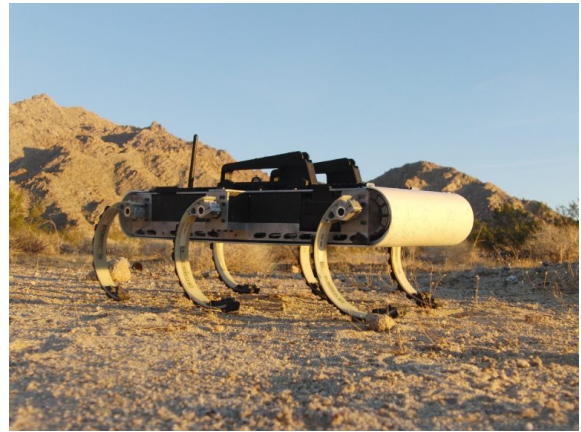
(b) X-RHex[2]

(c) Legged Squad Support System (LS3)[3]
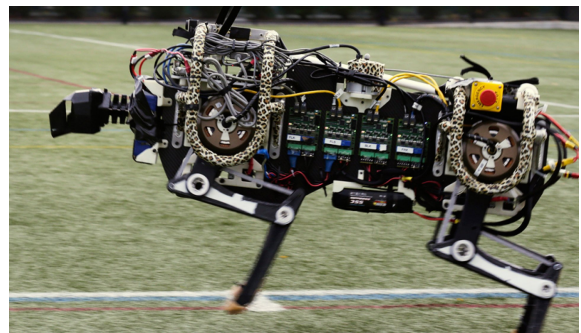
(d) MIT Cheetah[4]

Figure 3.9: Examples of hexapod robots with different number of joints and quadruped robots.

THALeR (Tri-Pedal Hyper Altitudinal Legged Robot) is a three-leg robot over three meters tall with 9 DOF that aims to using as few actuators as possible to achieve motion [181]. Its predecessors STRiDER 1 [73] and STRiDER 2 [111] were 90 cm and 120 cm tall, respectively. Although three legs are sufficient for static stability, the robot becomes unstable when any leg is lifted. The movement of the robot is therefore complex and relatively slow. Because the robot has under-actuated legs, it is not capable of normal walking. When moving, the swing leg slowly lifts and undergoes the A-frame formed by the remaining legs while maintaining balance. On the other hand, the low number of legs is beneficial in the case where the robot is not moving because it has low energy requirements. The final version of THALeR will be up to 10 m high, should be able to cross large obstacles and will serve as a mobile communication or surveillance platform. The robot is shown in Figure 3.10a.

---

[1]Figure taken from https://www.nasa.gov/sites/default/files/images/414103main_r_athlete_full.jpg, 15.7.2023.

[2]Figure taken from https://kodlab.seas.upenn.edu/wp-content/uploads/2017/10/xrhexdesert-1-768x576.jpg, 15.7.2023.

[3]Figure taken from https://cdn.arstechnica.net/wp-content/uploads/2013/12/LS3-AlphaDog_reduced.jpg, 15.7.2023.

[4]Figure taken from https://www.incimages.com/uploaded_files/image/1920x1080/cheetah-robot_44933.jpg, 15.7.2023.

COMET-IV is the fourth version of COMET hexapod robots designed for mine detection [83]. It has 24 hydraulic DOF that are driven by a hydraulic pump powered by two gasoline engines. The length, width and height of the robot are 2.8 m, 3.3 m and 2.5 m respectively and its weight is 2,950 kg. The robot uses impedance-based controller. The first version was COMET-I that exhibited a number of issues while walking and therefore its speed was very low [120]. Second version, COMET-II, was ten times faster than COMET-I. Its nonlinear controller is based on neural network so the robot can move autonomously. COMET-III was build as an scaled-up version of COMET-II. It weights 900 kg and it is 4 m long, 2.5 m wide and 0.8 m tall [121]. COMET-IV is shown in Figure 3.10b.

HexaTerra is an 18 DOF electrohydraulic hexapod robot designed for underwater operations [46]. The robot maintains stability using feedback from IMU, encoders and foot force sensors and can overcome various obstacles using wave gait. The robot is shown in Figure 3.10c.

LSHDSL (large scale hydraulically driven six-legged) robot is an 18 DOF electro-hydraulic robot with a weight of 10,000 kg [173]. The distributed control architecture consists of seven computers – one coordination computer and six leg computers.

TITAN XI is the latest version of the TITAN walking robots [76]. It has four legs – each leg has three DOF driven by hydraulic cylinders. The robot dimensions are 4.8×5×3 m and it weights 7,000 kg.

(a) THALeR[5]

(b) COMET-IV[6]

(c) HexaTerra[7]
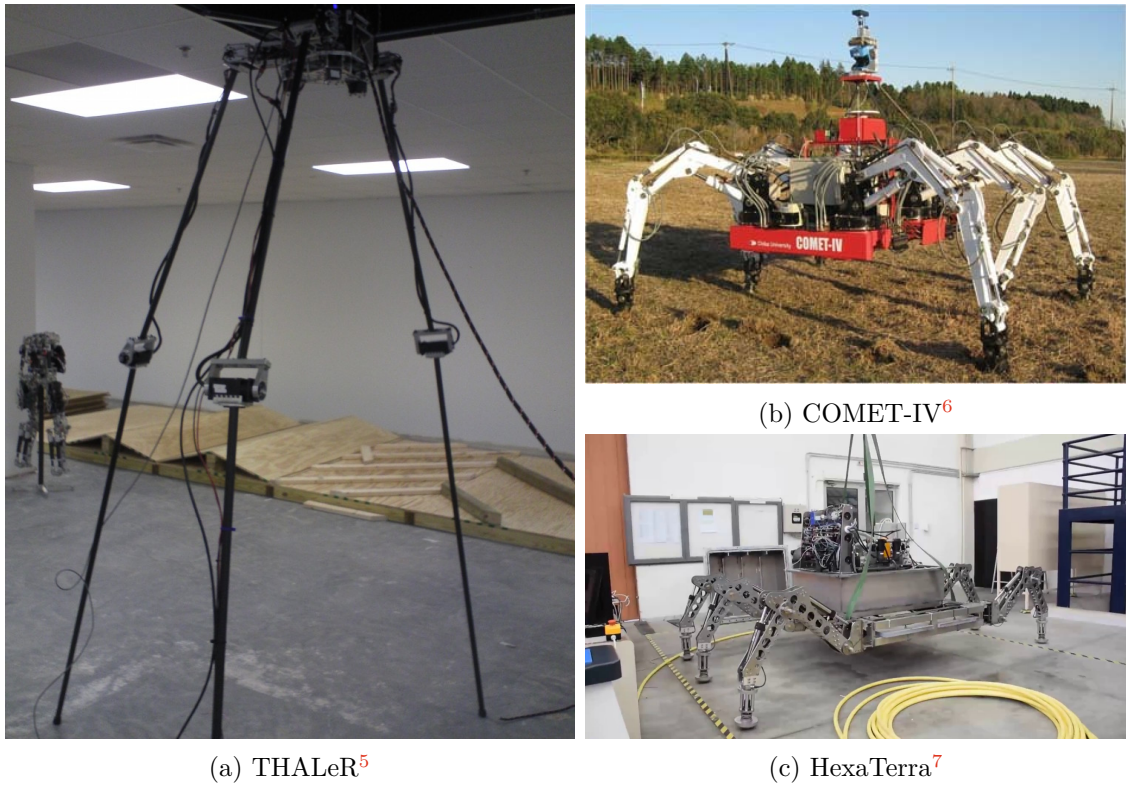
Figure 3.10: Examples of large scale legged walking robots.

(a) Dante II[8]

(b) HyQ (Hydraulic Quadruped)[9]

(c) AMOS II[10]
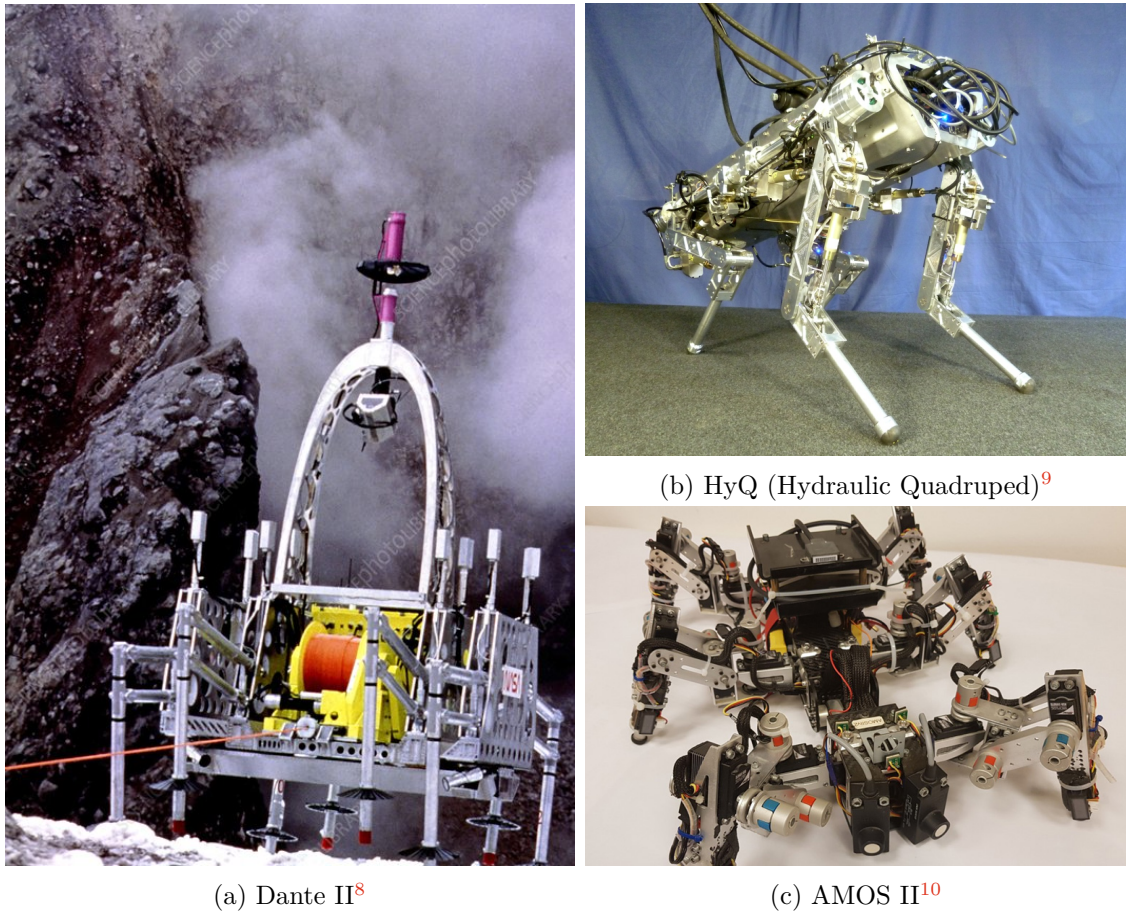
Figure 3.11: Examples of legged walking robots with different types of leg drive.

Dante II is eight-leg walking robot designed for space exploration [12]. Its pantographic legs are divided into two groups of four on the inner and outer frame. The robot movement is achieved by a single motor that moves the frames relative to itself. The frames can also rotate up to 7.5° relative to each other, allowing the robot to turn. Each leg can adjust its vertical position to avoid obstacles. The robot can move autonomously or can be teleoperated from a great distance. Dante II was tested on a five-day mission in a volcano. The robot was attached to a tether cable that was used to maintain stability while traversing a steep slope and minimize adverse structural load on the legs. The robot is shown in Figure 3.11a.

HyQ (Hydraulic Quadruped) is four-leg walking robot with 12 DOF (8 hydraulic and 4 electric) [159]. The robot weights 91 kg and uses torque-controlled hydraulically and electrically actuated joints. HyQ is 1 m long, 0.5 m wide and 0.98 m tall. The robot is shown in Figure 3.11b. Its successor HyQ2Max [158] is more rugged and has more powerful actuators. The movement skills of the robot have also been improved so that the robot can self right itself.

---

[7]Figure taken from https://i.ytimg.com/vi/sKu2AuVaTqI/maxresdefault.jpg, 15.7.2023.

[8]Figure taken from https://media.sciencephoto.com/t2/50/04/76/t2500476-800px-wm.jpg, 15.7.2023.

[9]Figure taken from https://assets.rbl.ms/25565755/origin.jpg, 15.7.2023.

[10]Figure taken from https://www.sdu.dk/-/media/images/nyheder_sduk/nyheder2018/insektrobot.jpg, 15.7.2023.

AMOS II is a hexapod robot with three DOF per leg and one DOF for active backbone joint [66]. The robot is controlled by reactive climbing control, which is composed of three neural networks – backbone joint control, leg reflex control and neural locomotion control. It allows the robot to efficiently negotiate over obstacles of different heights. The robot is shown in Figure 3.11c.

Weaver, a six-legged robot with 30 DOF, can climb slopes up to 30° and remain statically stable in the slope up to 50° [24]. The proposed hierarchical controller reduces the CoT of the robot and enables movement in rough terrain. This is achieved mainly by the capability of the robot to rotate its legs parallel to the gravitational acceleration. The robot is shown in Figure 3.12a.

Abigaille-III is a climbing hexapod with 24 active DOF [75]. The use of passive adhesion spares energy and allows the robot to climb nearly four hours. Unlike its predecessors [108, 96], the newer version of the robot uses active detachment using a dedicated motor. The parallel control architecture is based on a Field Programmable Gate Arrays (FPGA). The robot is shown in Figure 3.12b.

Multilegged Autonomous eXplorer (MAX) is an ultralight hexapod with 18 DOF [53]. The robot is 2.25 m tall and weights approximately 59.8 kg. The control architecture combines kinematics-based planning with impedance-based control. The robot uses pressure sensors to detect foot tip pressure on the ground. The robot is shown in Figure 3.12c.

Ambler is a six-legged robot designed for autonomous planetary and lunar exploration [93]. The robot is capable of traversing terrain with a slope of 30° and overcome ditches and boulders up to 1 m in size. The structure of the leg of the robot differs significantly from the structure of the leg of modern hexapods. Ambler has three DOF on each leg. The rotational and extensional joints in the horizontal plane are used for movement of the robot and the orthogonal joint in the vertical plane is used to compensate terrain irregularities. Ambler is 3.5 m long and 4.5 m wide. Its height varies between 4.1 and 6 m and its weight is 2,050 kg. The robot is shown in Figure 3.12d.

Ragno is a hexapod robot with 18 DOF [179]. Each leg has its own micro-controller that controls three hobby servomotors. One master microcontroller controls the movement of all legs based on commands from the control computer. Messor, successor of Ragno, has similar kinematic structure to the previous prototype, but its size is twice as big as Ragno, allowing the robot to perform more complex locomotion tasks and carry more sensors [178]. Messor II has better power to mass ratio than Messor [20]. It also has more powerful servomotors and the onboard control computer has more computing power. Force-sensitive resistors used as ground sensors have been replaced by micro-switches for greater durability.

DLR-Crawler is a six-legged robot developed from DLR-Hand II [33] as an experimental testbed for legged robots gait algorithms that uses joint torque, foot force-torque sensing and joint position. Each leg has four joints but only three DOF, because femur and tibia joins are coupled. The robot is powered by an external power supply and controlled by an external realtime PC [69]. The robot is shown in Figure 3.13a.

ASTERISK is a hexapod robot with 24 DOF [168]. The robot can be transformed to quadruped form and use two legs as arms and manipulate objects. The robot is equipped with pressure sensors to detect ground, gyrosensor and an acceleration sensor, cameras and infrared sensors. Thanks to the umbrella-shaped leg tip, the robot is able to climb on the wire ceiling grid. The robot is shown in Figure 3.13b.

Walking robots with hybrid legs form a special group of legged robots. These robots are able to achieve higher movement speeds due to their wheeled chassis. Thanks to their legs, they can also move in rough terrain. Some hybrid robots have only a small number of

joints on their legs, which they use rather to compensate uneven terrain while riding and are thus not capable of actual walking. An example of such a robot is Hylos.
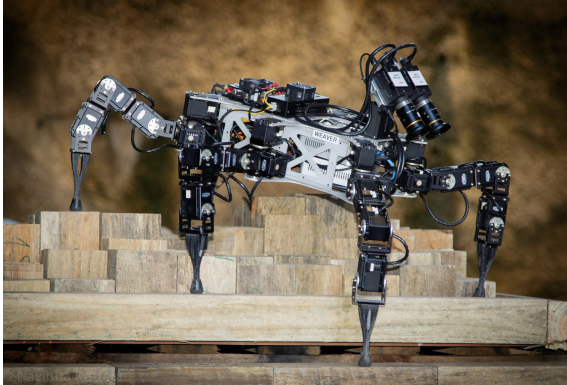
(a) Weaver[11]
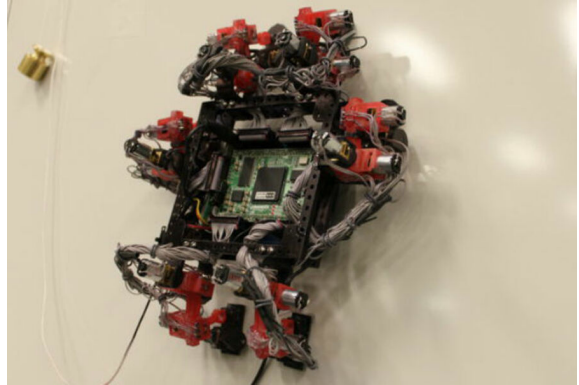
(b) Abigaille-III[12]

(c) MAX[13]

(d) Ambler[14]

Figure 3.12: Examples of hexapod robots with different leg types.

Hylos is a wheeled chassis rather than a walking robot [5]. However, it does have legs that are ended by wheels that can be rotated in different directions. It has 16 DOF (two on each leg and two as omnidirectional chassis). The controller combine posture and trajectory control [70]. The robot is shown in Figure 3.14a.

Other hybrid robots have a similar leg structure to walking robots and additionally have a motorized wheel at the end of the legs. So they can truly combine walking and riding. Examples of such robots include ASTERSIK H or Cassino Hexapod III.

ASTERISK H [192] is the successor of hexapod robot ASTERISK [168]. It has 30 DOF (three on each leg and two as omnidirectional chassis). The robot is able to detect the surface using encoder and torque sensors information, switch from riding to walking and overcome various terrain obstacles and irregularities.

---

[11]Figure taken from https://i0.wp.com/research.csiro.au/robotics/wp-content/uploads/sites/96/2016/09/WeaverOnTestbedNew1.jpg, 15.7.2023.

[12]Figure taken from https://www.usine-digitale.fr/mediatheque/7/3/8/000188837_896x598_c.jpg, 15.7.2023.

[13]Figure taken from https://i0.wp.com/research.csiro.au/robotics/wp-content/uploads/sites/96/2017/03/MAX_outdoor_new1.jpg, 15.7.2023.

[14]Figure taken from https://www.ri.cmu.edu/app/uploads/2018/11/ambler-cmu-frc.jpg, 15.7.2023.

(a) DLR-Crawler[15] (b) ASTERISK[16]
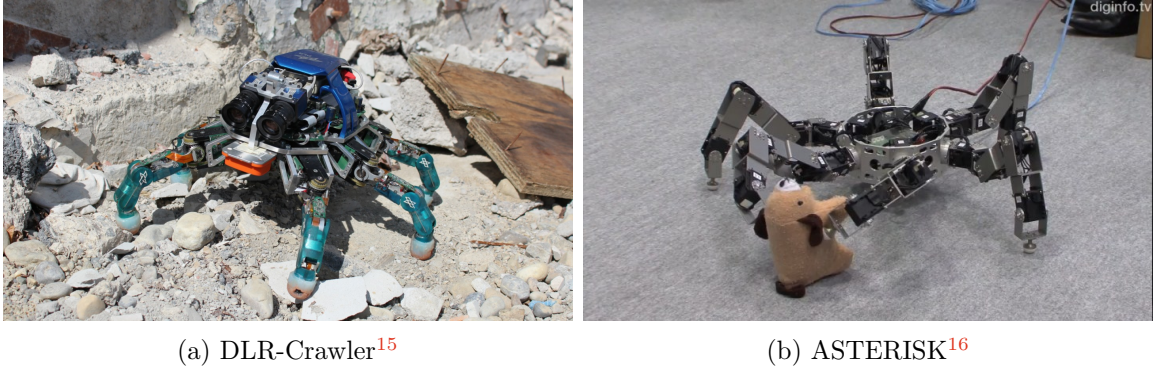
Figure 3.13: Examples of hexapod robots.

Cassino Hexapod III is a hybrid hexapod robot [171]. It has 18 DOF. Each leg is equipped with a mecanum-wheel (an omniwheel with angle of 45°). The robot is controlled by an Arduino board with servo shield an equipped with several sensors such as ultrasonic sonar or inertial measurement unit. The legs can only swing in the direction of movement. A detailed evaluation of locomotion performance of Cassino Hexapod III is described in [125]. Cassino Hexapod I [35] and Cassino Hexapod II [169], had very complex turning strategy due to the absence of omnidirectional wheels. The robot is shown in Figure 3.14b.

Unlike the previous two robots, Roller Walker does not have a motorized wheel, but only a passive wheel, which it uses for roller skating [54]. During walking, the wheel rotates towards the ground and forms the feet of the robot.

Other hybrid robots include ATHLETE [161], Creadapt Robot [85] (see Figure 3.15a) or ANYmal [25] (see Figure 3.15b).

The following Table 3.1 compares several characteristics of selected legged robots.

(a) Hylos[17] (b) Cassino Hexapod III[18]
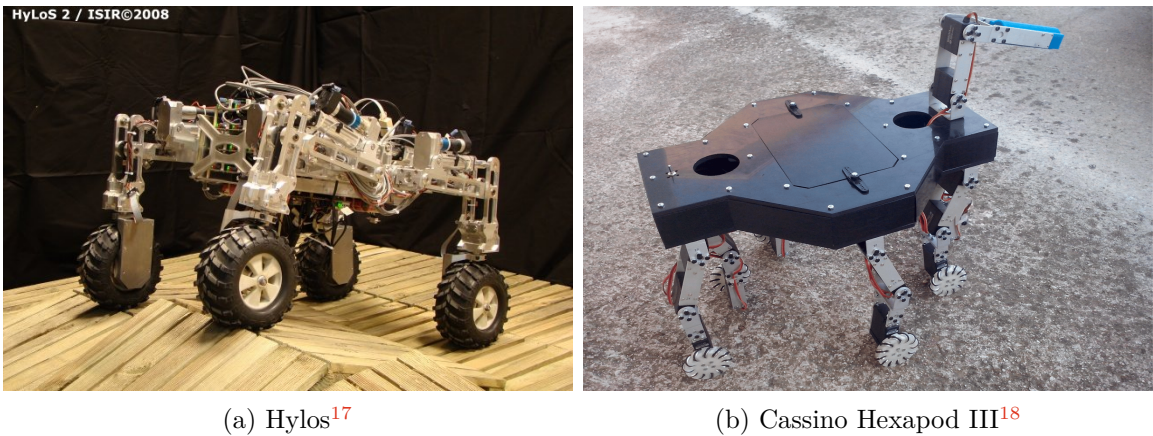
Figure 3.14: Examples of hybrid wheeled legged robots.

---

[15]Figure taken from https://www.dlr.de/rm/en/Portaldata/52/Resources/roboter_und_systeme/krabbler/Crawler_2011_Rubble_16_9_1440x809.jpg, 15.7.2023.

[16]Figure taken from https://robotnyheter.se/wp-content/uploads/2011/12/Asterisk_hexapod_insect_robot_with_prey.jpg, 15.7.2023.

[17]Figure taken from https://www.researchgate.net/profile/Philippe-Bidaud/publication/265752953/figure/fig6/AS:668299272675355@1536346371850/Hylos-II-a-hybrid-wheeled-legged-robot.jpg, 15.7.2023.
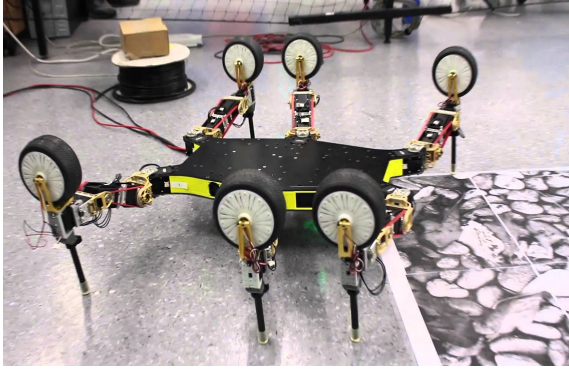
(a) Creadapt Robot[19]   (b) Wheeled ANYmal[20]

Figure 3.15: Examples of hybrid wheeled legged robots.

---

[18]Figure taken from https://pub.mdpi-res.com/robotics/robotics-06-00040/article_deploy/html/images/robotics-06-00040-g015.png, 15.7.2023.

[19]Figure taken from https://i.ytimg.com/vi/uIPErWYq1TI/maxresdefault.jpg, 19.8.2023.

[20]Figure taken from https://wired.me/wp-content/uploads/2022/11/Lead-swiss-mile-robot-.jpg, 19.8.2023.

Table 3.1: Comparison of legged robots. The table shows a comparison of several characteristics of the selected walking robots. The leg segment length ratios of the individual robots are also worth noting. Taken from [202].

Robot	Leg DOF	Dimensions L × W × H	Mass [kg]	Speed † [m/s]	Coxa [m]	Troch. [m]	Femur [m]	Tibia [m]	Tarsus [m]
R-Hex	1	0.5 × 0.4 × 0.1	7.0	0.55			0.175		
X-RHex	1	0.6 × 0.4 × 0.1	9.5	1.54			0.175		
MAX	3	2.4 × 2.1 × 2.3	60.0	0.07	0.08		0.8	1.5	
AMOS II	3	0.5 × 0.4 × 0.1	4.2		0.035		0.06	0.115	
Messor I	3	0.5 × 0.5 × 0.2	-		0.05		0.16	0.23	
Messor II	3	0.5 × 0.5 × 0.2	2.6		0,049		0.12	0.174	
Hector	3	1.0 × 0.5 × 0.2	13.0		0.032		0.26	0.28	
DLR-Crawler	4	0.5 × 0.5 × 0.2	3.5	0.20	0 ‡		0.075	0.04	0.04
HAntR	4	0.5 × 0.5 × 0.3	2.9	0.43		0.025	0.082	0.21	
ASTERISK	4	0.8 × 0.8 × 0.1	4.2		0.07	0.05	0.105	0.105	
Lauron V	4	0.9 × 0.8 × 0.7	43.5	0.14					
Weaver	5	0.6 × 0.6 × 0.3	7.0	0.12	0.067	0.062	0.107	0.088	0.135
WHexaR	5	0.6 × 0.6 × 0.4	8.8	0.12 / 0.2	0.073	0.064	0.127	0.124	0.095
Abigaille-III	3	0.2 × 0.2 × 0.1	0.6	0.001	0 ‡		0.03	0.03	
Cassino III	2	0.4 × 0.2 × 0.2		0.02 / 0.15					
ASTERISK-H	3	0.6 × 0.5 × 0.3	3.4	? / 0.30					

† The second number indicates the speed when using the wheels. ‡ Coxa and femur joints are united.

45

Chapter 4

WHexaR Mechanical, Electronic and Controller Design

The mechanical design of the robot is an important part of the walking robot design. It can be divided into two main parts, the mechanical design of the body and the mechanical design of the legs. In the case of the body, it is necessary to choose the shape and size that will correspond to the intended use of the robot. The size of the body determines the size of the leg. It is also possible to reverse this procedure and design the body size according to the leg size. This second approach was applied to the design of WHexaR (Wheeled Hexapod Robot – a robot built as part of this work).

The body of the robot will be used to house the control systems and batteries. The individual components will be placed inside the body of the robot and thus protected from possible damage. The legs will be placed in two groups of three on each side of the body. One leg at the front of the body, one in the middle and one at the back. Body weight should be kept as low as possible while maintaining sufficient strength. The estimated length of the robot body is about 0.5 m.

The task of the electronic system will be to control the robot, power the individual components and obtain information from the environment and actuators. The electronics will consist of a power supply, actuators, computing system and sensors.

The first part of this chapter describes the design of the leg structure and its forward and inverse kinematics. In the second part, the design of the robot controller is presented.

4.1   Leg Design

To design a walking robot leg, it is necessary to decide what type of leg the robot will have and how it will be attached to the robot body. Next, the type of actuators and their positioning relative to the leg joints must be chosen. Finally, the appropriate components can be selected to connect the actuators to form the leg and its joints.

An aracnid type leg with a frontal orientation on a rectangular body was selected for WHexaR, combining features of a bio-inspired leg and a non zoomorfic hybrid leg. To simplify the design of the leg, its joints will be formed directly by actuators. Each leg will have seven degrees of freedom. Five actuators will be used to position the leg. Two more actuators will form a wheeled chassis. The lengths of the segments will be based on the size of the leg of the insect. For easier riding in the terrain, the robot will be equipped with rubber wheels. The proposed leg structure is in Figure 4.1.
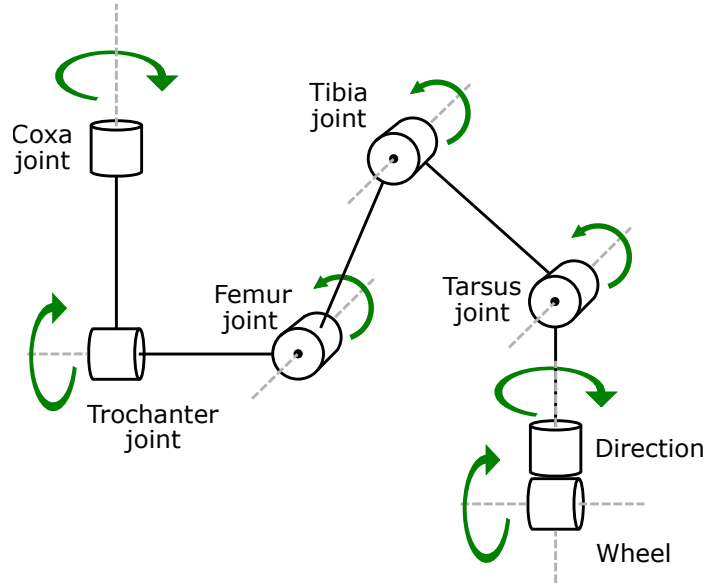
Figure 4.1: Scheme of the proposed leg structure. The leg has seven joints. Coxa, trochanter, femur, tibia and tarsus are used to position the leg. The trochanter joint allows rotation of the entire leg, which will be beneficial especially in sloping terrain. The last two joints form the wheeled chassis. The first joint allows the wheel to turn, the second joint drives the wheel.

The first joint, the coxa, will be used to rotate the leg forward and backward. Its range should be at least 180°, so that the leg can be used not only for movement but also for manipulating objects in the environment. The second joint, the trochanter, will allow the entire leg to rotate relative to the body. The third joint, the femur, will be used to lift the rest of the leg during the swing phase and will provide the most support during the stance phase. Its actuator should be selected accordingly. The remaining two joints, the tibia and tarsus, will be used to adjust the trajectory of the leg during walking. The load on the tibia joint depends on the current stance. Its main task will be to support the body during the stance phase. The tarsus joint is assumed to be parallel to the acceleration of gravity, and thus should not bear a heavy load since it will only maintain the balance of the leg joint.

4.1.1 Forward Kinematics

The leg will consist of seven servomotors that will be connected together using aluminum brackets. To create a mathematical model of the robot, each leg is numbered according to its position $l \in \{0, ..., 5\}$, each joint is numbered as $j \in \{0, ..., 6\}$, where coxa joint is 0 and wheel joint is 6, and each servomotor will be assigned a unique number $i \in \{1, ..., 42\}$ (see Figure 4.2). The following applies:

$$i = 7l + j + 1 \tag{4.1}$$

$$j = (i - 1) \bmod 7 \tag{4.2}$$

$$l = \frac{i - j - 1}{7} \tag{4.3}$$

Equation (4.1) determines the servomotor number based on the leg and joint number, Equation (4.2) determines the joint number from the servomotor number and Equation (4.3) determines the leg number based on the joint and servomotor number.
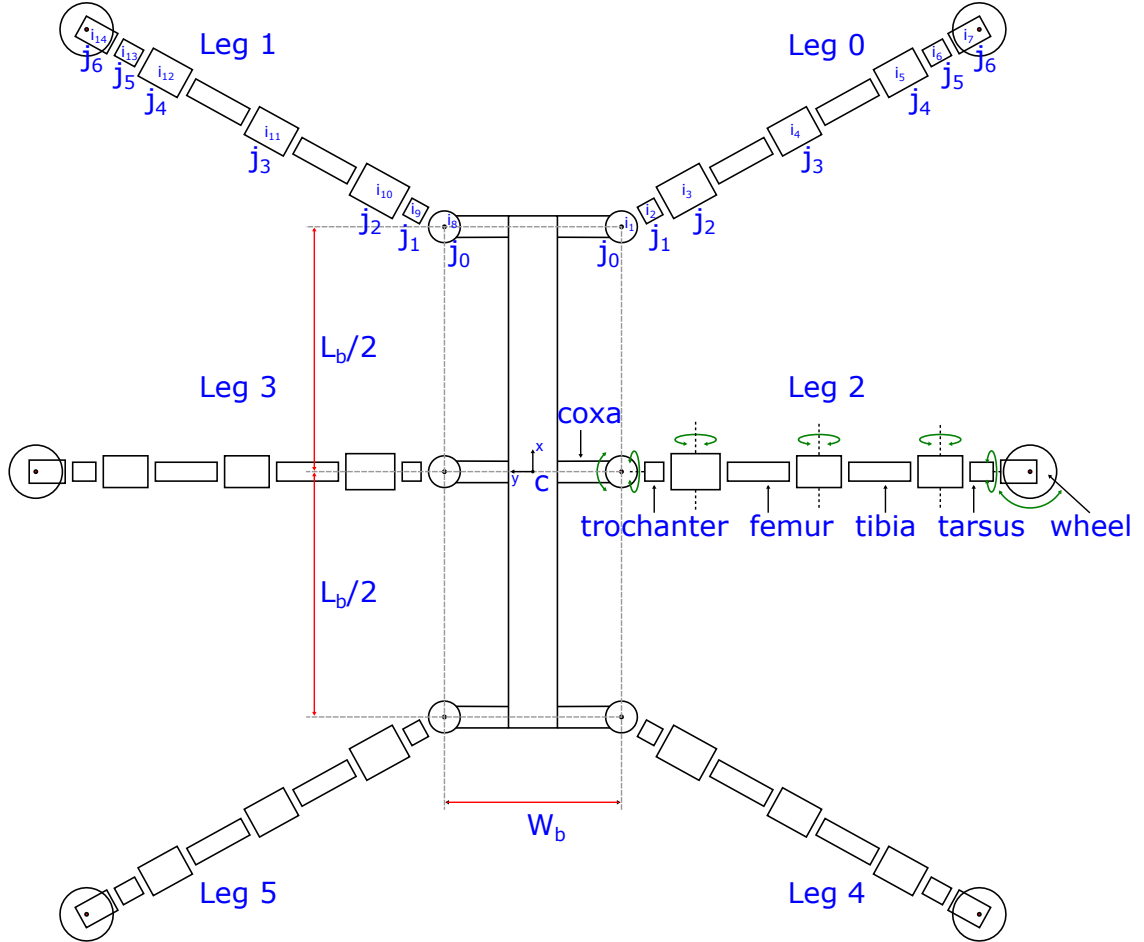
Figure 4.2: Robot leg numbers. The legs are numbered in sequence, right front, left front, right middle, left middle, right rear and left rear. Joint 0 corresponds to the coxa joint, joint 6 corresponds to the wheel. Servomotors are numbered from coxa joint of leg 0 to wheel servomotor of leg 5. Point C represents the centre of the robot body. Body width W_b is the distance between the coxa joints of the left and right pairs of legs, body length L_b is the distance between the coxa joints of the front and rear legs. The figure is inspired by [92].

The forward kinematics problem deals with the relationship between the individual joints of the robot leg and the position and orientation of the foot tip [164]. The leg of the robot can be considered as a set of links (brackets) connected to each other by joints (servomotors) that have only one degree of freedom. The Denavit-Hartenberg (D-H) [164]

convention was chosen to describe the relationships between the individual joints. This convention describes a general open kinematic chain using a series of homogeneous transformations. Each of these homogeneous transformations is represented by Equation (4.4) as the product of four basic transformations, rotation by θ_i about the z axis, translation of d_i along z axis, translation of a_i along x axis and rotation by α_i about the x axis:

$$
\begin{aligned}
A_i \;=\;& Rot_{z,\theta_i} Trans_{z,d_i} Trans_{x,a_i} Rot_{x,\alpha_i} \\[4pt]
=\;& \begin{bmatrix} c_{\theta_i} & -s_{\theta_i} & 0 & 0 \\ s_{\theta_i} & c_{\theta_i} & 0 & 0 \\ 0 & 0 & 1 & 0 \\ 0 & 0 & 0 & 1 \end{bmatrix}
\begin{bmatrix} 1 & 0 & 0 & 0 \\ 0 & 1 & 0 & 0 \\ 0 & 0 & 1 & d_i \\ 0 & 0 & 0 & 1 \end{bmatrix}
\begin{bmatrix} 1 & 0 & 0 & a_i \\ 0 & 1 & 0 & 0 \\ 0 & 0 & 1 & 0 \\ 0 & 0 & 0 & 1 \end{bmatrix}
\begin{bmatrix} 1 & 0 & 0 & 0 \\ 0 & c_{\alpha_i} & -s_{\alpha_i} & 0 \\ 0 & s_{\alpha_i} & c_{\alpha_i} & 0 \\ 0 & 0 & 0 & 1 \end{bmatrix} \\[4pt]
=\;& \begin{bmatrix} c_{\theta_i} & -s_{\theta_i}c_{\alpha_i} & s_{\theta_i}s_{\alpha_i} & a_i c_{\theta_i} \\ s_{\theta_i} & c_{\theta_i}c_{\alpha_i} & -c_{\theta_i}s_{\alpha_i} & a_i s_{\theta_i} \\ 0 & s_{\alpha_i} & c_{\alpha_i} & d_i \\ 0 & 0 & 0 & 1 \end{bmatrix}
\end{aligned} \tag{4.4}
$$

where s_x denotes $sin(x)$, c_x denotes $cos(x)$, quantities $a_i, \alpha_i, d_i, \theta_i$ represent the parameters of the corresponding links i and joints i as translation along x, rotation around x, translation along z and the rotation around z, respectively (sometimes called link length, link twist, link offset, and joint angle, respectively) [164]. The D-H leg parameters will be measured on the 3D model and will be adjusted according to the real robot.

The transformation matrix T_{j+1}^{j} between the coordinate system of leg joint j and the coordinate system of leg joint $j+1$ is given by Equation (4.5).

$$
T_{j+1}^{j} = \begin{bmatrix} c_{\theta_j} & -s_{\theta_j}c_{\alpha_j} & s_{\theta_j}s_{\alpha_j} & a_j c_{\theta_j} \\ s_{\theta_j} & c_{\theta_j}c_{\alpha_j} & -c_{\theta_j}s_{\alpha_j} & a_j s_{\theta_j} \\ 0 & s_{\alpha_j} & c_{\alpha_j} & d_j \\ 0 & 0 & 0 & 1 \end{bmatrix} \tag{4.5}
$$

where s_x denotes $sin(x)$, c_x denotes $cos(x)$ and $a_j, \alpha_j, d_j, \theta_j$ are the DH parameters of the joint j. The mapping between the global coordinate system and the foot tip coordinate system is given by Equation (4.6).

$$
T_f^0 = T_1^0 T_2^1 T_3^2 T_4^3 T_f^4 \tag{4.6}
$$

where f is the foot tip frame.

4.1.2 Inverse Kinematics

The task of inverse kinematics is to calculate the joint angles $\theta^l = \{\theta_0, \theta_1, \theta_2, \theta_3, \theta_4\}$ of the individual servomotors of the leg l so that the foot tip is located at the specified coordinates. Unlike forward kinematics, whose task is to determine the end position of the foot tip based on the rotation of individual servomotors, inverse kinematics may not find a solution or may find infinitely many solutions. To avoid this issue, one solution is to add a constraint as in [24]. However, the proposed solution to avoid an infinite number of solutions is the reduction of controlled degrees of freedom of the leg. The control of the trochanter joint will be based on data from the inertial measurement unit (IMU), which senses the tilt of

the robot's body, and is controlled by the reactive layer. The tarsus joint will also be controlled by the reactive layer that will keep the joint parallel to the gravitational force. The resulting system has only three degrees of freedom. The inverse kinematics can then be solved using the following Equations (4.7)–(4.17), where x_t, y_t and z_t are the coordinates of tarsus joint, d_1 is trochanter offset (the distance between trochanter and femur joints), a_2 is femur length, a_3 is tibia length, L is the distance between coxa joint and tarsus joint, L_t is the distance between femur joint and tarsus joint and θ_0, θ_2 and θ_3 are the angles for coxa, femur and tibia joints [202]. The established coordinate system is shown in Figure 4.3.

First the distance L between the coxa joint C and the tarsus joint W must be determined. By considering the xz-plane of the tarsus joint, Pythagorean theorem can be used (Equation (4.7)).

$$L = \sqrt{x_t^2 + z_t^2} \tag{4.7}$$

Next, the distance L_t between the femur joint F and the tarsus joint W must be calculated. By considering the right triangle FWX, it is possible to use the Pythagorean theorem again. The distance between points W and X can be determined as the difference between L and d_1 and the distance between F and X corresponds to y_t (Equation (4.8)).

$$L_t = \sqrt{(L - d_1)^2 + y_t^2} \tag{4.8}$$

Before calculating the angles $\theta_0, \theta_2, \theta_3$, it is first necessary to determine the auxiliary angles α, β, γ. First the angle γ. Knowing the distances L_t, $|FX|$ and $|WX|$, the trigonometric functions can be used (Equation (4.9)).

$$\gamma = arccos\left(\frac{y_t}{L_t}\right) \tag{4.9}$$

The angle β can be determined using the Law of Cosines (Equation (4.10)). With appropriate modifications, Equation (4.11) can be derived.

$$c^2 = a^2 + b^2 - 2ab\,cos\gamma \tag{4.10}$$

$$\beta = arccos\left(\frac{a_2^2 + L_t^2 - a_3^2}{2a_2L_t}\right) \tag{4.11}$$

Using the Law of Sines (Equation (4.12)), the value of the angle α can be found (Equation (4.13)).

$$\frac{a}{sin\,\alpha} = \frac{b}{sin\,\beta} = \frac{c}{sin\,\gamma} \tag{4.12}$$

$$\alpha = arcsin\left(\frac{L_t sin\,\beta}{a_3}\right) \tag{4.13}$$

Alternatively, the α angle can be calculated without using the second trigonometric function using the Law of Cosines (Equation (4.14)).

$$\alpha = arccos\left(\frac{a_2^2 + a_3^2 - L_t^2}{2a_2a_3}\right) \tag{4.14}$$

Finally, the angles $\theta_0, \theta_2, \theta_3$ can be calculated using Equations (4.15)–(4.17). The method of their calculation is obvious from Figure 4.3. By considering the xz-plane of the tarsus joint, angle θ_0 can be calculated using trigonometric functions. The angle θ_2 can be determined as the difference of $\pi/2$ and the sum of the angles β and γ. Angle θ_3 is equal to the difference between π and α.

$$\theta_0 = arctan\left(\frac{z_t}{x_t}\right) \tag{4.15}$$

$$\theta_2 = \frac{\pi}{2} - (\beta + \gamma) \tag{4.16}$$

$$\theta_3 = \pi - \alpha \tag{4.17}$$

Equation (4.18) can be used to calculate the angle of the trochanter joint θ_1.

$$\theta_1 = \theta_{body\_pitch} \tag{4.18}$$

where θ_{body_pitch} is the pitch angle of the body of the robot acquired from IMU. The tarsus angle θ_4 can be determined using Equation (4.19) based on the angles θ_2 and θ_3 and the assumption that the tarsus will always be parallel to the gravitational acceleration, i.e. perpendicular to the flat surface.

$$\theta_4 = -\frac{\pi}{2} - \theta_2 - \theta_3 \tag{4.19}$$

4.2   WHexaR Controller Design

The controller, together with the hardware, is the most important part of the robot. It handles actuator operation, sensor control and higher robot functions such as navigation or task planning. A neural network will not be used to control the robot. The structure of the insect's nervous system is not sufficiently explored and the resulting controller could not copy its structure. Instead, reflexes and behaviors observed in insects will be mimicked. Since the control of a walking robot with a large number of joints is a non-trivial task, a hierarchical controller architecture can be chosen to allow the control to be divided into smaller parts, which can then be more easily implemented or replaced with a new version without affecting the other parts. However, the hierarchical control architecture is more suitable for static environments. In dynamic environments that change frequently, the planning phase causes the response to these environmental changes to be too slow [84].
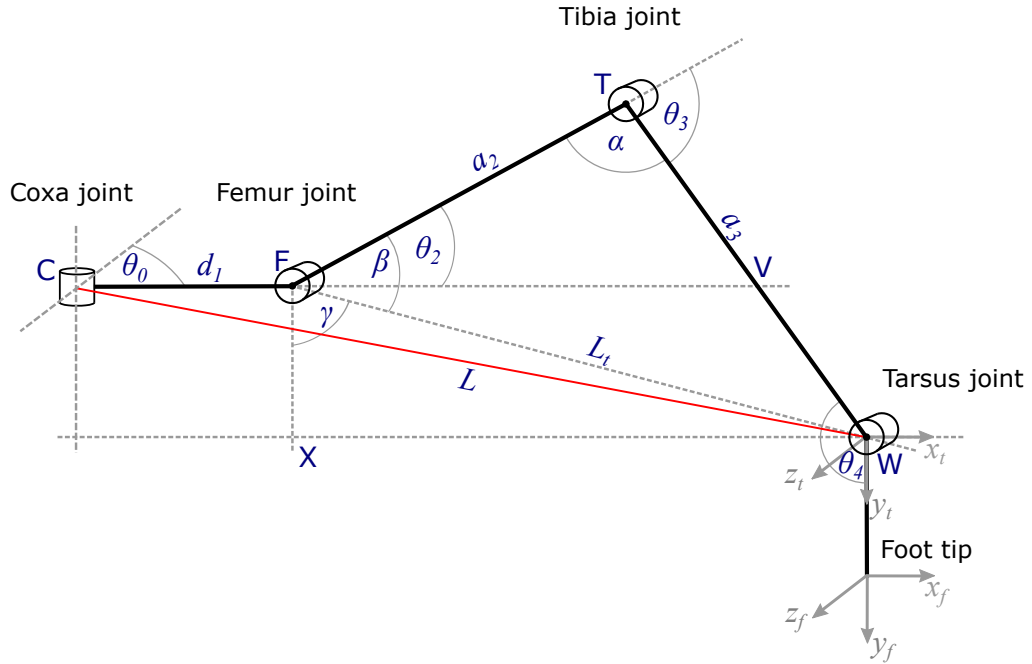
Figure 4.3: The leg coordinate system established for the purposes of inverse kinematic calculations. d_1 is trochanter offset, a_2 is femur length, a_3 is tibia length, L is the distance between coxa joint and tarsus joint, L_t is the distance between femur joint and tarsus joint, θ_0, θ_2 and θ_3 are the angles for coxa, femur and tibia joints, α, β and γ are angles used during inverse kinematic calculations and x_t, y_t and z_t are the tarsus joint coordinates. Both trochanter and tarsus joints are controlled by a reactive layer and are, thus, not included in the inverse kinematic calculations. The figure is inspired by [51].

A reactive control architecture could be used because it has a fast response to changes in a dynamic environment. However, this architecture lacks the possibility of any planning. For these reasons, a hybrid architecture that combines the fast response of a reactive architecture and the planning capability of a hierarchical architecture was chosen for the robot controller.

The proposed controller will consist of several parts. A scheme of the control system is shown in Figure 4.4. The first part of the controller is represented by a reactive layer which receives data from the sensors. This layer evaluates whether any of the reflexes have been activated based on the sensor data. If so, the reactive layer sends an instruction to the leg controller of the respective leg.

The sensor data is then sent to the terrain controller that analyses the data obtained from the sensors and evaluates the terrain characteristics. This information is then used by next block of the movement controller, the gait selector. Its task is to select the most appropriate gait considering the terrain. The next block of the movement controller is the leg coordinator, which synchronizes the movement of each leg by sending control signals to the leg controllers. Each leg has its own leg controller that manages all its joints following the commands from the leg coordinator.
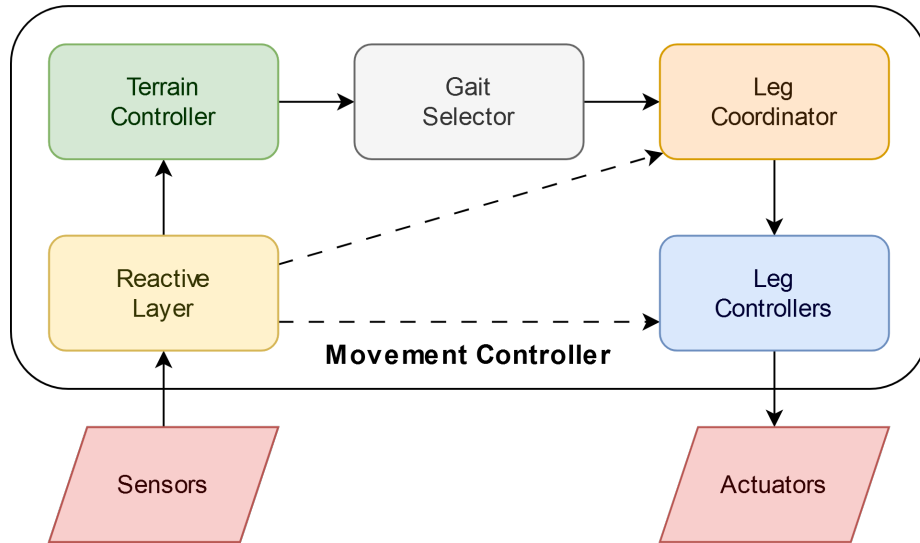
Figure 4.4: Scheme of the designed robot controller. The sensors provide data to the reactive layer, which can directly control the legs in the event of a threat. Data from the sensors are simultaneously sent to the input of the terrain controller, where they are analyzed and used by the gait selector to choose the most appropriate gait for the current terrain. The selected gait is then executed by the leg coordinator, which controls the leg controllers. Taken from [201] and modified.

4.2.1 Sensor Layer

The sensors are the only source of data for the robot about itself and its environment. The sensors of the robot will be designed largely as proprioceptive. Specifically, the robot will be equipped with force-sensitive resistors (FSR) and an inertial measurement unit (IMU). The sensor layer will also read data from all servomotors such as present position, current and temperature. The only exteroceptive sensors will be several rangefinders that will detect obstacles in front of the robot. Data obtained from sensors and servomotors will be passed to the reactive layer.

4.2.2 Reactive Layer

The reactive layer of the movement controller is used to react quickly to unexpected changes in the environment. These changes are detected by analyzing the data obtained from the sensors of the robot. These rapid responses are inspired by reflexes observed in insects. Based on the input, an immediate unconscious reaction is triggered. The reactive layer will implement several reflexes that will ensure stability and constant body support of the robot.

The first reflex will control the rotation of the whole leg at the trochanter joint based on data from the IMU. Leg rotation will occur mainly on sloping terrain and should reduce the required power of the servomotors. This will reduce the energy consumption of the robot and extend the battery life. Less stress on the servomotors will also extend their lifetime and reduce the risk of failure. Unlike conventional hexapods, which usually do not have a trochanter joint, the WHexaR should be able to move on much steeper terrain. This situation is outlined in Figure 4.5.
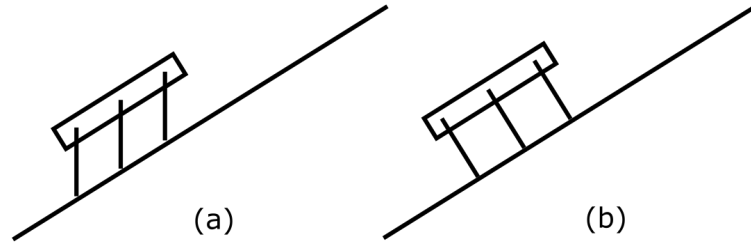
Figure 4.5: Difference between hexapod with (a) and without (b) trochanter joint. Hexapod with trochanter joint can rotate its legs so the foot tip is parallel to the gravity vector. This reduces power consumption, better supports the body and allows the robot to climb more difficult and inclined terrains. This extra joint can also be used to turn the legs when the robot falls on its back. Taken from [201].

The second reflex is the stepping reflex. It is used to increase the support of the body in case of leg slippage. This reflex is illustrated in Figure 4.6a.

The elevator reflex is another leg reflex that is activated when the leg hits an obstacle during the swing phase and cannot complete its movement. The elevator reflex causes the leg to attempt to repeat the movement, but the step height is increased. This reflex is illustrated in Figure 4.6b.

The searching reflex is used when the leg does not find support at the expected location. The leg begins to iteratively search the immediate area and attempts to find another foothold to support the body and finish the step. This reflex is illustrated in Figure 4.6c.

The robot should also be able to overcome various obstacles. Low obstacles can be stepped over or overcome by walking, where the leg movement will be stopped at the obstacle. Higher obstacles can be avoided or climbed over. Rangefinders are used to decide whether an obstacle can be climbed over or should be avoided. The robot stops in front of the obstacle and measures its height. If the obstacle is not too high, it starts climbing. Otherwise, it will have to avoid the obstacle.
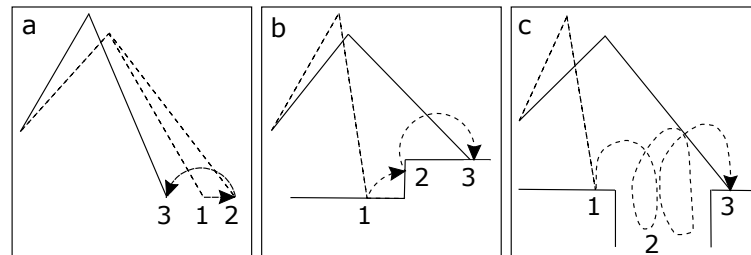
Figure 4.6: Reflexes implemented in the reactive layer of the robot controller. (a) Stepping reflex. The leg can step from the position (2) to the position (3) to better support the body. (b) Elevator reflex. If the leg encounters an obstacle (2), it tries to lift the leg higher to step over the obstacle and find new position for the foot tip (3). (c) Searching reflex. If the leg cannot reach ground at the expected location (2), it tries to find another foothold (3). Taken from [57, 201].

4.2.3 Terrain Controller

The terrain controller will analyze data from sensors, namely IMU, encoders, torque meters and thermometers of the servomotors, and rangefinders, and will evaluate the characteristics of the terrain in which the robot is currently moving. Based on the acquired terrain data, the gait selector will choose the most appropriate gait. The terrain controller will monitor the following metrics [201]:

- the height of the step – if a leg does not hit any obstacle on the ground while lifted only to specific threshold, the terrain is considered flat. Otherwise the terrain difficulty is increased.

- the tilt of the body – if the body reaches threshold tilt the terrain difficulty is increased. Different counters will be used for pitch and roll of the robot as it has different impact on the gaits.

- count of obstacles – increased number of obstacles in the environment indicates higher difficulty of the terrain. There are two kinds of obstacles. Either the robot can overcome the obstacle or the robot has to circumvent the obstacle. Only the first type of obstacles have impact on the terrain difficulty because the second type of obstacles is avoided by navigation of the robot and does not have effect on the gait selection. Conversely, the number of obstacles that can be overcome indicates difficult terrain leading to an increase in terrain difficulty to prevent the robot from falling.

- vibrations, bumps and impacts detected by the IMU – if the robot travels on wheels, the higher count of bumps means the robot is travelling through difficult terrain and the robot should change to some walking gait.

- count of disappeared leg support – when the robot often loses leg support, it indicates unstable or interchangeable terrain. Once a threshold is reached, the terrain difficulty is increased.

4.2.4 Gait Selector

The gait selector will use information from the terrain controller to select the most appropriate gait. The chosen gait is then passed to the leg coordinator which starts to execute it. The goal will be to select the fastest, most energy efficient and sufficiently stable gait for the given terrain conditions. The selection of the most suitable gait will be made on the basis of individual terrain characteristics and their thresholds. If the threshold value for at least one parameter is exceeded, the gait will be changed to a more stable one.

4.2.5 Leg Coordinator

Gaits consist of synchronized sequences of swing and stance phases of each leg. The resulting gait is shaped by the time intervals between leg movements. The task of the leg coordinator is to synchronize these movements so they form the gait selected by the gait selector. This will be accomplished by sending signals to the leg controllers. The sent signal will identify the command to start the swing phase of the leg with defined parameters.

The leg coordinator will control the speed of movement, the step height and the step length. These parameters will be passed to the leg controllers and will influence the resulting foot tip trajectory and robot locomotion speed.

4.2.6 Leg Controller

Each leg will have its own leg controller that will control it. It will receive information about the desired leg movement from the leg coordinator and will generate the desired leg trajectory. The leg coordinator specifies only basic step parameters such as its height or length. This information will need to be converted into a trajectory consisting of several points so that the leg movement is smooth and satisfies the specified parameters.

However, the leg consists of rotating servomotors where only the angle of rotation can be adjusted. It will therefore be necessary to convert the desired foot tip position to a set of individual servomotor angles. This problem can be solved using inverse kinematics, which task is to find such values of the angles of individual servomotors that the foot tip ends at the given coordinates.

Chapter 5

WHexaR Implementation

The construction of the robot and implementation of the controller followed the design described in Chapter 4. First, suitable actuators were selected to meet the required parameters. Then six legs were constructed according to the design and attached to the body of the robot. Next, the components of the robot control and power supply system were selected and suitable sensors were chosen. The communication with the selected servomotors and sensors was implemented. The resulting six-legged robot WHexaR (Wheeled Hexapod Robot) is able to travel by gait and wheels.

5.1 Leg Actuators Selection

The selection of suitable actuators depends on the desired characteristics of the robot, especially its size. If the resulting robot has to be able to carry a person and tens of kilograms of payload, it is appropriate to use hydraulic actuators, which are characterized by high load capacity. For large robots, the presence of additional equipment, such as a hydraulic pump or motor that drives it, is not an issue. For smaller robots, it is convenient to use electric actuators that are relatively light, easy to operate and have sufficient power. Due to the planned size of the robot, electric rotary actuators, specifically servomotors, were chosen. They will be positioned directly in the leg joints. The advantage of servomotors is that there is a clear relationship between the control electrical signal sent and the resulting horn position.

There are a number of servomotors on the market that vary in size, design, torque or price. Several criteria were investigated to find the most suitable servomotors.

5.1.1 Torque

One of the main parameters to watch when selecting a servomotor is its torque, i.e. with what force the servomotor is able to turn the horn. The torque of the selected servomotors must be sufficiently large to support the weight of the robot and potential payload. It should also have enough reserve so that the servomotors do not run at their limits.

The torque is often dependent on the input voltage of the servomotors, which can usually be in a certain range. Therefore, it is necessary to know what power supply will be used to power the robot and what voltage will be used to power the servomotors.

When moving, servomotors produce heat, which mostly reduces their torque. This results in a reduction in servomotor performance during continuous movement of the robot,

which also needs to be considered in the design. A detailed analysis of the calculation of the required actuator performance is described in [198].

5.1.2 Mechanical Construction

From the perspective of mechanical design, the size of the servomotors should be considered. It should correspond to the expected dimensions of the resulting leg and robot. The servomotor does not have to form only the leg joint itself. It may also form part of the relevant leg segment. The servomotor body itself should be adapted to the conditions in which the robot will be operated, such as dusty or humid environments, high or low temperatures, or the possible occurrence of fire or water.

Weight is also an important factor, especially if the servomotors are used directly in the leg joints. A heavy leg can affect the centre of gravity of the robot during movement and therefore its stability. The gearbox, which most servomotors are equipped with, is usually made of plastic or metal gears. Metal gears are of higher quality and can handle a greater load, but they are also heavier.

5.1.3 Control

Control in most servomotors is either by PWM signal or by more complex communication based on some protocol. In the case of PWM control, a $50\,\mathrm{Hz}$ signal is sent with a duty cycle ranging from $5\,\%$ to $10\,\%$, which corresponds to a $0°$ or $180°$ rotation of the servomotor. Most of these types of servomotors are hobby servomotors for models. They are usually not capable of a larger range of movements.

Protocol control of servomotors involves sending instructions to the servomotors typically via a bus to which all servomotors are connected simultaneously. In addition to setting the goal position of the servomotor, other parameters such as movement speed or acceleration can be set. Unlike hobby servomotors, information can be retrieved from protocol-controlled servomotors, e.g. about their position or current temperature. Thanks to the bus connection, motors can often be daisy-chained to a single cable, reducing the number of cables needed for communication, but their control is more complicated.

Besides the way of position control and possible data reading, it is also important to examine other parameters such as the resolution of the servomotor. Servomotor resolution refers to the smallest possible shift (step) that the servomotor is capable of. For example, if the resolution were $2°$, then with a segment length of $15\,\mathrm{cm}$ the end of the segment would be moved more than $0.5\,\mathrm{cm}$ and the movement would not be smooth.

Last but not least, we can focus on different motion modes of the servomotor such as wheel mode, in which the servomotor rotates infinitely and has no end points. Or the possibility to set endpoints so that incorrectly entered target position does not damage the servomotor or the robot.

5.1.4 Price and Availability

The price of servomotors and their availability can also be a decisive factor. In the event of failure or damage to a servomotor, it is good to be able to obtain a replacement easily and quickly. With custom manufactured servomotors, this may not be possible or there may be a long wait for a new part.

To simplify the robot design and servomotor control, it was decided that the selected servomotors must meet the following criteria:

- protocol-based control with the possibility of reading servomotor position and load

- possibility of bus connection

- sufficient torque

- resolution of at least 0.5°

- range of movement at least 270°

- wheel mode option

The Dynamixel MX servomotors [139] were selected based on the established criteria. They are controlled using TTL Half Duplex Asynchronous Serial bus, can be daisy chained, have sufficient torque and acceptable size and weight. The range of motion is 360°, their resolution is 0.088°, they can be limited in end positions and have a wheel mode. Besides the goal position, acceleration and other motion characteristics can be changed, and the present position, load or temperature of the servomotor can be read. Servomotors also have overheat, overvoltage, undervoltage or torque and speed limit functions. Another interesting feature is the ability to reverse the direction of rotation, thanks to which the servomotors can be controlled by the same signals on the left and right side of the robot.

Because each of the leg joints is stressed differently, and because the servomotors at the end of the leg should have rather lower weights in order to maintain stability during walking, three different servomotor sizes were chosen for different joints of the robot (see Table 5.1 for the parameters of the selected servomotors).

Table 5.1: Parameters of selected Dynamixel servomotors.

Parameter	MX-28	MX-64	MX-106
MCU	ARM CORTEX-M3		
Motor	Coreless(Maxon)		
Baud Rate [kbps]	$8-4500$		
Resolution [pulse/rev]	$4096\ (\sim 0.088°)$		
Input Voltage [V]	$10.0-14.8$		
Standby Current [A]	0.1		
Operating Temperature [°]	$-5-80$		
Range [°]	$0-360$		
Weight [g]	77	135	153
Width [mm]	35.6	40.2	40.2
Height [mm]	50.6	61.1	65.1
Depth [mm]	35.5	41	46
Stall Torque at 12 V [Nm]	2.5	6.0	8.4

Coxa, tibia and tarsus joints are driven by MX-64 servomotors. These joints are not subjected to as much stress and the middle size of the servomotor is sufficient. In contrast, the trochanter and femur joints are the most stressed joints. The trochanter rotates the

entire leg of the robot and its use will be especially in the terrain. The femur lifts the weight of the entire rest of the leg. Therefore, the largest servomotors in the series were chosen – MX-106. For the construction of the wheeled chassis, two MX-28 servomotors were chosen, which are relatively small and lightweight and therefore will not disturb the centre of gravity of the robot. Also, these servomotors are not loaded during the robot walk. The servomotor that turns the chassis is only loaded during its movement and not during body support. The servomotor that drives the wheel is loaded when it is moving or when the robot is standing on inclined terrain. All the selected servomotors have a metal front cover that reinforces the servomotor body structure and also serves as a heat sink.

5.2   Leg and Body Construction

First, the six legs of the robot were assembled. The legs differ only in the orientation of the coxa and trochanter servomotors. Those on the front and rear legs point towards the body so that they do not extend outwards from the body. The servomotors that form the leg joints are connected by aluminum brackets. These provide sufficient strength and are lightweight. M2.5 screws of various lengths and corresponding nuts were chosen to fasten the servomotors and brackets. The dimensions of the brackets determined the final size of the leg. When selecting the brackets, the aim was to mimic the structure and dimensions of an insect leg. The size of the coxa segment in insect is around 10 % and the trochanter is 2 - 8 % of the total leg length [61]. Femur and tibia are usually the same size or femur is longer than tibia. The tarsus in insects usually consists of 3 to 7 segments.

The size of the coxa of the resulting robot leg is approximately 13 % and the trochanter approximately 11 % of the length of the entire leg. The femur is the longest segment followed by the tibia segment. In the case of a robot leg, however, the tarsus will have only one part. The constructed leg has a length of 558 mm. The lengths of the segments and the ranges of each joint of the leg are shown in Table 5.2.

Table 5.2: Joint angle ranges and leg dimensions.

Part name	Joint angle ranges [°]	Dist. to the next joint/ground [mm]	Dynamixel servomotor	% of the total leg length
Body	-	74	-	-
Coxa	$\langle -135, 135 \rangle$	0	MX-64	13.26
Trochanter	$\langle -360, 360 \rangle$	63	MX-106	11.29
Femur	$\langle -120, 120 \rangle$	127	MX-106	22.76
Tibia	$\langle -150, 150 \rangle$	124	MX-64	22.22
Tarsus	$\langle -155, 170 \rangle$	95	MX-64	17.03
Direction	$\langle -360, 360 \rangle$	42	MX-28	7.53
Wheel	endless	33	MX-28	5.91

During the design of the leg structure, the option of interchanging the coxa and trochanter joints was considered. The servomotor rotating the leg (trochanter) would be first and the servomotor moving the leg forward and backward (coxa) would be second (see Figure 5.1). This option was eventually rejected because the weight of the coxa servomotor would rest on the trochanter joint. The current proposal assumes that the trochanter will only rotate

the servomotors further from the femur and thus be less loaded. Since in the trochanter joint, the rest of the leg is connected through only one point (the horn of the trochanter servomotor), it is important that this joint is stressed as little as possible.
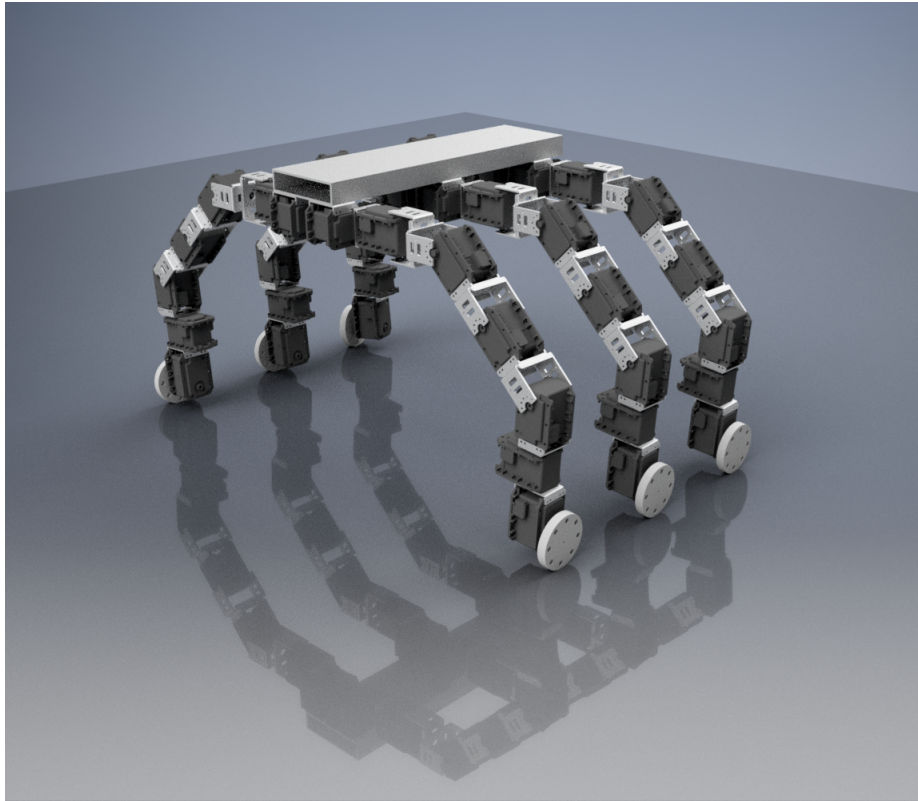
Figure 5.1: Early CAD robot design. This design was not implemented because the weight of the entire leg would rest on only one point, the horn of the first servomotor. On the other hand, this design has conveniently housed the first servomotor, inside the body of the robot, which would increase the overall stability.

The selected wheels, which the robot will use when moving on flat terrain, are large and soft in order to provide sufficient adhesion to the surface and prevent the legs from slipping, especially in sloping terrain. The larger wheel radius will also increase the maximum speed of the robot when driving. The chosen wheels were originally designed for racing car models. Their strong and lightweight construction together with rubber tyres ensure long durability and high grip. The wheels are shown in Figure 5.2.

The servomotors were interconnected by three-wire cables that provide power and communication. Each leg creates its own bus. These are then connected on the body of the robot to form one complex bus that will be connected to the control system. The connection of the leg buses is realized by a power hub. It provides the interconnection of the communication buses and is used to supply power from the power source. During the experiments, power was provided by an industrial power supply which was connected using a long $2.5\,\text{mm}^2$ copper cable.

The design of the robot body is based on the dimensions of the resulting leg. It is important to determine what working space will be available to each leg to avoid collisions when moving the legs. Alternatively, collisions can be prevented within the control system and the leg working spaces can be larger and overlapping. The distance of the legs on the

Figure 5.2: Wheels with rubber tyres. The inside of the rim is filled with foam reinforcement to strengthen the structure.[1], 21.7.2023.

robot body was set to 30 cm. This distance will give the legs sufficient working space for basic gaits. In order to increase this working space, the control system will prevent possible collisions. The total body length will therefore be approximately 60 cm. This size of the robot is sufficient to overcome obstacles in the real world.

The body is made of aluminium rectangular tube with dimensions $60 \times 10 \times 6$ cm. Inside the profile there is space for batteries, control units and other equipment. The D-H parameters obtained from the real robot leg are shown in Table 5.3. The resulting leg prototype and its dimensions are shown in Figure 5.3 and the robot is shown in Figure 5.4.

Table 5.3: Values of the Denavit-Hartenberg parameters of the leg.

Link	i	d_i [mm]	a_i [mm]	α_i [rad]	θ_i [rad]
coxa	0	0	0	$\pi/2$	θ_0
trochanter	1	65	0	$\pi/2$	$\theta_1 + \pi/2$
femur	2	0	127	0	θ_2
tibia	3	0	124	0	θ_3
tarsus	4	0	95	0	θ_4

5.3 Electronics System

The electrical control system consists of a Raspberry PI 4 model B mini computer, an ATmega2560 microcontroller on an ArduinoMega2560 development board and sensors such as inertial measurement unit (IMU), force-sensitive resistors (FSR) and rangefinders. These components were interconnected as follows. Raspberry Pi and ATmega2560 are connected

---

[1]Figure taken from https://eshop.reichard.cz/media/catalog/product/cache/1/image/9df78eab33525d08d6e5fb8d27136e95/5/0/500900551_00-2.jpg
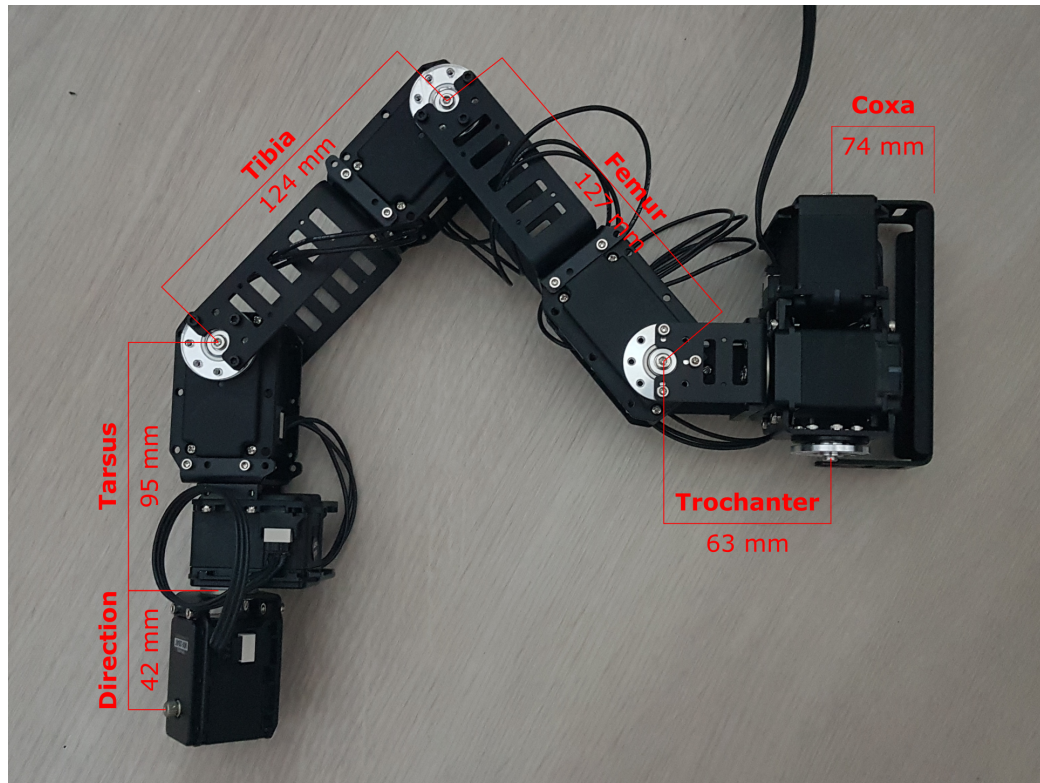
Figure 5.3: A prototype of the robot's leg. The coxa and trochanter joints are linked in a single bracket. The femur and tibia are the longest segments of the leg. The last two servomotors on the bottom left are used to turn and drive the wheel. The servomotors are connected by a three-wire cable that provides power and communication.

via serial link through USB port. The IMU is connected directly to the Raspberry Pi. The FSRs and the rangefinders are connected to the analogue pins of the ATmega2560. Servomotors and electronic components are powered from a central power source.

5.3.1 Power Supply

The power source will provide electrical power to the entire robot system. It will power the servomotors and the control electronics with sensors. Selected servomotors require a power supply in the range of 10 V to 14.8 V. The recommended voltage value is 12 V. As the voltage increases, the torque and current also increase. The dependence of torque on current and other dependencies are shown in Figure 5.5. For experiments in controlled conditions, the robot will be connected to a switching industrial power supply with a voltage of 12 V, which corresponds to the recommended servomotor voltage. This prevents voltage fluctuations caused by the gradual discharge of the batteries. Also, the lifetime of the batteries will not be reduced if they are not used.

When selecting batteries, in addition to the battery voltage, the capacity of the battery and the maximum current it can deliver must also be considered. A three-cell Li-Po battery with a nominal voltage of 11.1V was selected for the robot. This battery can reach a voltage of up to 12.6 V because the voltage value of one fully charged cell is up to 4.2 V. For these reasons, a four-cell Li-Po battery was not considered, although it has a nominal voltage
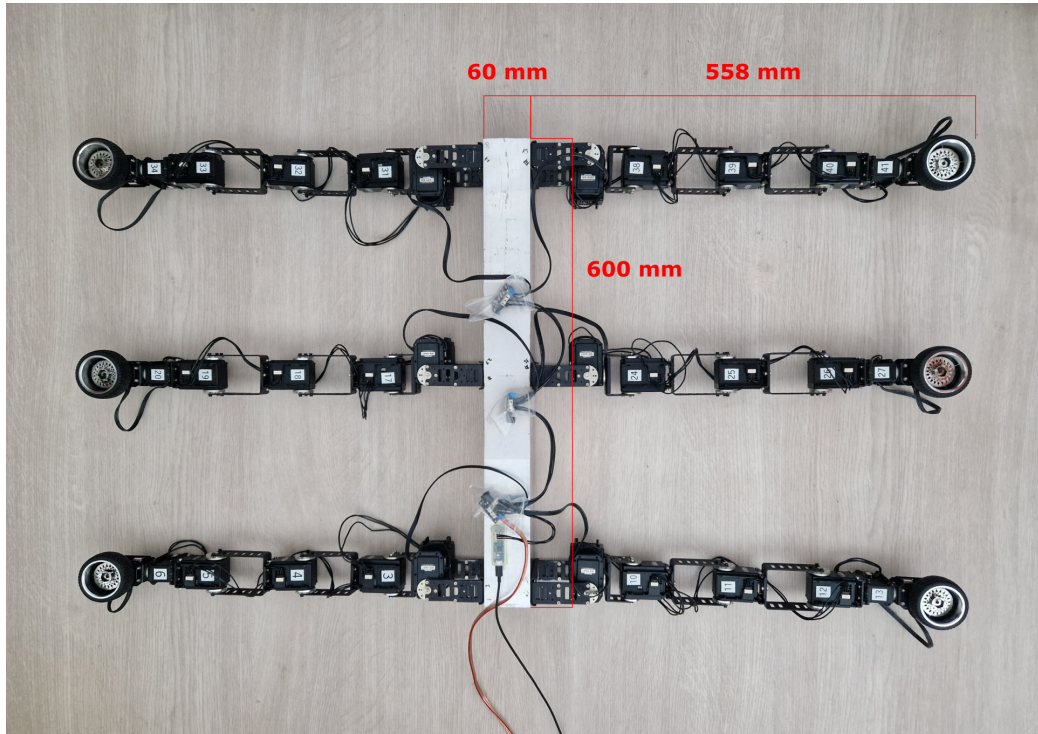
Figure 5.4: A prototype of the robot. It is 60 cm long, 117,6 cm wide and 10 cm high.

of 14.8 V, which is within tolerance for the selected servomotors. However, its voltage will reach up to 16.8 V when fully charged, which already exceeds the maximum voltage allowed for servomotors. Thus, it would be necessary to use an additional voltage regulator. The lowest voltage that a three-cell Li-Po battery can have is between 9.6 V and 9.9 V. Below this value there is already a risk of damage to the battery and such a situation should never occur. This voltage is slightly below the value of 10 V, which is specified as the minimum for proper operation of servomotors. The control system will therefore monitor the current battery voltage and interrupt the operation of the robot in time.

However, the computing systems that will drive the robot usually require 5 V. Therefore, it is necessary to use a voltage regulator to reduce the voltage of the power supply to the desired value of 5 V.

It is difficult to estimate the battery life of the robot in advance because the consumption of the servomotors during operation is unknown. From the documentation can only be obtained the current at stall torque, which is for MX-106 5.2 A, for MX-64 4.1 A and for MX-28 1.4 A at 12 V. Assuming that none of the motors are blocked in their movement, an average motor current of about 0.5 A can be expected. Considering that some servomotors are not loaded, their current will be close to the standby value, which is 0.1 A. When using the tripod gait, an average of 6 servomotors are moving simultaneously. With 36 servomotors in standby and 6 servomotors moving, the estimated current is 6.6 A. Electric power can be calculated using Equation (5.1) as the product of voltage and current.

$$P = UI \tag{5.1}$$

where P is electric power, U is voltage and I is current.
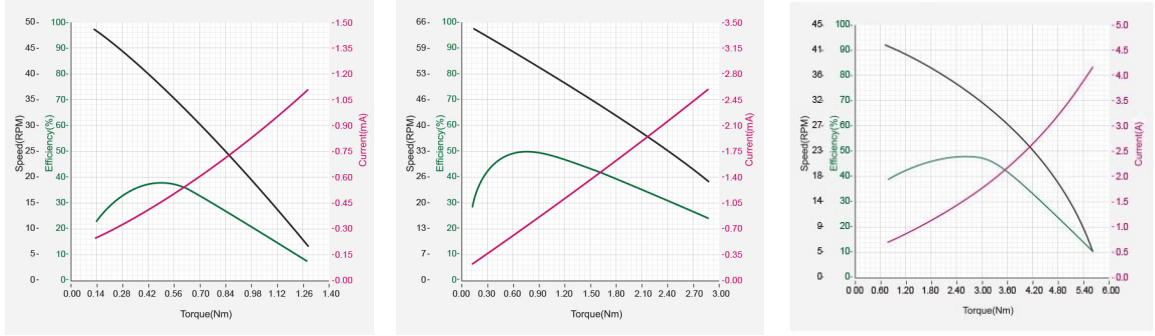
Figure 5.5: Dynamixel servomotors performance charts. From left, MX-28, MX-64 and MX106. The charts show the dependence of torque (x axis) on current (right y axes, red line), on speed (left y axes, black line) and on efficiency (left y axes, green line).[2]

This corresponds to approximately 80 W at 12 V. Furthermore, the power consumption of the control system and sensors must be considered. The estimated power consumption is about 5 W (1 A at 5 V). With a battery capacity of 6 Ah, voltage of 12 V and an instantaneous robot consumption of 85 W, the expected operating time t can be calculated using Equation (5.2).

$$t = \frac{CU}{P} \tag{5.2}$$

where C is electric capacity of battery, U is the battery voltage and P is the power consumed by the system. This can be simplified by substituting one equation into the other to obtain Equation (5.3).

$$t = \frac{C}{I} \tag{5.3}$$

The resulting operating time is about 50 minutes. This time can be extended by adding a second battery connected in parallel. Due to the increase in weight of the robot and the need for higher performance of the servomotors, the resulting operating time will be less than double.

5.3.2 Computing System and Sensors

Every robot needs a control system that commands its actuators and thus determines its movement and behavior in the environment. This usually consists of a computing system that runs the operating software of the robot and sensors that collect data both from the environment and about the robot itself. Choosing the right sensors is important because these are the only „senses" the robot will have. Various forms of rangefinders, such as lidars or sonars, are often used to detect obstacles in the environment. They use laser

---

[2]Figures taken from https://emanual.robotis.com/assets/images/dxl/mx/mx-28_ntgraph.jpg, https://emanual.robotis.com/assets/images/dxl/mx/mx-64_ntgraph.jpg, https://emanual.robotis.com/assets/images/dxl/mx/mx-106_ntgraph.jpg, 21.7.2023.

beams or sound waves reflected in the environment to determine the distance to obstacles. A map of the nearest environment in which the robot is moving can then be constructed. More advanced sensors such as cameras capture images of the surroundings. This is then processed by a computing system to identify obstacles or terrain complexity. Other sensors, for example, are capable of creating depth maps of the surrounding environment and can be used to detect the roughness of the terrain.

The sensors used must be considered when selecting the computing system. For simple lidars or sonars, a small development board with a single-chip processor such as Arduino is sufficient. For high-resolution camera data processing, a more powerful device such as an ODROID [123] or Raspberry Pi [138] mini computer is needed.

The communication with the selected servomotors can be implemented by several methods. Their communication is realized using a TTL Half Duplex Asynchronous Serial Bus, which is routed on a single wire. One wire allows communication in one direction only, i.e. it is not possible to send commands to servomotors and read values at the same time. However, since most processors support only the full duplex variant and therefore have two pins, where one sends data and the other simultaneously receives data, it is necessary to use additional hardware that allows the connection of these pins into one. It is possible to use e.g. integrated circuit 74LS241 [112], which allows switching RX and TX pins to the single wire bus. Another option is to emulate communication on any input/output pin of the processor. This approach is relatively difficult. Various converters can also be used. The variant with the 74LS241 integrated circuit was chosen to control the robot servomotors. The circuit will be connected to the ATmega2560 microcontroller [109] on the Arduino Mega 2560 [6] development board. The main control system will be on a Raspberry Pi 4 model B microcomputer [137]. This will be connected to the ATmega2560 microcontroller via a serial line. A scheme of the proposed electronic system is on Figure 5.6.

Raspberry Pi 4 model B is a single board computer with a size of 8.5×5.6 cm. It features a quad-core 64-bit processor, 4 GB RAM, gigabit Ethernet port, 2.4/5.0 GHz wireless LAN and four USB ports. It can also connect a speaker, microphone or camera. Its maximum power consumption is between 5 W and 6 W and approximately 0.6 W while idling. Its input power supply is 5 V. The Raspberry Pi will run a control script written in Python.

ATmega2560 is an 8-bit microcontroller equipped with 256 KB ISP flash memory, 8KB SRAM and 4KB EEPROM. The chip has 86 general purpose I/O lines, PWM, four USARTs and a 16-channel A/D converter. Its input power supply is 5 V.

The robot will be equipped with an inertial measurement unit (IMU) and several rangefinders. The IMU will be used to monitor the position of the body of the robot and to detect any bumps or shocks. The rangefinders will detect obstacles around the robot.

Load sensors in the form of force-sensitive resistors (FSR) will be built into the legs to detect ground. FSR can be replaced by switches that detect when a certain position is reached. The authors of [20] replaced the FSR with switches because of their longer lifetime. Unlike FSRs, switches provide only 1 or 0 values at the output (e.g., touching the ground, not touching the ground). FSRs, on the other hand, provide a continuous value about the leg load.

5.3.3 Force-Sensitive Resistors

Force-sensitive resistors will be built into the legs of the robot because the legs have wheels at their end and it is not possible to place these sensors in the foot tip. The most suitable
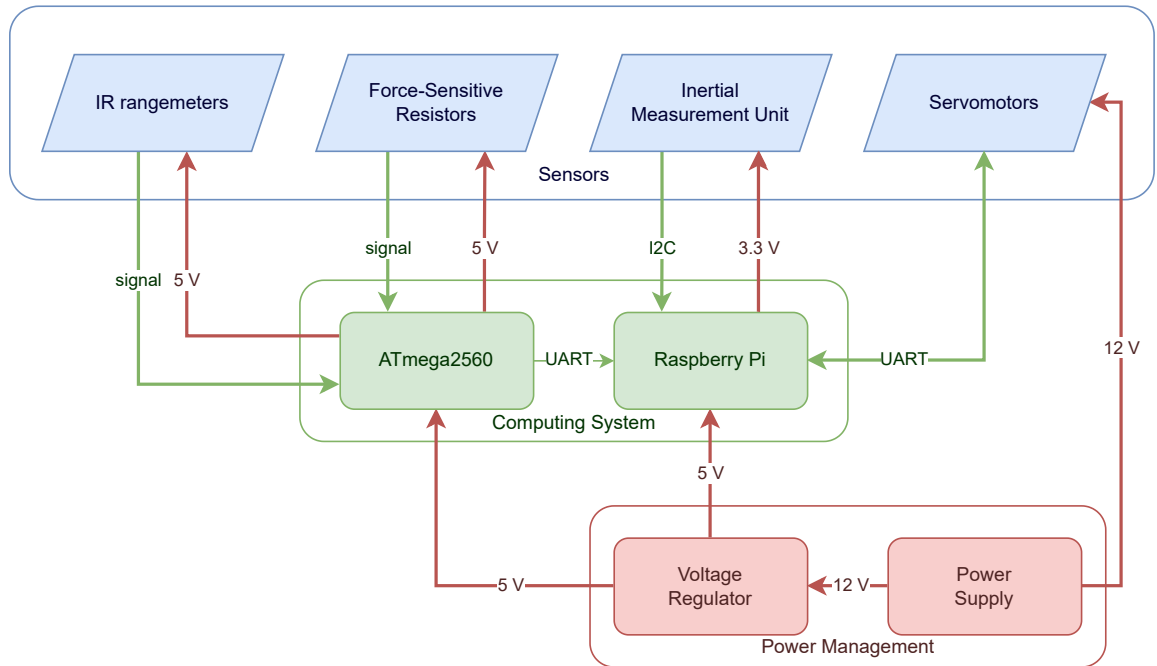
Figure 5.6: Scheme of the robot's electronic system. The core of the system consists of a microcomputer Raspberry Pi 4 model B and an microcontroller ATmega2560 on an Arduino development board. The Raspberry Pi communicates with the ATmega2560 and the servomotors using the UART buses. Furthermore, an inertial measurement unit is connected via an I2C interface. Force-sensitive resistors and infrared rangefinders are connected to A/D converter of the ATmega2560 microcontroller. The servomotors are powered directly from the power supply or battery. Computing units and sensors require a voltage of 5 V, which is created by a voltage regulator.

placement for the sensor is the tarsus segment, which will always be perpendicular to the surface. FSRs are available in different sizes. Larger sensors have a larger surface area and therefore better detection capability. However, large sensors cannot be built into the leg of the robot. It is therefore necessary to choose the largest possible size of FSR that can be placed in the leg.

At the same time, two wires will need to be run to each sensor so that data can be read from them. The FSR itself has no output signal. Its principle is the decrease of resistance with increasing load. The current resistance of the FSR can be converted to voltage using a voltage divider [186]. The voltage value can be read e.g. by an A/D converter, which is available on the ATmega2560 chip. The voltage divider is created by connecting one pin of the FSR to +5 V and the other to a $10\,\text{k}\Omega$ resistor, which is connected to ground, and to a pin of the microcontroller. The circuit scheme is shown in Figure 5.7.

A voltage divider is a circuit that gives part of the input voltage at the output depending on the ratio of resistors in the divider. Its principle is based on Ohm's law and can be written as Equation (5.4).

$$V_{out} = V_{in} \frac{R_2}{R_1 + R_2} \tag{5.4}$$

where V_{out} is the output voltage, V_{in} is the input voltage and R_1 and R_2 are the values of the resistances in the divider.
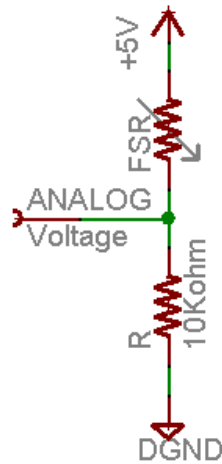
Figure 5.7: Force-sensitive resistor (FSR) circuit scheme. The FSR is connected as a voltage divider. The resulting voltage value is measured using an A/D converter on the ATmega2560.[3]

The force-sensitive resistor is located in the tarsus segment of the leg. It consists of three servomotors. The first one directly forms the tarsus joint, the second one is used to turn the wheel and the third one drives the wheel itself. The FSR cannot be placed on the wheel or in any of the servomotors. Therefore it will have to be placed in the servomotor linkage. Since the rotation servomotor is directly connected to the wheel servomotor, there is only one place where the FSR can be installed and that is on the bracket between the tarsus and the direction servomotor. The proposed location of the FSR is shown in Figure 5.8. The advantage of this placement is that the reactive layer ensures that the tarsus segment is always parallel to the gravitational acceleration and the FSR will be evenly loaded. To allow the FSR to bend, a spacer is inserted between the bracket of the rotation servomotor and the FSR.

The FSR itself consists of three layers [29]. The first, active layer, consists of a pattern of conductors that are connected to the input leads. The second layer is a non-conductive spacer that creates an air gap between the other two layers. The third layer consists of a flexible substrate which is covered with a thin conductive film at the active area. When an external force is applied to the sensor, the active layer flexes and comes into contact with the conductive film on the third layer. As the pressure increases, the amount of contact increases and the resistance of the sensor decreases. The structure of the FSR is shown in Figure 5.9.

If the leg is not loaded, pressure must not be applied to the FSR. For this reason, the bolts connecting the brackets will be tightened only partially to make space for the FSR. The leg load will bring these segments closer together and create a load on the FSR.

---

[3]Figure taken from `https://cdn-learn.adafruit.com/assets/assets/000/000/435/medium800/force___flex_fsrpulldownsch.gif?1447975571`, 23.7.2023.
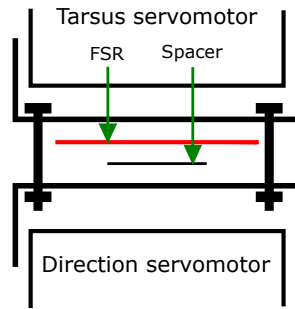
Figure 5.8: Placement of the force-sensitive resistor (FSR) in the leg. The FSR is located between the brackets of the tarsus servomotor and the direction servomotor. When the leg is loaded, a force is applied to the FSR and its resistance changes. This change is detected by the microcontroller and used to evaluate the leg load. To allow the FSR to bend, a spacer is inserted between the bracket and the FSR. Taken from [201] and modified.
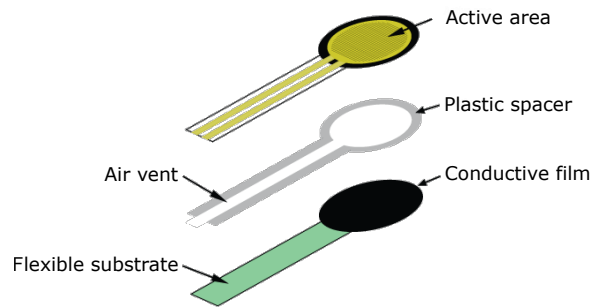
Figure 5.9: Force-sensitive resistor structure. The sensor consists of three layers. The first layer contains a pattern of conductors. The second layer serves as a separator. The third layer connects under pressure the conductive pattern of the first layer.[4]

5.3.4 Inertial Measurement Unit

An inertial measurement unit (IMU) is an electronic device that combines several separate sensors. An accelerometer is a sensor that is capable of measuring acceleration forces acting on an object [44]. Acceleration forces can be classified as static and dynamic. Static forces are forces that are unchanging, such as gravity. Dynamic forces are forces caused by motion. The second sensor that is usually included in the IMU is the gyroscope. This sensor is capable of measuring angular velocity. There can also be a magnetometer in the IMU that measures the magnetic field and can be used, for example, as a compass to measure the Earth's magnetic field. All these three sensors are usually able to measure in three different axes simultaneously. For the purpose of detecting the current orientation of the robot, the accelerometer would be sufficient. The remaining sensors could be used for other purposes.

The inertial measurement unit was chosen with respect to the presence of the mentioned sensors, but also with respect to the interfaces that the IMU has to make data reading simple. Therefore, an IMU LSM9DS1 [165] on a breakout board that has I2C and

---

[4]Figure taken from https://sensorwiki.org/_media/sensors/fsr_diagram.png, 23.7.2023.

SPI interface support was selected [1]. It is connected via I2C interface to Raspberry Pi. A python library is used to read the data.

5.3.5 Rangefinders

To measure the distance of the robot from obstacles, simple infrared rangefinders were chosen, which are able to detect an object up to 150 cm away. The main factor in choosing rangefinders was their size because they will be placed on the front legs of the robot. The output of these rangefinders is a voltage value corresponding to the measured distance. To function properly, the rangefinders must first be calibrated, which involves measuring the output voltage for several reference distances and creating a function of this dependence. Figure 5.10 shows the dependence of the measured distance on the output value from the A/D converter of the microcontroller. By interleaving the points with the trend line, a mathematical relationship was determined as Equation (5.5). The reference calibration distances and corresponding output voltages are shown in Table 5.4. The measured output value is the average of 500 values with a sampling rate of 4 Hz. A second meter – a tape measure – was used as a distance reference.
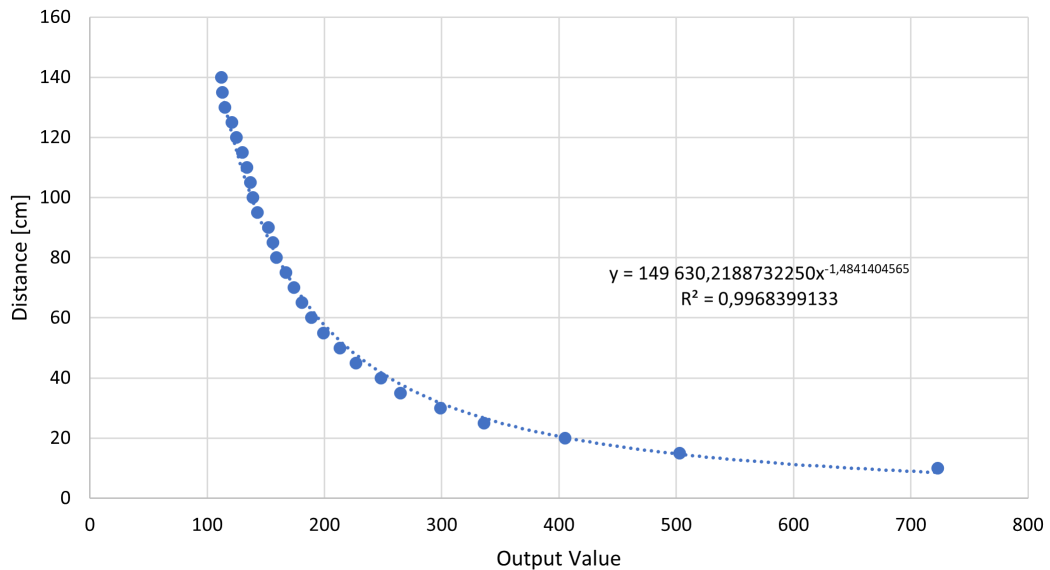
Figure 5.10: Calibration of IR rangefinders. The graph shows the dependence of the measured distance on the output value from the A/D converter of the microcontroller. By interleaving the points with the trend line, a mathematical relationship was determined.

$$y = 149,630.2188732250x^{-1.4841404565} \tag{5.5}$$

where y is the resulting distance in centimeters and x is the output value of the A/D converter.

Table 5.4: Reference distances and output A/D values for rangefinder calibration.

Distance [cm]	Output Value	Distance [cm]	Output Value
10	723	80	159
15	503	85	156
20	405	90	152
25	336	95	143
30	299	100	139
35	265	105	137
40	248	110	134
45	227	115	130
50	213	120	125
55	199	125	121
60	189	130	115
65	181	135	113
70	174	140	112
75	167		

5.3.6 Communication with Servomotors

Selected Dynamixel servomotors are controlled by TTL half duplex asynchronous serial bus, which is implemented over a single wire. In one moment, data can be read or written over the bus, but not both at the same time. However, the selected ATmega2560 microcontroller has only a standard serial interface, which has one RX pin for receiving and one TX pin for transmitting. To connect the servomotors to the controller, a 74LS241 integrated circuit was selected. This approach was tested but did not bring the expected results. Communication was unstable, with packets being lost or corrupted. The source of these issues could not be clearly identified. Most likely the issue was the large number of servomotors. When communicating with two servomotors, there were almost no errors. Therefore, an alternative option was chosen, specifically a USB converter U2D2 [145], which is connected on one side to the PC via a USB port and on the other side to the servomotor bus. This converter is connected to the Raspberry Pi.

Communication with the servomotors is achieved via the Dynamixel protocol. At the beginning of the project the Dynamixel Protocol 1.0 [140] was used because the Protocol 2.0 was not supported for the MX series servomotors. The servomotors are identified by a unique ID from the range $0 - 253$ (ID 254 can be used for broadcast). This unique ID corresponds to the unique number i introduced in Section 4.1.1. Communication is realized by sending Instruction packets to servomotors that respond with a Status packet (see Table 5.5 for the Instruction packet structure and Table 5.6 for the Status packet structure). Both packets start with a 2-byte Header with fixed 0xFF values. This is followed by the 1-byte number, which represents the servomotor ID. The packet also contains the Length, which indicates the Byte size of the Instruction, Parameter and Checksum field. Next is the identification of the Instruction and its Parameters. The last value is Checksum, which is calculated as binary complement of sum of ID, Length, Instruction, Parameter1, ..., Parameter N. The structure of the Status packet is similar, but instead of an Instruction

there is an Error describing the result. Besides the success status, the servomotor may report one of the following errors: instruction error, overload error, checksum error, range error, overheating error, angle limit error or input voltage error. The instructions that can be sent to the servomotors are listed in the documentation [144]. These include setting a new goal position, speed or reading the present current or position of the servomotors. Some instructions have length one byte, others two bytes.

Table 5.5: Instruction packet structure of Dynamixel protocol 1.0. The two-byte header is followed by the ID of target servomotor, length of the packet, instruction identifier, parameters and packet checksum.

Header1	Header2	Packet ID	Length	Instruction	Param 1	...	Param N	Checksum
0xFF	0xFF	Packet ID	Length	Instruction	Param 1	...	Param N	CHKSUM

Table 5.6: Status packet structure of Dynamixel protocol 1.0. The two-byte header is followed by the ID of servomotor that sent the response, length of the packet, result of the communication (success or error), response parameters and packet checksum.

Header1	Header2	Packet ID	Length	Error	Param 1	...	Param N	Checksum
0xFF	0xFF	Packet ID	Length	Error	Param 1	...	Param N	CHKSUM

The servomotors have ten different communication speeds ranging from 9600 bps to 2 Mbps. The experiments reported in [23] recommend setting the highest possible servomotor communication speed for maximum bus throughput. Therefore, the speed was set to the highest possible, i.e., 2 Mbps. Furthermore, the USB port latency has been adjusted to the lowest possible according to [143].

Because communication is only over one wire, it is not possible to transmit and receive at the same time. Therefore, the servomotors do not send any information unless explicitly prompted to do so by the appropriate command. In order to differentiate the communications and to give the converter time to switch from transmit mode to receive mode, there is a time delay called Return Delay Time between receiving the Instruction packet and sending the Status packet. The communication scheme is showed in Figure 5.11. To increase the bus throughput, the Return Delay Time parameter was set to 20 µs.
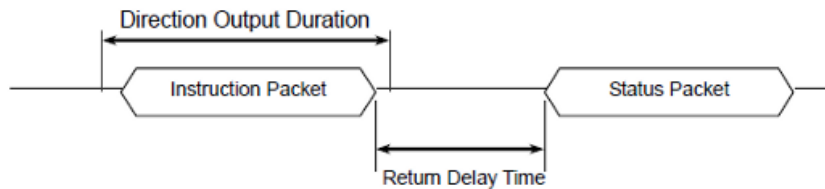
Figure 5.11: Dynamixel communication scheme. After the Instruction packet is received by the servomotor, a Status packet with the required values is sent. The time delay between receiving the Instruction packet and sending the Status packet is defined by the adjustable parameter Return Delay Time.[5]

The Dynamixel software development kit (SDK) [142] was used to communicate with the servomotors using the specified protocol. It supports many programming languages such as C, C++, C#, Java or Python. Functions for setting the position and speed of the servomotors were created using this Python SDK. Each servomotor was set to a default stance position. The resulting robot stance is shown in Figure 5.12.
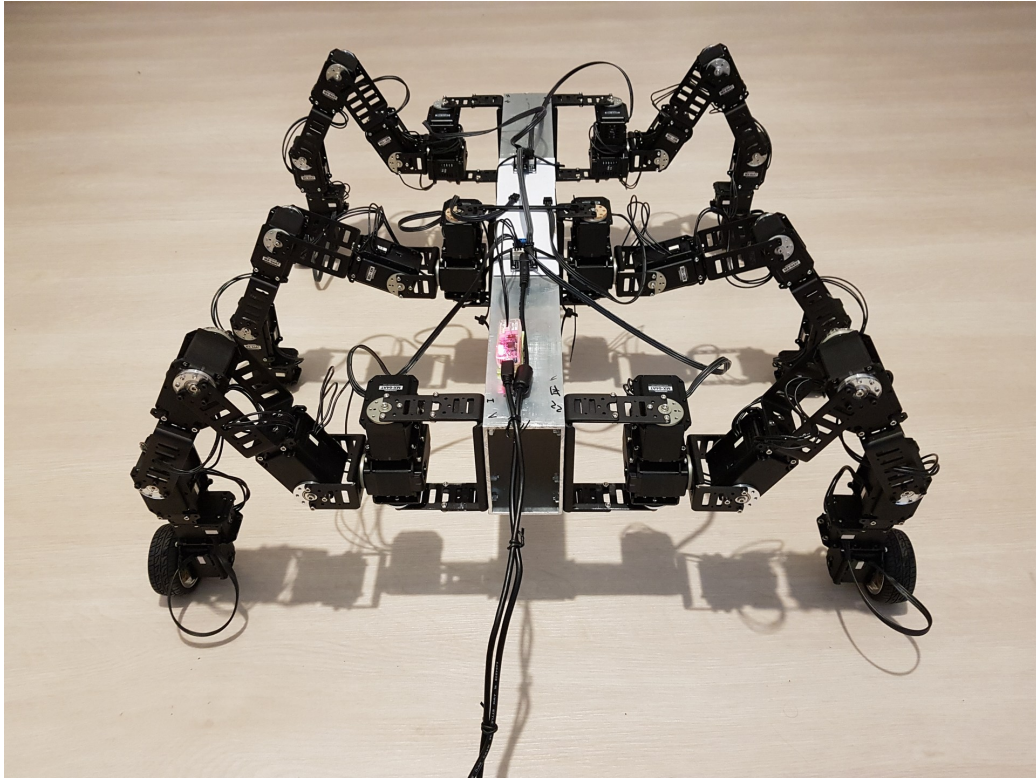
Figure 5.12: WHexaR in default stance.

During the development of the project it became possible to install the Dynamixel Protocol 2.0 [141] also in the MX series servomotors. Protocol 2.0 has better support for bulk control and reading data from servomotors. Therefore, the firmware in each servomotor was updated, which involved a complete disconnection of the buses, because only one servomotor can be connected to the controller during the update. Protocol 2.0 works similarly to its predecessor, but it has more features. Therefore, the structure of the Instruction and Status packets are different (see Table 5.7 for the Instruction packet structure and Table 5.8 for the Status packet structure). The biggest difference is in the number of bytes for each item. The header has four bytes (three with value and one reserved with zero value), the length and CRC now have two bytes instead of one.

Table 5.7: Instruction packet structure of Dynamixel protocol 2.0. The four-byte header is followed by the ID of the target servomotor, two-byte length of the packet, instruction identifier, parameters and two-byte packet checksum.

Header 1	Header 2	Header 3	Header Reserved	Packet ID	Length 1	Length 2	Instruction	Param	Param	Param	CRC 1	CRC 2
0xFF	0xFF	0xFD	0x00	ID	Len_L	Len_H	Instruction	**Param 1**	...	Param N	CRC_L	CRC_H

Table 5.8: Status packet structure of Dynamixel protocol 2.0. The four-byte header is followed by the ID of servomotor that sent the response, two-byte length of the packet, instruction identifier (in the case of Status Packet its always 0x55 – Status), result of the communication (success or error), response parameters and two-byte packet checksum.

Header 1	Header 2	Header 3	Header Reserved	Packet ID	Length 1	Length 2	Instruction	ERR	PARAM	PARAM	PARAM	CRC 1	CRC 2
0xFF	0xFF	0xFD	0x00	ID	Len_L	Len_H	Instruction	Error	Param 1	…	Param N	CRC_L	CRC_H

5.4 WHexaR Controller

The robot controller implementation reflects the proposed controller structure. The flow diagram of the controller is in Figure 5.13. The Python scripting language was chosen for the implementation. The controller layers are represented in the program by classes. The source codes can be found on the attached storage media.
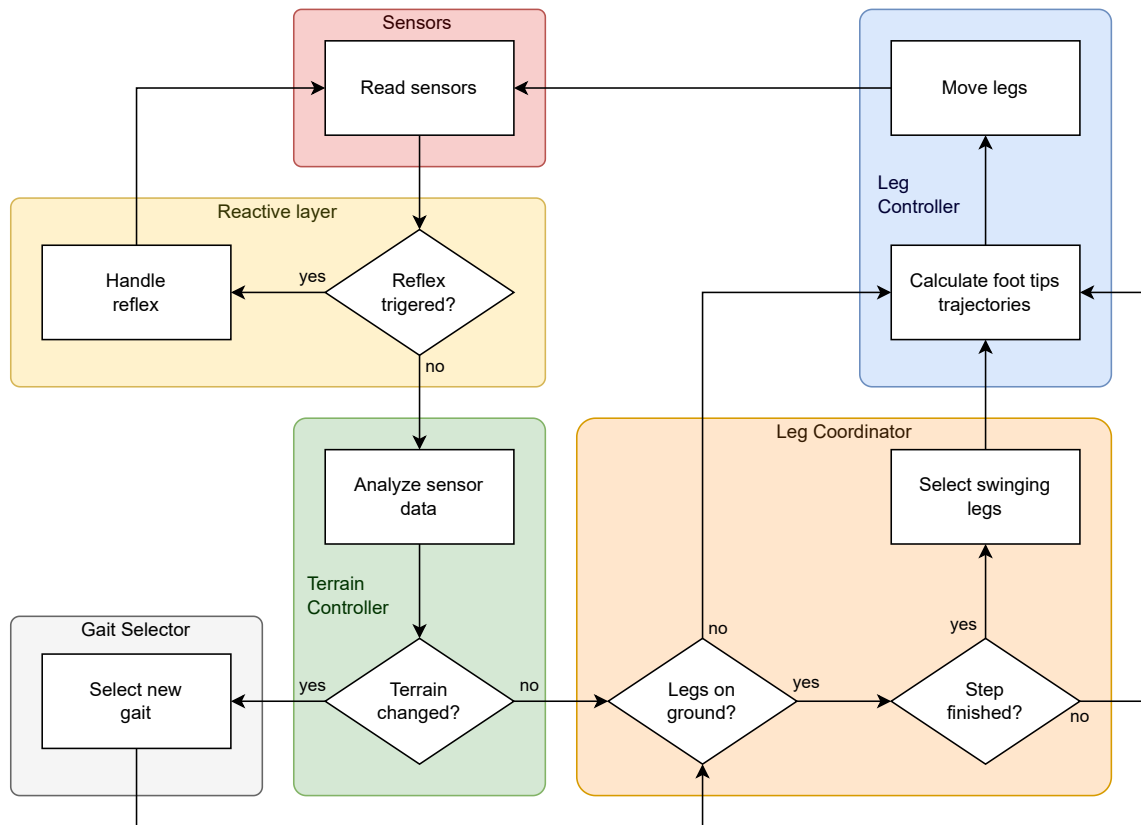
Figure 5.13: Controller flow diagram. Sensors provide data to the reactive layer, that can control leg movement directly in case of reflex activation. Sensor data is also sent to the terrain controller, where the data are transformed and used by the gait selector to determine the most appropriate gait for the current terrain. The chosen gait is executed by the leg coordinator, which controls the leg controllers.

Sensor Layer The `Sensors` class integrates the management of the sensors, their control and the reading of new values. The class has the `update()` method that refreshes all sensor values. This includes updating the accelerometer values from the inertial measurement unit (IMU) and calculating the current tilt angles, reading the present positions and currents from the servomotors, and parsing the incoming data from the ATmega2560 microcontroller, which periodically sends the values of the infrared rangefinders (IRR), force-sensitive resistors (FSR) and eventually from the IMU. The program for ATmega2560 is written in C++ programming language. The frequency of sending messages with sensor data is 20 Hz. A simple text protocol was implemented, where individual values are marked with a unique identifier and separated by the ; character. Each message is terminated with a # sign. The message sent by the protocol is as follows.

```
ir1=5;ir2=7;accx=0;accy=1;accz=2;fsr0=5;fsr1=7;fsr2=3;fsr3=2;fsr4=6;fsr5=8#
```

Values of IRR are read at 50 Hz, averaged and filtered for outliers. The relationship obtained during calibration is used to calculate the distance from the sensor output voltage (Equation (5.5)). The communication speed between Raspberry Pi and ATmega2560 over the serial line is 1 Mbps.

The I2C bus on the Raspberry Pi is used to read data from the IMU registers. A library was used to operate the I2C bus. The obtained values represent the accelerations in the x, y and z axes, which must be converted into tilts in each axis. The terms roll, pitch and yaw are used for these tilts and have their origins in avionics. Roll represents left and right roll about x axes, pitch represents up and down roll about y axes and yaw represents rotation about the vertical z axis (see Figure 5.14).

The tilts can be determined by trigonometric functions using Equation (5.6) for roll and Equation (5.7) for pitch. Yaw will not be used to control the robot.

$$\phi = arctan\left(\frac{acc_x}{acc_z}\right) \tag{5.6}$$

$$\theta = arctan\left(\frac{acc_y}{acc_z}\right) \tag{5.7}$$

where acc_x, acc_y, acc_z are the acceleration values in the x, y, z axes, respectively. These equations are implemented in the `updateAccelAngles()` method, which also converts the angles from radians to degrees.

The `updateServomotorsPositions()` and `updateServomotorsCurrents()` methods use synchronous communication and read in bulk the present position and current from all servomotors. The `readSerialSensors()` method is used to read and parse sensor data sent by the microcontroller over the serial line. The sensor layer also provides the possibility to create logs of the motion of the robot, which contain the present and goal position of the servomotors and their present current and velocity.
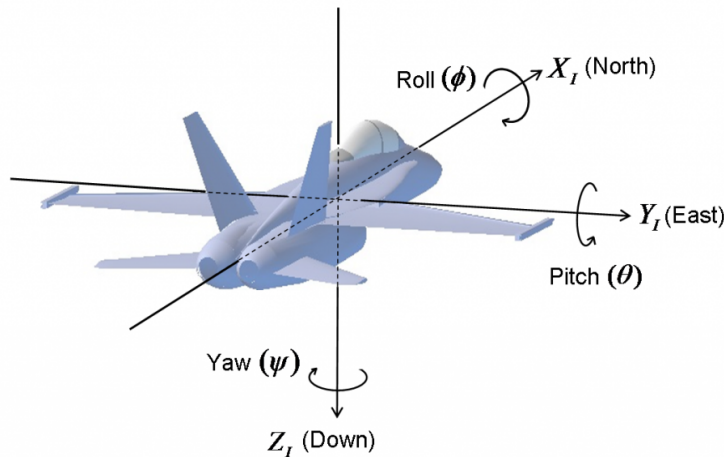
Figure 5.14: Roll, pitch and yaw. Roll represents tilt left and right, pitch represents tilt up and down and yaw represents rotation about vertical z axes.[6]

Reactive Layer The `ReactiveLayer` class forms the reactive layer of the controller. The methods define the behaviour of the different reflexes of the robot. The `checkReflexes()` method is used to check all reflexes (namely trochanter, tarsus, stepping, searching and elevator reflexes) simultaneously and is called from the main control loop of the program. The reactive layer also detects obstacles.

The trochanter reflex is activated when the body tilt detected by the IMU exceeds a threshold value. If this situation occurs, the leg rotation is adjusted using the trochanter joint.

Terrain Controller The `TerrainController` class represents the Terrain Controller block, whose task is to analyse the complexity of the terrain. In order to do this, it uses data from the sensory layer and information from leg controllers about leg movements. The step height changes when the elevator reflex is activated or can be set by the operator when the robot is activated. The body tilt is sensed by the IMU. Obstacles are detected using rangefinders. The number of disappeared leg supports is based on the number of activations of the searching reflex.

Gait Selector The `GaitSelector` class represents the Gait Selector block, which selects the most suitable gait based on the terrain information obtained from the Terrain Controller. It monitors step height, body inclination, number of obstacles, vibrations and disappeared foot supports. The proposed values of the thresholds of the these parameters are shown in Table 5.9. If any of the parameters exceeds the threshold value, it will change to a more stable gait. This approach requires ranking the gaits according to the degree of stability they provide to the robot during its movement and their expected ability to traverse complex terrain.

Riding on wheels is suitable mainly on flat, easy terrain, even though it has all six legs in contact with the ground at all times and therefore high stability. Unfortunately, the

---

[6]Figure taken from https://i.stack.imgur.com/ge9sN.png, 16.8.2023.

wheels are unlikely to be able to negotiate larger holes or rocks. The specific size of these obstacles that the robot will be able to overcome using only the wheels will have to be determined experimentally, but given the size of the selected wheels it will be in the order of centimetres. Anyway, riding on wheels should be the fastest and most energy-efficient locomotion the robot will be capable of.

Table 5.9: Proposed Gait Selector thresholds. The gaits are ordered according to stability of movement and usability in difficult terrain. For each gait, the threshold values of the parameter are given, which, if exceeded, will lead to a change to a more stable gait.

Move-ment	Max. step high [mm]	Body tilt [°]	Obstacles count	IMU bumps count	Disappeared supports count
Wheels	-	$\langle -7, 7 \rangle$	0	≤ 10	≤ 3
Tripod	100	$\langle -20, 20 \rangle$	> 0	> 10	≤ 3
Tetrapod	120	$\langle -25, 25 \rangle$	> 0	> 10	≤ 4
Ripple	220	$\langle -30, 30 \rangle$	> 0	> 10	≤ 5
Wave	350	$\langle -30, 30 \rangle$	> 0	> 10	≤ 5

Tripod gait is the fastest possible gait. Its disadvantage, however, is that the robot rests most of the time on only three legs. While this number satisfies the static stability conditions, the stability of a robot resting on three legs can easily be disturbed by the dynamics of its own motion or by external interference such as external forces or changes in the environment. The energy consumption of the tripod gait is also expected to be rather higher, because the entire body weight rests on only three legs and the servomotors have to exert more torque. Regardless of these features, the tripod gait is the most used gait for both insects and hexapods.

Tetrapod gait is a modification of tripod gait. Instead of three legs, the robot always rests on at least four legs and only two legs are in the swing phase. This increases the stability of the robot during movement, but also reduces its speed, because instead of two groups of legs there are three groups. Energetically, the tetrapod gait should be slightly less demanding compared to the tripod gait.

Wave gait is the most stable gait because there is always only one leg in the swing phase. This also results in its low speed, which is approximately three times lower than in the tripod gait. The energy consumption of the wave gait should be the lowest possible because the weight of the robot is distributed over the maximum possible number of legs. This gait is particularly suitable for rugged, difficult terrain.

Ripple gait is a modification of wave gait and in terms of stability, speed and energy consumption it is between wave and tetrapod gaits. There is no more than two legs in the swing phase. The second leg starts its swing phase when the first leg is in the middle of its swing phase. Its period is thus one half compared to the wave gait, which makes the ripple gait faster. The time the robot rests on only four legs is also half compared to the tetrapod, making the ripple gait a more stable gait.

In addition to these gaits, it would be possible to include a hybrid gait that combines the features of gaits and riding on wheels. However, its characteristics are far from clear and therefore it will not be part of the gait selector in the first version. This type of locomotion could use e.g. tripod gait combined with riding on wheels. This could theoretically achieve even higher movement speeds than using a gait or riding on wheels separately.

Based on the listed characteristics of each gait, a ranking of gaits from gaits suitable for flat terrain to gaits suitable for difficult terrain was made as follows: riding on wheels, tripod gait, tetrapod gait, ripple gait, wave gait.

Leg Coordinator The `Whexar` class represents the Leg Coordinator block. Its task is to synchronize the movement of the legs. The Leg Coordinator runs the main control loop of the program. There are also methods for initializing the robot. There are several methods for generating and managing gaits and riding on wheels. Different gaits are generated by sequences of movements of the legs. Movement by riding on wheels has several types. The first type is a straight drive, where the robot moves along a straight line. The second type is sideways movement, where the robot body stays in the original direction of movement, but moves sideways depending on the current rotation of the direction servomotors. The last two types of movement on wheels are rotation on the spot and riding along a circle. In both cases, the wheels are rotated towards the centre of rotation. The location of the centre of rotation and the direction of rotation of the wheels determine the resulting motion (see Figure 5.15).

(a)   (b)   (c)   (d)
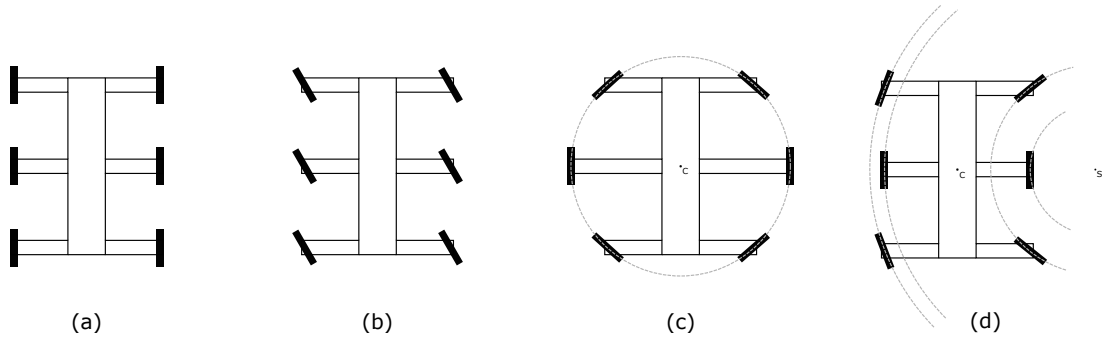
Figure 5.15: Movement types using wheels. (a) Straight movement. The wheels are not turned. (b) Movement sideways. The robot maintains its body direction and moves sideways. (c) Rotation on the spot. The wheels move in a circle and the robot rotates on the spot. (d) Turning. By turning the wheels properly, the robot can turn. The wheels move on concentric circles with different radii. The rotation speed of the wheels depends on the radius of the circle.

When rotating on the spot, the wheels must be rotated parallel to the tangents of the circle on which they move. To determine these angles, it is necessary to calculate the position of the wheels relative to the centre of rotation, which is the same as the centre of the robot body. The angle of rotation can then be determined using trigonometric functions. The situation is illustrated in Figure 5.16a. If the center of the robot, denoted by point C, is the origin of a coordinate system with coordinates $[0, 0, 0]$ and the end of the leg is at point P with leg coordinates $[x, y, z]$, then the position of the end of the leg P' relative to the center of the body C can be expressed using Equations (5.8) and (5.9).

$$P'_x = \frac{W_b}{2} + P_x \tag{5.8}$$

$$P'_z = \frac{L_b}{2} + P_z \tag{5.9}$$

78

where P' is the point of the end of the leg relative to the centre of the body C, W_b is the distance between the coxa joints of the front legs, L_b is the distance between the coxa joints of the front and middle legs, P_x and P_z are the coordinates of the end of the leg in the leg coordinate system. The angle α of the direction servomotor is then defined by Equation (5.10).

$$\alpha = arctan\left(\frac{P'_z}{P'_x}\right) \tag{5.10}$$

For wheels on middle legs, the angle α of the direction servomotors is 0. The rotation angle for the other direction servomotors can be obtained by adding $pi/2$, pi and $3pi/2$ to the α angle.

When rotating around a point that is off the axis of the body of the robot, the robot rides on concentric circles. In this case, the rotation angle needs to be expressed relative to the rotation point S. This situation is illustrated in Figure 5.16b. For the direction servomotors of the middle legs, the angle of rotation remains 0 assuming that the axis of the leg points to the point of rotation. For the remaining direction motors two cases can be distinguished. Servomotors on the far side relative to the rotation point S (in the Figure the left side of the robot) with rotation angle α_1 and on the near side relative to the rotation point S (in the Figure the right side of the robot) with rotation angle α_2. As in the case of rotation on the spot, it is necessary to express the positions of the ends of the legs relative to the centre of rotation S. These can be obtained using Equations (5.11)–(5.14).

$$P'_{1x} = R - \frac{W_b}{2} - P_1x \tag{5.11}$$

$$P'_{1z} = \frac{L_b}{2} + P_1z \tag{5.12}$$

$$P'_{2x} = R + \frac{W_b}{2} + P_2x \tag{5.13}$$

$$P'_{2z} = \frac{L_b}{2} + P_2z \tag{5.14}$$

where P'_1 and P'_2 are the points of the ends of the legs relative to the centre of rotation S, W_b is the distance between the coxa joints of the front legs, L_b is the distance between the coxa joints of the front and middle legs, $P_{x1}, P_{z1}, P_{x2}, P_{z2}$ are the coordinates of the ends of the legs in the leg coordinate system and R is the distance between the centre of the body C and the point of rotation S. The angles $\alpha 1$ and $\alpha 2$ can be expressed using Equations (5.15) and (5.16).

$$\alpha_1 = arctan\left(\frac{P'_{1z}}{P'_{1x}}\right) \tag{5.15}$$

$$\alpha_2 = arctan\left(\frac{P'_{2z}}{P'_{2x}}\right) \tag{5.16}$$

The rotation angle for the direction servomotors on the rear legs can be obtained as the inverse of α_1 and α_2, respectively. It can be seen that rotation on the spot is just a special case of rotation around a distant point where R is 0. Because the wheels move along different trajectories, they must rotate at different speeds. The angular velocity is defined by Equation (5.17).

$$\omega = \frac{\Delta\theta}{\Delta t} \tag{5.17}$$

For the speed v then applies Equation (5.18).

$$v = r\omega \tag{5.18}$$

where r is the turning radius. Since all wheels must move with the same angular velocity, their speed depends only on the distance r from the centre of rotation.
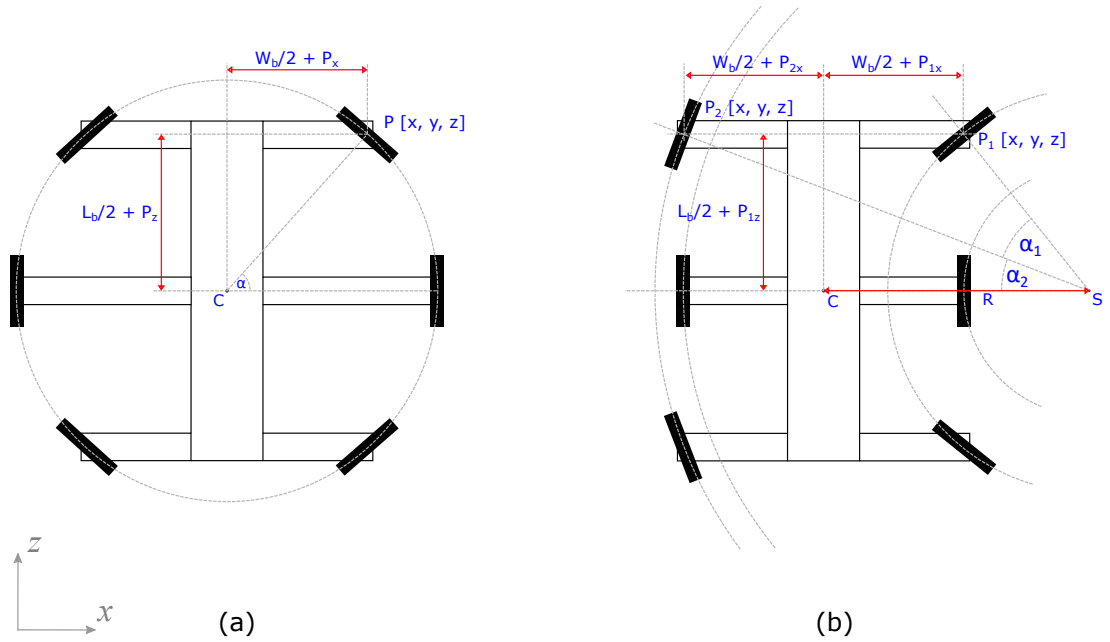
Figure 5.16: Turning using wheels. (a) Rotation on the spot. Direction servomotors are rotated by an angle α to the center of rotation, which lies in the center of the robot body C. W_b is the distance between the coxa joints of the front legs, L_b is the distance between the coxa joints of the front and middle legs, $P[x, y, z]$ are the coordinates of the end of the leg in the leg coordinate system. (b) Turning around a point off-center of the body of the robot. The wheels on the left side of the body are at a different angle to the wheels on the right side of the body. The rotation of the wheels is towards the point of rotation S.

Leg Controller   The `Leg` class represents the Leg Controller that integrates the control of all seven joints (servomotors) of one leg. Using various methods, it allows to change the properties of each joint, such as their speed, acceleration, PID controller settings, return delay time, goal position or torque on and off. The `calculateFK()` and `calculateIK()` methods calculate the forward and inverse kinematics of the leg, respectively. Other methods are used to activate the swing or stance phase and to perform the parts of the step of the leg. There are also methods for calculating the rotational effect of the force (torque) acting on the leg segments. These methods use the value of the present current in the servomotors and information about the length of the segments. The resulting torque is calculated using Equation (5.19).

$$F_i = \frac{I_i}{L_i sin(\alpha_{i+1})} \tag{5.19}$$

where F_i is the resulting torque acting on servomotor i, I_i is the current I flowing through servomotor i, L_i is the length of segment i to the next joint, and α_{i+1} is the present angle of the next servomotor. Torque can be used to detect leg contact with a surface or obstacle and can replace the FSR function.

Actuators   The `Dynamixel` class uses methods from the Dynamixel SDK to control the servomotor bus and to send Instruction packets.

Additional Classes   The `Robot` class represents the robot and all its legs and provides an interface to control all legs simultaneously. This is used e.g. when setting the stances or initializing the robot.

The `VRepHexapod` class provides an interface for communication with a simulated robot in the CoppeliaSim (formerly V-REP) simulation environment. The class contains the basic methods for connecting to the simulator API and handling objects in the simulation.

The `Base` class contains helper methods. The `objects` module contains helper classes especially for data storage.

The `LogPlotter` class can process logs generated by the robot control system and create graphs containing the present and goal position, velocity and current of each servomotor.

Chapter 6

Experiments

To verify the proposed robot design, a series of experiments were performed with both simulated and real robot. The simulated experiments were performed in the simulation environment V-REP (now Coppelia Sim). The robot was controlled by the proposed controller and its actions were transmitted using an API to the simulated environment. Experiments with a real robot used artificial obstacles. The robot was connected to a power supply during the experiments to prevent the results of the experiments from being affected by the fading battery. The robot controller was run on a desktop computer.

The proposed experiments aimed to verify the functionality of individual parts of the robot such as sensors or servomotor control, but also the functionality of the robot as a whole and its ability to navigate in rough terrain. The last part of the experiments is focused on the energy consumption of the robot.

6.1 Servomotors, Sensors and Computing Units

Several experiments were designed to verify the correct functioning of the servomotors and sensors. In the case of servomotors, the maximum frequency of reading and writing was investigated. For the sensors, the output values were examined and compared with other meters.

6.1.1 Servomotor Control

Experiments focused on servomotors were aimed at finding the most appropriate servomotor communication setup to obtain data from servomotors as often as possible. The search for suitable parameters was based mainly on [23]. The authors concluded that it is desirable to use the highest baud rate provided by the servomotors and to use the sync functions for reading and writing. The servomotors were therefore set to a baud rate of $3\,\mathrm{Mbps}$.

When the power was turned on, the bus experienced a large number of errors and the servomotors could neither be found nor controlled. After lowering the baud rate to $2\,\mathrm{Mbps}$, it was possible to find the servomotors, but there were a number of dropouts in the responses during synchronous reads. Only after setting the baud rate to $1\,\mathrm{Mbps}$ communication without errors was achieved.

The following two types of experiments investigated the maximum possible frequency of reading and writing of servomotor values. The sync read and sync write functions of the Dynamixel protocol were used in these experiments. These functions allow reading and writing different values to the same registers of several servomotors. Unlike bulk functions,

which allow different values to be written to different registers of several servomotors, sync functions have a smaller instruction packet length, which results in a lower load on the communication bus and therefore a higher frequency of reads and writes.

Maximum Reading Frequency

In this experiment, current temperature, position and current data were read from the servomotors and the frequency of data reading was measured. The goal was to determine how many times per second data could be retrieved from the servomotors. In the first part of the experiment the temperature value was read, in the second the position value was read and in the third the position value and the current.

Each measurement was performed for 5 seconds, when the servomotors were cyclically queried for data using sync read functions. Ten of these measurements were taken and the resulting values were averaged. The results of the experiments are shown in Table 6.1.

When reading only servomotor temperature value from all 42 servomotors, the average measured reading frequency was 118.18 Hz with a variance of 0.6. The result shows that the communication was stable as the frequency does not change much throughout the experiment.

Reading only value of servomotor present position from all 42 servomotors, the average measured reading frequency was 100.2 Hz with a variance of 0. It can be seen that the communication was very stable as the frequency does not change throughout the experiment.

When reading two values (servomotor present position and current) from all 42 servomotors, the average measured reading frequency was 52.8 Hz with a variance of 0. Again, the communication was stable. Interestingly, the frequency is not half as expected, but slightly higher. This is due to the length of the data being transmitted. While the present servomotor position is 4 bytes long, the present servomotor current is 2 bytes long and the present temperature is only 1 byte long. In order to verify the correct measurement of the present position and current of the servomotor, the frequency of the servomotor current reading was measured separately.

When reading only one present current value from all 42 servomotors, the average measured reading frequency was 111.2 Hz with a variance of 0. Again, the communication was very stable. The measured data confirms the previously measured frequency of reading position and current of the servomotor of 52.8 Hz.

Table 6.1: Tested servomotor registers during reading experiments.

#	Register Name(s)	Reg. Size [B]	Frequency [Hz]	Variance
1	Present Temperature	1	118.18	0.6
2	Present Current	2	111.20	0.0
3	Present Position	4	100.20	0.0
4	Present Position, Present Current	4+2	52.80	0.0

It is therefore not possible to clearly determine the maximum frequency of reading values from the servomotors because it depends on the length of the registers being read. However, the frequency of reading a single value from all servomotors exceeds 100Hz in both cases, which is more than sufficient for robot control purposes. If multiple values need to be read simultaneously, it is necessary to consider how often the present value is actually needed

and whether it is necessary to know it for all servomotors. Similar values were achieved on the Raspberry Pi in all experiments.

Maximum Writing Frequency

In this experiment, the value of the goal position was written to all servomotors and the frequency of writing was measured. The goal was to determine how often a new goal position could be sent to all servomotors. It should be noted that the servomotors were not active during this experiment, i.e., they did not perform any movement to avoid damage due to frequent writing of the desired position change.

Each measurement was performed for 5 seconds, when a new goal position was sent to the servomotors using sync write functions. Ten of these measurements were taken and the resulting values were averaged. The results of the experiments are shown in Table 6.2.

When writing a new goal position to all 42 servomotors, a writing frequency of 446.6 Hz with a variance of 0 was achieved. It can be seen that the communication was very stable even during writing as the frequency does not change throughout the experiment. The measured frequency is relatively high. It is because only one packet is sent to the servomotors during the writing of the new goal position. In the case of reading, each servomotor responds individually.

During the experiment, the same value of the servomotor goal position was sent over and over again. The frequency remains the same even if the value of the servomotor target position is changed between write cycles.

The size of the servomotor goal position register is 4 bytes. In contrast, the servomotor goal current register has a size of 2 bytes. The achieved frequency of writing to this register was 714.6 Hz with a variance of 0. Writing in a register of size 1 byte has not been tested because it is usually not used. Registers with a size of 1 byte are mainly used to initialize servomotors and are not useful for servomotor control.

As in the case of reading data from servomotors, the frequency of writing depends on the length of a particular register. The maximum observed write frequency is several times greater than the read frequency. For robot control purposes, this frequency is sufficient. Similar values were achieved on the Raspberry Pi in all experiments.

Table 6.2: Tested servomotor registers during writing experiments.

#	Register Name(s)	Reg. Size [B]	Frequency [Hz]	Variance
1	Goal Position	4	446.6	0.0
2	Goal Current	2	714.6	0.0

6.1.2 IR Rangefinders

In order to verify the accuracy of the output values, an experiment was designed to compare the IR rangefinder output values with a second meter – tape measure. Ten distances were measured. The measured distances and the results of the experiment are shown in Table 6.3. One measurement consisted of averaging the rangefinder output values. The output values were sampled at a frequency of 50 Hz for 5 seconds.

Table 6.3: Tested distances and rangefinder output values.

#	Distance [mm]	Average Measured Value [mm]	Variance [mm]	Error [mm]
1	50	53.9	0.00	-3.9
2	100	84.7	0.01	15.3
3	150	137.7	0.03	12.3
4	200	193.0	0.06	7.0
5	250	245.5	0.26	5.5
6	300	302.9	0.25	-2.9
7	500	504.2	2.74	-4.2
8	750	762.6	19.92	-12.6
9	1,000	998.7	27.65	1.3
10	1,250	1,257.4	27.46	-7.4

The measured values show that infrared rangefinders have a relatively high measurement error. Especially at longer distances, the variance of the measured values increases significantly. The influence of these deviations can be mitigated by suitable filtering of the output values. More accurate values could be achieved by calibrating with a smaller step. The sensors will be sufficient for basic orientation of the robot in the environment. However, more reliable rangefinders would be needed to create a map of the surrounding environment.

6.1.3 Inertial Measurement Unit

In an experiment with an inertial measurement unit (IMU), the accelerometer output was tested. The dependence of the IMU roll about x axis on the output value and the calculated roll angle was investigated. The tilt of the IMU was verified using an external meter. Individual measurements were taken in 10° increments ranging from -90° to +90°. Table 6.4 shows the individual measurements and the results obtained.

The measured values show that the accuracy of the accelerometer is relatively high and sufficient for the purpose of measuring body tilt. The cause of the deviation from the expected gravitational acceleration of the earth of 9.81 is explained by imperfect calibration of the accelerometer, however, the resulting values are not significantly affected.

6.1.4 Raspberry Pi

To verify the performance of the selected Raspberry Pi 4 model B computing device, an experiment was designed to investigate at what frequency the computing system is able to execute the main control loop of the program. This involves reading new values from all sensors and servomotors, writing new goal positions to the servomotors and evaluating the movement controller tasks. During the experiment, new goal positions were written to servomotors that were inactive to prevent damage to them.

The measured frequency of the main loop of the program was 48 Hz, which is relatively low. However, this value was expected given the results of previous experiments where only servo motors were communicating. Based on these experiments, the method of data collection from the servomotors was modified so that only the necessary values are read. The

present position for the wheel and trochanter joint servomotors is not needed for normal control. The values can be obtained by a special command if necessary. The present position of the direction servomotor is also not needed when walking. After applying these adjustments, the frequency increased to 80 Hz.

Table 6.4: Tested angles and output values of inertial measurement unit.

#	Angle [°]	X [m/s²]	Y [m/s²]	Z [m/s²]	Calculated Angle [°]
1	-90	-0.06	-10.00	0.08	-90.45
2	-80	-0.09	-9.81	1.72	-80.04
3	-70	-0.25	-9.30	3.36	-70.13
4	-60	-0.53	-8.51	4.88	-60.17
5	-50	-0.39	-7.48	6.25	-50.10
6	-40	0.30	-6.23	7.40	-40.13
7	-30	-0.38	-4.82	8.32	-30.06
8	-20	-0.25	-3.27	8.98	-20.00
9	-10	0.34	-1.66	9.35	-10.05
10	0	0.00	0.00	9.79	0.00
11	10	-0.10	1.66	9.31	10.08
12	20	-0.30	3.23	8.87	20.05
13	30	0.16	4.76	8.16	30.26
14	40	-0.42	6.09	7.24	40.07
15	50	-0.55	7.23	6.03	50.14
16	60	-0.21	8.29	4.80	59.96
17	70	-0.32	9.01	3.28	70.02
18	80	-0.29	9.49	1.67	80.03
19	90	-0.28	9.66	-0.01	90.09

6.1.5 ATmega2560

A similar experiment as for the Raspberry Pi was also designed for the ATmega2560 micro-controller, in which the frequency of the main program control loop was monitored. In the case of the microcontroller, however, the situation is different. The microcontroller operates rangefinders that emit infrared rays into the environment. These bounce off obstacles and return to the sensor detector, where the distance is evaluated and converted to an output signal. These rays are constantly emitted into the environment and the sensor output value changes continuously. Thus, although it is theoretically possible to read distances at high frequency, this is not desirable. The microcontroller is not able to send such a large amount of data over the serial line. Furthermore, processing this data would put an unnecessary load on the Raspberry Pi. Therefore, the sampling interval of the sensor outputs was chosen to be 50 Hz. The frequency of sending data to the Raspberry Pi was then set to 10 Hz due to the low speed of the movement of the robot. These read and send frequencies were then tested. Communication and measurements were performed without issues. Force-sensitive resistors behave in a similar way as rangefinders. The read and send frequency values were set in the same way as for rangefinders.

6.2 Forward and Inverse Kinematics Experiments

To verify the correctness of the proposed forward (FK) and inverse kinematics (IK) and their correct implementation, an experiment was designed in which the leg was moved to a given coordinate and it was verified whether the leg arrived at the target location with sufficient accuracy. Next, the angles calculated by IK were used to calculate the position of the tarsus servomotor using FK. The result was compared with the coordinates at which the foot moved. Only one leg was tested because all legs are the same design and the results would be identical. Several test points were selected. Their list and the resulting values of forward and inverse kinematics are shown in Table 6.5.

The results show that the design and implementation of FK and IK are correct. During the experiment, it was found that the servomotors are not able to achieve the exact angle set for them. Thus, there is a deviation within millimeters when calculating the FK from the angles obtained from the present positions of the servomotors.

Table 6.5: Coordinates of tested points, angles calculated by inverse kinematics and coordinates of points calculated by forward kinematics from angles of inverse kinematics.

#	Goal Coordinates [x, y, z]	Coxa [°]	Femur [°]	Tibia [°]	Tarsus [°]	FK Coordinates [x, y, z]
1	[190, 120, 0]	0.00	1.80	-92.69	0.90	[190, 120, 0]
2	[190, 160, 100]	27.76	-18.09	-58.39	-13.52	[190, 160, 100]
3	[190, 80, -100]	-27.76	18.59	-94.90	-13.68	[190, 80, -100]
4	[150, 120, 0]	0.00	-1.50	-108.28	19.78	[150, 120, 0]
5	[240, 120, 0]	0.00	-2.58	-64.58	-22.84	[240, 120, 0]

6.3 Stances

In these experiments, different stances that the robot is able to achieve were tested. In different stances, the resulting dimensions of the robot varied, allowing it to overcome obstacles of different shapes and sizes. The different stances are shown in Figure 6.1. During the experiments it was found that the reflex that controls the position of the tarsus joint to always point parallel to the gravitational acceleration is not fast enough, because it reacts only to the present position of the other servomotors and therefore there is a delay in movement caused by reading the present positions of the other servomotors and activating the tarsus servomotor. Therefore, the control of the tarsus joint was moved to the inverse kinematics calculation, where the new position of the tarsus servomotor is calculated based on the calculated values of the other servomotors. The tarsus reflex is implemented in the reactive layer but is turned off. Some stances are affected by dead zones of servo motors. This effect is amplified by the relatively long length of the femur, tibia and tarsus segments.
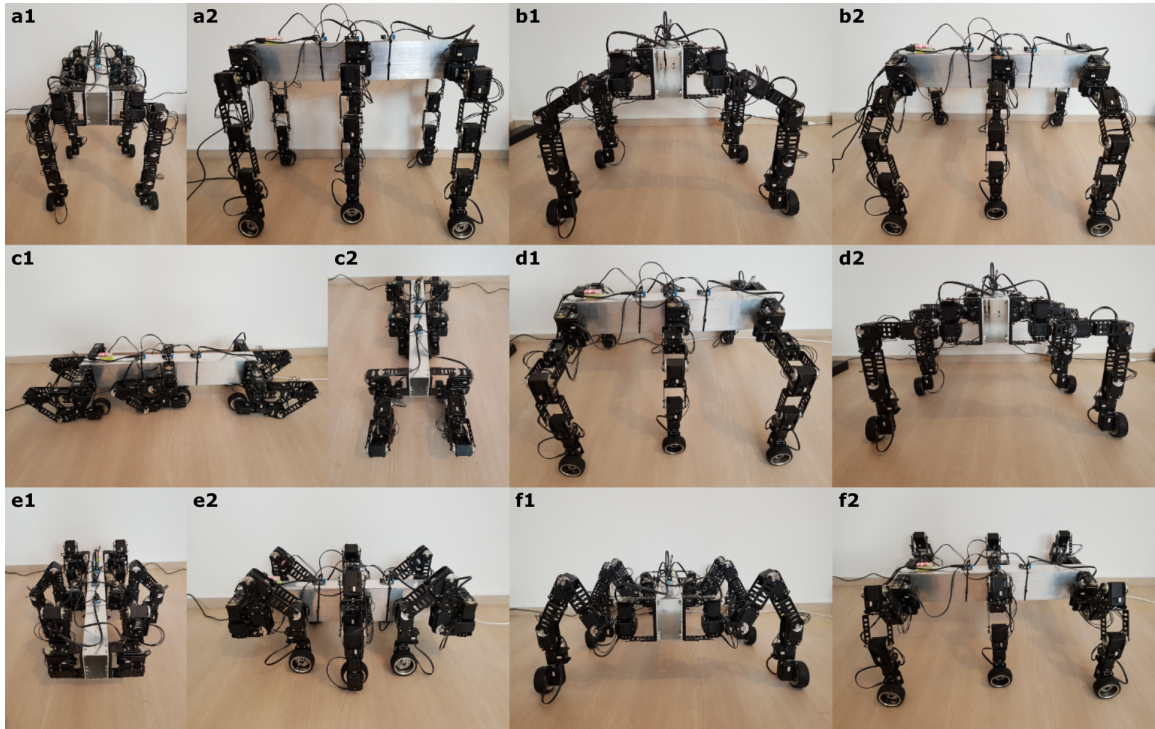
Figure 6.1: WHexaR stances. Several different stances are shown in this figure. Each stance can be used to overcome obstacle of different size and shape. (a1), (a2): The highest stance the robot is capable of. This stance can be used to get over high obstacles up to 38 cm. (b1), (b2): One of the basic basic stance of the robot that is used during ordinary movement. (c1), (c2): Stance with the smallest height (only 20 cm) can be used to crawl under a low obstacle. (d1), (d2): This stance is lower modification of the basic stance and is also used during ordinary movement. (e1), (e2): The shortest stance. (f1), (f2): Third variant of the basic stance, which is the lowest.

6.4 Movement using Gaits

The gait testing of the robot was performed on a flat surface. All the basic gaits, tripod, wave, ripple and tetrapod, were investigated. The robot moved with the selected gait and its speed and stability were analyzed.

Present positions, goal positions and servomotor current were monitored during movement. It was investigated whether the goal positions matched the actually achieved positions of the servomotors. The graphs in Figure 6.2 show the goal and actually achieved positions of coxa, femur, tibia and tarsus servomotors of the first leg in time during tripod gait. From the graphs it can be seen that the movement of the individual servomotors relatively corresponds to the desired goal position. In the end positions, especially at the femur and tarsus joints, there are slight deviations due to servomotor clearance. The initial differences in the graphs are due to the absence of a target position.

During walking experiments with the tripod gait, the robot exhibited occasional instability (when the rear legs were swung forward, it did not have sufficient support and leaned backwards). This issue was fixed by adjusting the default stance with the front and rear legs rotated 25° forward and backward, respectively. The inertial forces of the robot's motion

(a) Coxa

(b) Femur
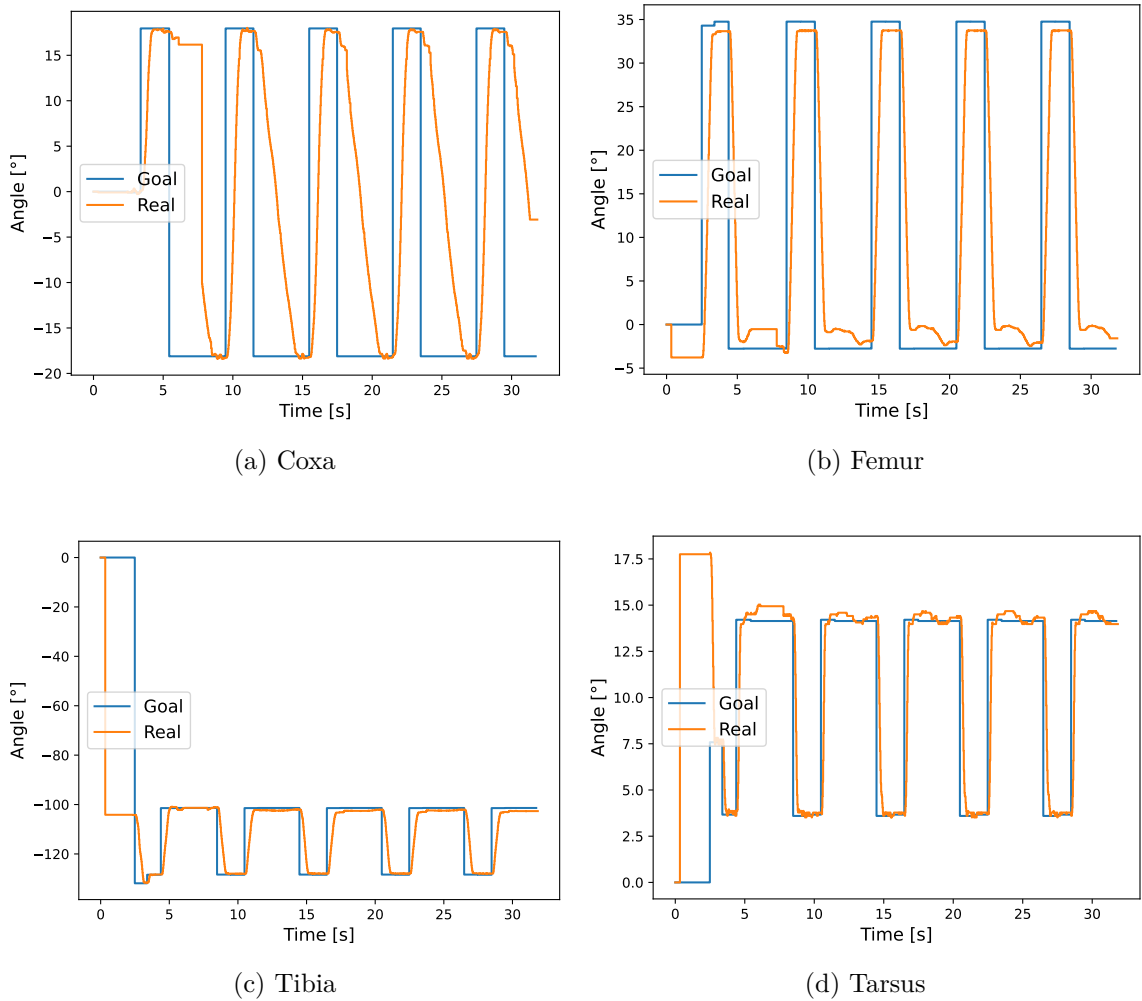
(c) Tibia

(d) Tarsus

Figure 6.2: Goal and actually achieved positions of the first leg coxa, femur, tibia and tarsus servomotors during tripod gait.

were also evident during movement, especially at longer stride lengths. These effects were mitigated by adjusting the speed and acceleration of the coxa servomotors.

6.5 Movement using Wheels

In these experiments, the omnidirectional chassis characteristics during ride were tested. Both, straight driving and turning were examined. During these experiments, the robot was moving on a flat surface. The robot was connected to a power supply and a control computer by cables.

6.5.1 Straight Movement

Straight driving on wheels was tested on a 2 metre long track. The robot gradually accelerated to its maximum speed. At the end of the track, it slowed down in a similar manner. The straightness of the trajectory was verified. The maximum speed of the robot was also measured.

The robot was able to maintain its direction of travel during its movement and traveled the track in 10 seconds. The maximum speed achieved was 0.2 m/s. The graphs in Figure 6.3 show the velocity of all wheels and the angles of the coxa, femur, tibia and tarsus servomotors of the first leg. These angles change slightly due to the load on the robot structure and wheel movement.

(a) Velocity of all wheels.

(b) Coxa, femur, tibia and tarsus angles.
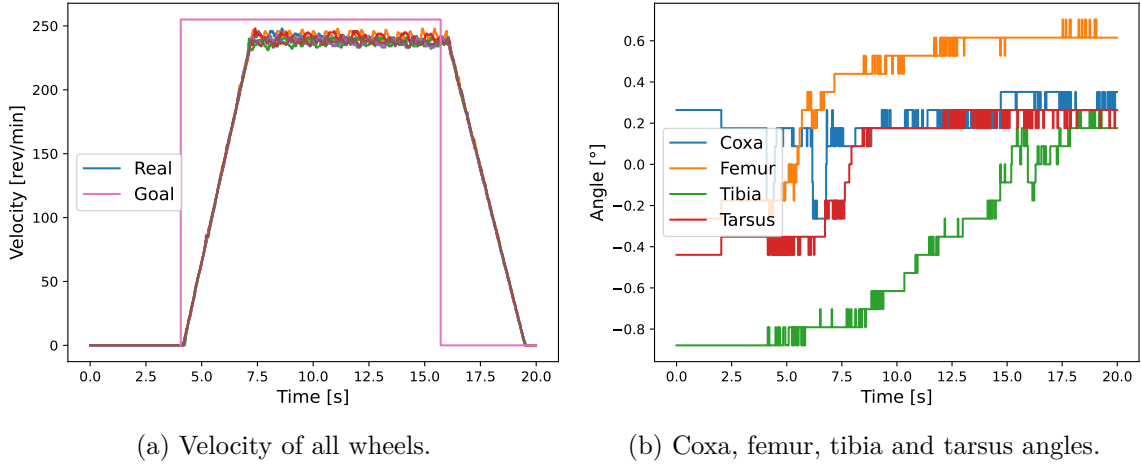
Figure 6.3: Straight movement using wheels. The tibia angle was shifted by $\pi/2$ when plotted on the graph for better readability.

6.5.2 Turning

There are two ways of turning the robot while moving on wheels. The first variant uses the direction servomotors for turning, where all wheels are turned in the same direction. The robot then starts moving in the direction of the wheels. Its body remains rotated in the direction of the original motion. After the direction servomotors are rotated to the initial position, the robot continues driving in the original direction. Thus, the robot does not turn, but moves sideways and can therefore go around possible obstacles without the body going off course.

The second variant of turning also uses direction servomotors. However, their rotation varies across the legs. This causes the whole robot to turn or to rotate on the spot depending on the direction of rotation of the individual wheels. The trajectories of the wheels are formed by concentric circles of different radii. In the experiments, both turning variants were analyzed because each of them is suitable for a different way of movement.

Driving Sideways

The testing of sideways driving on wheels was similar to the testing of straight driving. The robot moved along a 2 metre long track. The robot gradually accelerated to its maximum speed. At the end of the track, it slowed down in a similar manner. The direction servomotors were rotated to 45° and -45°, respectively. The straightness of the trajectory was verified. The maximum speed of the robot was also measured.

The robot was able to maintain its direction of travel during its movement and traveled the track in 10 seconds. The maximum speed achieved was 0.2 m/s.

Rotation on the Spot

Testing of rotation on the spot while riding on wheels was conducted on a flat surface. The aim of the experiment was to verify that the robot maintains a stable centre of rotation. After reaching a constant speed of rotation, the robot was rotating at 4 revolutions per minute. The speed of rotation could be increased by reducing the radius of the circles on which the wheels move, but at the expense of stability. The robot remained stable at the initial point of rotation throughout the experiment.

Riding along a Circle

Testing of riding on wheels along a circle was performed on a flat surface. The robot moved along a circular track. The speed of each wheel was monitored. The main objective of the experiment was to verify the repeatability of the movement of the robot, i.e. whether the robot is able to arrive back at the starting point after traversing the whole circle.

After completing two circuits, the robot returned to the original starting point with a deviation of 1.5 cm. During the movement, occasional tension was observed on the inner legs, because their wheels have a low rotation speed and do not keep turning.

6.6   Movement using Gait and Ride

When moving by walking, the robot puts its legs in the direction of movement and leans on them. When driving, it only stands on its legs and the movement is provided by rotating wheels. However, these two methods can be combined to create hybrid gait, in which robots move using walking and riding simultaneously. The ripple gait pattern was chosen to be combined with wheeled locomotion because of its high stability. The robot moved similarly to the previous experiments on a flat surface in order to achieve the maximum possible speed.

The robot completed the 2 metre long track in 9 seconds. Despite the slight increase in speed of movement of the robot compared to riding, there are significant vibrations during the combined movement and therefore this movement is suitable mainly for flat surfaces. The robot also has a higher power consumption. The graphs in Figure 6.4 show the goal and actually achieved positions of coxa, femur, tibia and tarsus servomotors of the first leg in time. It can be seen that the goal positions are in most cases close to the actually achieved positions.

6.7   Movement in Terrain

Movement in terrain can be divided into movement on a flat surface with potential obstacles and movement on sloping terrain. Some obstacles the robot is able to overcome, others it must avoid. When traveling on inclined terrain, the robot uses trochanter joints to rotate the entire leg parallel to the acceleration of gravity, which increases its stability and reduces the load and energy consumption of the servomotors. Reflexes help to overcome irregular terrain and respond to sudden changes in the environment. The robot is able to change the type of movement according to the current terrain conditions.

(a) Coxa

(b) Femur
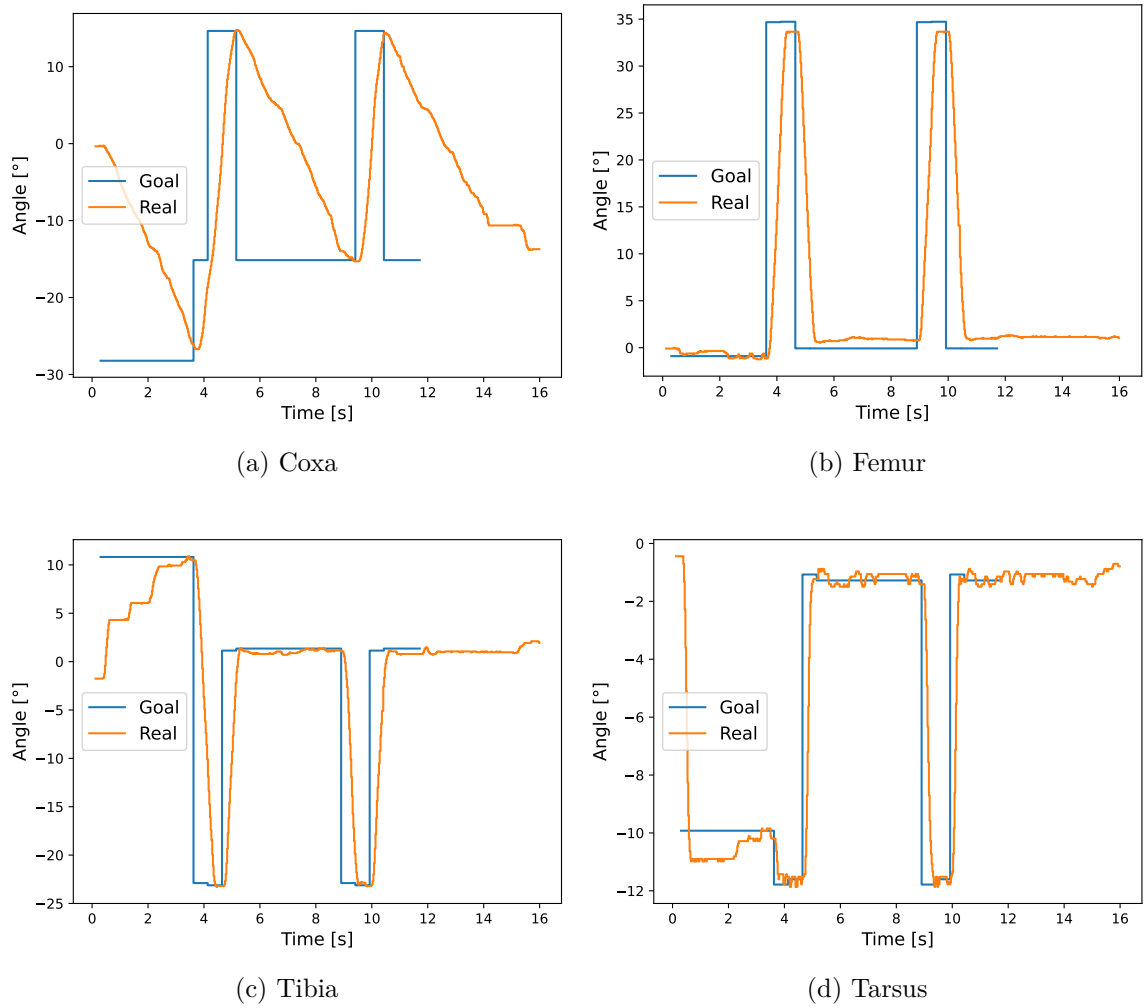
(c) Tibia

(d) Tarsus

Figure 6.4: Goal and actually achieved positions of the first leg coxa, femur, tibia and tarsus servomotors during hybrid gait that was generated using ripple gait and riding on wheels.

6.7.1 Stepping Reflex

Stepping reflex was tested on a flat surface. The robot was moving by gait. During the movement, one of the legs was prevented from reaching its goal position. It was observed whether the activated stepping reflex returns the leg to its original position. During the testing, other reflexes were also activated and therefore disabled for the duration of this experiment. After activation of the stepping reflex, the leg returned to its original direction of movement.

6.7.2 Elevator Reflex

To verify the correct operation of the elevator reflex, an experiment was designed in which the robot moved on flat terrain and during the movement one of the legs encountered an artificial static obstacle. The reaction of the leg was observed and its trajectory of the new movement was analyzed. The activation of the reflex occurred in all cases. Based on the

results of the experiment, the torque coxa joint threshold for activation of this reflex was adjusted.

Furthermore, the reflex was tested during movement in sloping terrain without using the trochanter joint. During testing, several incorrect activations caused by loads on the coxa joints due to the slope of the terrain occurred. These problems did not occur when moving on inclined terrain with the use of the trochanter joint.

Moreover, a situation where the obstacle is very light and the robot is able to shift it by moving its leg was tested. When the leg encountered such an obstacle, no reflex was activated during testing, but the obstacle was pushed by the robot's leg. This behaviour is not entirely desirable as it puts unnecessary load on the leg servomotors. However, lowering the threshold is not possible because the reflex would be activated too often.

These experiments revealed that the activation threshold of the elevator reflex may depend on the actual terrain, the robot stance and the character of the obstacle. Setting a universal threshold is therefore difficult. In the end, a higher threshold was chosen to ensure that the reflex is activated only when necessary, at the expense of a higher load on the servomotors as the leg may push an obstacle.

6.7.3 Searching Reflex

Several experiments were conducted to verify the behaviour of the searching reflex. The first was to determine whether the leg is able to find a new foothold when it loses its support during the stance phase, i.e. when the leg supporting the body loses its foothold. The leg detects the surface and thus the transition from the swing phase to the stance phase using a force-sensitive resistor (FSR). If there is a change in the amount of pressure the leg applies on the surface, the searching reflex is activated and attempts to find a new foothold, first in the downward direction and eventually in other directions.

The loss of leg support during the stance phase always triggered the searching reflex. However, finding a new foothold takes some time and therefore the robot may be destabilized. This was observed especially in the tripod gait, where loss of support of any leg caused the robot to fall. For more stable gaits, the robot compensated the loss of support of one leg and the searching reflex found new foothold. This reflex significantly improves movement in rugged terrain.

As part of the searching reflex, the function of stopping the leg when stepping early on a surface or obstacle has also been implemented. The experiment tested whether the leg stops its movement on an obstacle even though it has not yet reached the expected goal position. During the experiment, the robot stood still and its front leg stepped on an obstacle. Two alternatives were tested to determine the moment of stopping the leg movement. The first used information about the current flowing through the femur joint, i.e., with how much force, if any, the servomotor is pushing on the ground. The second alternative used the present values from force-sensitive resistors (FSR). When the threshold value of the monitored metric was exceeded, the leg movement was stopped. The threshold was set according to the initial load on that leg after the robot was calibrated. During the experiments, the alternative using FSRs performed better because their values show less fluctuation.

6.7.4 Obstacles Negotiation

During its movement on a flat terrain the robot may encounter different types of obstacles. The first type of obstacles can be considered as uneven terrain and when using gait, they

will be crossed or the leg will stop its movement on them. The second type are obstacles that the robot is unable to step on or step over during normal walking because they are too high, but it should be able to climb over them. At such obstacles, the robot stops and measures their height and depth using a rangefinder. If the height of the obstacle is within a threshold, the robot starts climbing over the obstacle. Insects exhibit similar behaviour when moving. It uses its antennae to detect obstacles. The robot has no antennae, so it has to use its sensors or legs. The last type is high obstacles that the robot must avoid.

6.7.5 Terrain Controller and Gait Selector

Testing of the Terrain Controller and the Gait Selector was performed simultaneously because their functioning is related. The robot moved in different terrain conditions and indicators of terrain complexity, their threshold values and stability of robot movement were monitored. Based on the experiments, the thresholds for the activation of each type of movement were adjusted. For wheeled movement, the possible tilt of the robot has been increased to 20°. For the number of disappeared supports, a floating time window was specified in which the values are registered. The window length was set to one gait cycle.

6.7.6 Inclined Terrain

Two types of experiments were designed in inclined terrain. The first experiment involved placing the robot on a wooden board with an adjustable slope. Different inclinations of the board were sequentially set and the movements of the robot generated by the reactive layer were observed (see Figure 6.5a). In the second experiment, the robot moved on flat terrain with a transition to an inclined plane (see Figure 6.5b).

In the first experiment, the robot was able to respond to a change in the tilt of the plate. This response is not instantaneous because the servomotors take a while to initiate their movement. For this short period of time, the legs are perpendicular to the body of the robot and not parallel to the gravitational acceleration, and they have a higher energy consumption and provide less stability.

Tripod gait and riding on wheels were used to test locomotion on inclined terrain. The robot was able to move by gait up to a 32° inclination, ride up to a 40° inclination, and maintain balance while standing statically up to a 50° inclination.

6.7.7 Discussion

The performed experiments have shown that each part of the movement controller is functional. Furthermore, the robot's ability to overcome terrain irregularities was confirmed. It was also found that the selection of thresholds for the activation of different reflexes affects the way the robot walks. The advantage of using explicit thresholds is that they can be easily adjusted.

Experiments in sloping terrain proved that the combination of trochanter joint and the terrain controller allows WHexaR to walk up to an inclination of 32°, to ride inclined terrains up to 40° and remain statically stable on slopes up to 50°. This is an improvement compared to LAURON [148], which is able to walk at an inclination of 25° and stand stably up to 42° and Weaver [24], which is capable of walking up to 30° and remain stable until 50°. Using wheel locomotion, the robot should be able to negotiate steeper slopes. Unfortunately, at higher inclinations of the test bed there was considerable wheel slippage. The same applied for gait movement.
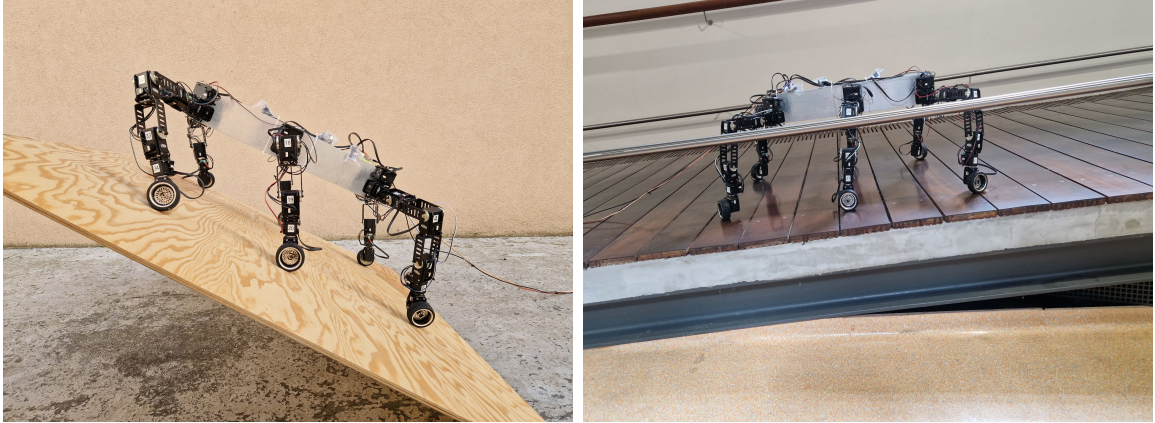
(a) Posture of the robot on a inclined board with the legs rotated using trochanter joints.

(b) Movement of the robot on an inclined plane with the legs rotated using trochanter joints.

Figure 6.5: Experiments in inclined terrain.

6.8 Robot Energy Consumption

The goal of these experiments was to determine the actual energy consumption of the robot, which was moving with tripod gait and riding on all six wheels on both flat and sloping terrain [202]. The goal was also to verify whether the use of a trochanter joint would reduce the energy consumption of the robot when moving in sloping terrain. The robot was powered by a 12 V power supply and the servomotors were controlled by an U2D2 controller from desktop computer. The inclined terrain was simulated by a wooden board with an adjustable slope. The load on the individual servomotors was measured as the current flowing through the servomotor. The actual current of each servomotor was read from the servomotor present current register. Another way to measure the load on the servomotors would be the usage of an external current sensor. However, one sensor would need to be attached to each servomotor, which would be very complicated. In addition, the servomotors themselves measure their current with a resolution of 3.36 mA, which is sufficient accuracy for this experiment. The total current of the robot was measured at 50 Hz using a hall effect-based linear current sensor ACS712 [4], which was connected to the Atmega2560 on a development board Arduino Mega 2560.

Three different static stances and two movements (tripod gait with a maximum speed of 0.12 m/s and a period of 1.6 s and ride using six wheels with a maximum speed of 0.2 m/s) were tested at six different inclinations (see Table 6.6). All tested stances were based on the default stance of the robot (Figure 6.6a). The first derived stance (No. 1) did not use the trochanter joint and all legs were at the same height (Figure 6.6b). The second derived stance (No. 2) also did not use the trochanter joint, but the individual legs were at different heights that corresponded to the slope of the tested terrain (Figure 6.6c). Finally, the third derived stance (No. 3) used the trochanter joint and all legs were at the same height. The angle of rotation of the trochanter joint was identical to the slope of the tested terrain (Figure 6.6d).

Table 6.6: The parameters of the proposed experiments. This table describes the parameters of each experiment, specifically the slope of the terrain, the stance used and its characteristics. Each experiment was performed for static stance, walking using tripod gait and driving all six wheels.

Terrain Slope [°]	Stance No.	Trochanter Joint Angle [°]	Stance
0	1†	0	same height
14	1	0	same height
14	2	0	different height
14	3	14	same height
23	1	0	same height
23	2	0	different height
23	3	23	same height
32	1	0	same height
32	2	0	different height
32	3	32	same height
40	1	0	same height
40	2	0	different height
40	3	40	same height
50	1	0	same height
50	2	0	different height
50	3	50	same height

† In terrain with zero slope, there was no point in testing the other two stances because they corresponded to stance number 1.

Each stance was measured three times. Measurements of static stance contained 40 values, which were then averaged. Measurements of the moving robot were collected at a frequency of 50 Hz. In some cases, the servomotor did not respond within the specified limit or the response was corrupted. These occurrences were removed from each measurement. The resulting value of the servomotor current was determined according to Equation (6.1).

$$I_s = \frac{\sum_{i=1}^{n} |x_i|}{n} \tag{6.1}$$

where I_s is the current of the servomotor with ID s, x_i is the ith value of the measurement and n is the count of accepted values in the measurement.

The resulting total leg current was given by Equation (6.2).

$$I_l = \sum_{s=1}^{m} I_s \tag{6.2}$$

where I_l is the total current of the leg with ID l, I_s is the current of the servomotor with ID s and m is count of servomotors in the leg.

The resulting current for the given stance was determined using Equation (6.3).
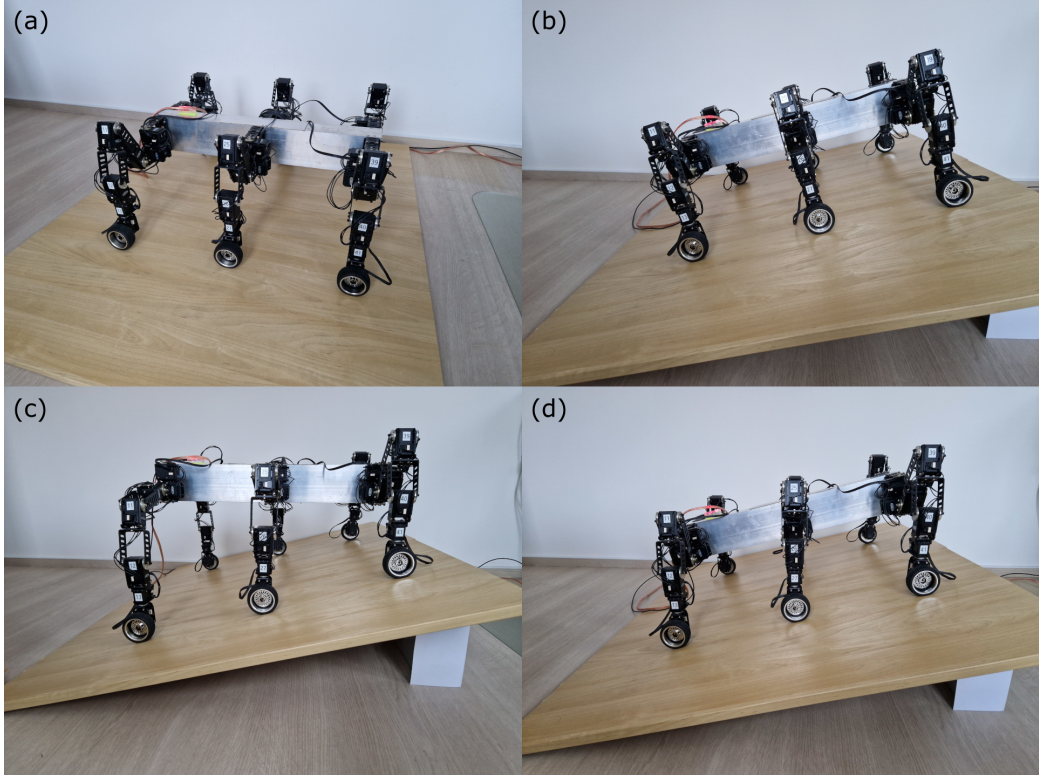
Figure 6.6: Robot stances during experiment. (a) The default stance. (b) The trochanter joint is not used and the legs have the same height. (c) The trochanter joint is not used, but the leg height is adjusted according to the slope. (d) The angle of rotation of the trochanter joint is adjusted to the slope of the tested terrain.

$$I = \sum_{l=1}^{6} I_l \qquad (6.3)$$

where I is the resulting current of the given stance and I_l is the current of the leg with ID l.

The power indicator energetic cost of transport (CoT) was used to compare the energy consumption with other robots. It is defined as the energy required to move a unit mass over a unit distance [119, 92]. By substituting energy for power, we can write CoT as Equation (6.4).

$$e = \frac{P}{mgv} \qquad (6.4)$$

where P is the power consumed by the robot during the motion, m is the mass of the robot and v is the speed of the robot. The power can then be determined by Equation (6.5).

$$P = UI \qquad (6.5)$$

where U is the supply voltage of the robot and I is the current drawn from the power supply.

6.8.1 Results

All measurements were calculated according to the presented methodology. The results for each stance and movement are shown in the following charts. Figure 6.7a shows a chart of the total current of the robot at three static stances. The stance using the trochanter joint had the lowest current value and, therefore, the lowest power consumption. The stance with different leg heights had low energy requirements compared to the stance that did not use the trochanter joint, which had a significant increase in energy consumption with increasing terrain slope. The stance using the trochanter joint was more than 23 % more energy-efficient in the case of a 32° slope.

The chart also shows that the robot was no longer able to stand stably on slopes greater than 32° without the use of a trochanter joint.

Figure 6.7b shows a chart of the current of the robot during tripod gait and wheeled movement with, and without, the usage of the trochanter joint. Up to 40 % energy could be saved when using the wheeled locomotion. When driving on wheels on 40° slopes, there was already considerable slipping. The robot was no longer reliably able to ride on such a slope without using the trochanter joint. This could also be seen in the drop in the current of the robot at an inclination of 40°.

(a) Static stances.   (b) Movement using tripod and wheels.
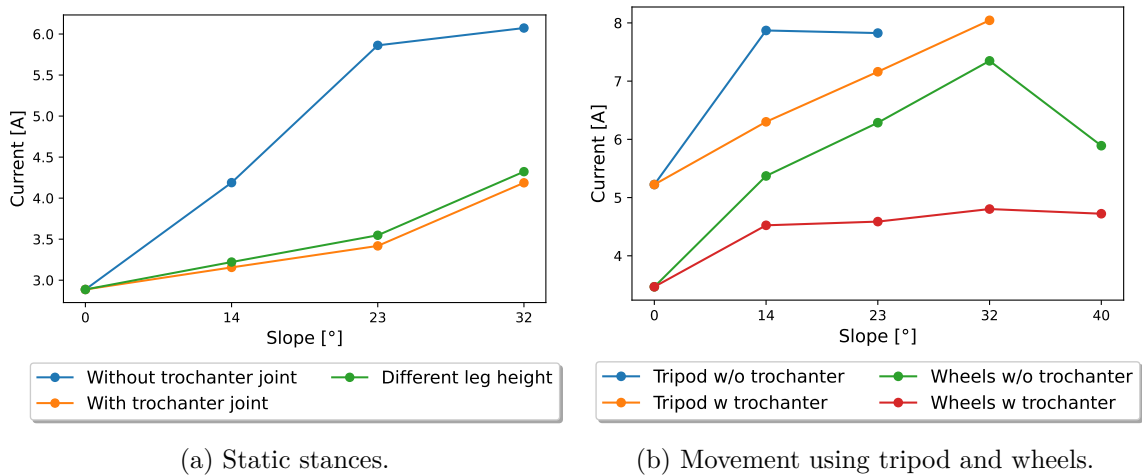
Figure 6.7: Overall current on different slopes for static stances and movements. 'w/o' stands for without and 'w' stands for with. (a) Static stances: The graph shows that the stance using the trochanter joint and the stance with different leg heights had almost the same energy requirements. In contrast, the basic stance required more and more energy as the terrain slope increased. (b) Tripod and wheel mode: The movement with the usage of the trochanter joint had a lower power consumption in all measured inclinations. The use of a trochanter joint also reduced the power consumption when using wheels.

The results are presented in more detail in the graphs, which show the current of individual servomotors of each leg on 0° and 32° terrain slopes for three static stances (see Charts a–d in Figure 6.8). It can be seen that, as the slope of the terrain increased, the robot's centre of gravity shifted backwards, increasing the load on the rear legs. In contrast, the front legs were loaded significantly less. Furthermore, the coxa servomotors were significantly more loaded when standing without a trochanter joint at a 32° inclination.

The graphs also show uneven loading on the legs. This was mostly due to minor slippage of the legs on the surface and the tolerance of the controller that controlled the leg loading.

(a) Slope 0°.

(b) Slope 32°.

(c) Slope 32° with different leg heights.

(d) Slope 32° with trochanter joint.
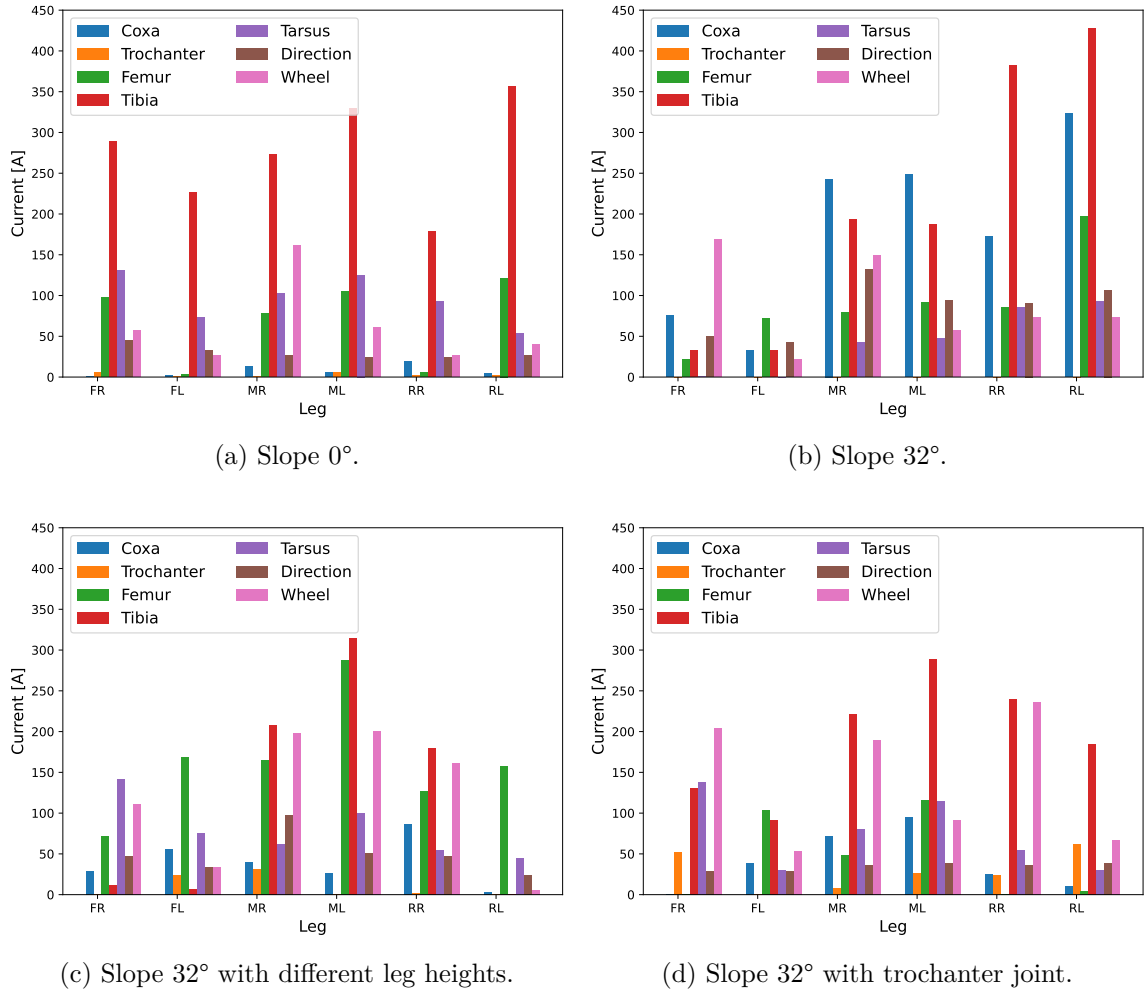
Figure 6.8: Charts of all legs and servomotors for 0° and 32° slopes in different static stances. The graphs show the load on each servomotor of each leg in different terrain slopes using basic stance, stance with different leg heights and stance using the trochanter joint. The abbreviations used for the leg names are as follows: FR—front right, FL—front left, MR—middle right, ML—middle left, RR—rear right, RL—rear left.

It can also be observed that the difference between the stance using the trochanter joint and the stance with different leg heights was relatively small. It appeared that the use of these stances had similar energy demands. Even so, a robot with a trochanter joint can use more stances and tilting the robot on sloping terrain is easier than using a stance with different leg heights. In the case of our robot, the trochanter joint was also used in case the robot fell on its back. The robot can use the trochanter joint to rotate its legs by 180° and continue its movement.

The charts in Figure 6.9 show the current of the robot when moving using tripod gait and wheeled locomotion with, and without, the use of the trochanter joint on flat terrain and on a 23° slope. The speed of the tripod gait ranged from 0.07 m/s to 0.12 m/s and its period was 1.6 s. The tripod gait on flat terrain had the lowest energy consumption and regular swing phase of the legs. When walking on sloping terrain, small slips occasionally occurred, especially when using the stance without the trochanter joint.

(a) Tripod. (b) Wheels.
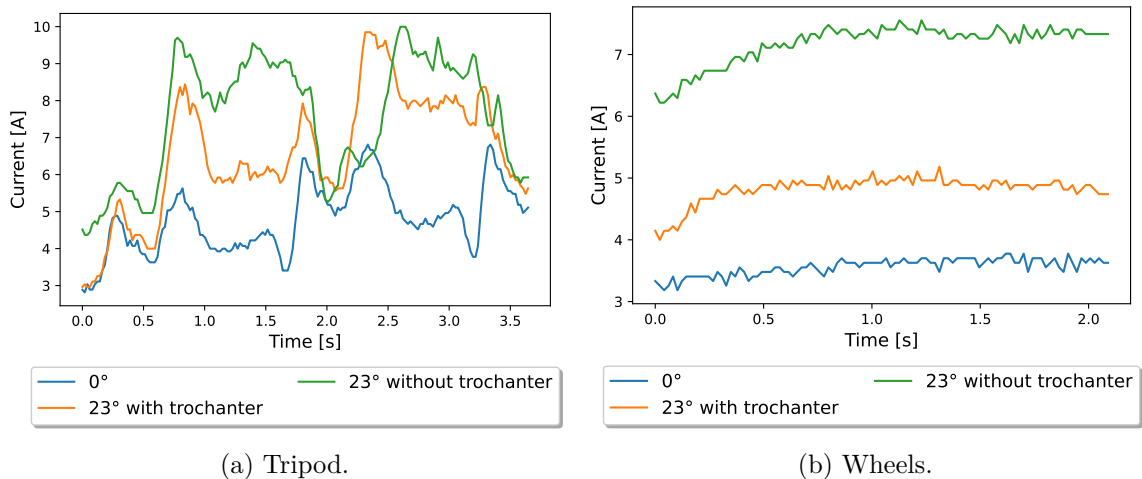
Figure 6.9: Current during movement in different slopes. (a) Current of the robot when moving using tripod gait with, and without, trochanter joint on 0° and 23° slopes. The chart shows two periods of tripod gait (one period was 1.6 s). Between 0.4 and 2 s, respectively, 2 and 3.6 s, the stance phase was followed by the swing phase of one group of legs and, at the same time, the swing phase was followed by the stance phase of the other group of legs. The maximum speed of the robot using the tripod gait was 0.12 m/s. (b) Current of the robot when moving using wheeled locomotion with, and without, trochanter joint on 0° and 23° slopes. The chart shows the first two seconds of the movement. In the first part, the robot accelerated to its maximum speed and the current gradually increased. In the second part, the speed of the robot no longer changed and the current oscillated around a constant value. The maximum speed of the robot using the wheeled locomotion was 0.2 m/s.

When using wheels, the energy consumption was constant throughout the movement except for minor fluctuations. At the beginning of the movement, we observed a gradual increase in power consumption caused by the acceleration of the robot. The power consumption when riding on wheels with the trochanter joint was up to 36 % lower than when riding without it. The maximum speed of the robot moving by wheeled locomotion was 0.2 m/s.

The power indicator energetic cost of transport (CoT) was used for comparison with other robots. It was calculated with a robot mass of 8.8 kg, power supply voltage of 12 V and a gravitational acceleration of 9.81 m/s². The CoT for each experiment is given in Table 6.7. The CoT ranged from 6.05 to 15.97 for the tripod gait and from 2.41 to 5.11 for wheeled locomotion, depending on the slope of the terrain and the usage of the trochanter joint.

6.8.2 Discussion

The experiments showed that the proposed leg structure reduces the energy consumption of the robot and allows it to traverse steep slopes that would be impossible for the robot to navigate without the trochanter joint. As can be seen in the charts showing the current of the individual servomotors, using a trochanter joint significantly reduces the load on the coxa joint. There is also better load distribution across all leg servomotors. The energy consumption of the movement is further reduced by the wheeled chassis, which is suitable for movement on flat terrain. In addition, this chassis increases the speed of the robot

and can also be used to climb slopes without terrain irregularities. The novel leg design also increases the stability of the robot, especially when navigating steep slopes. The experiments showed that, at a certain inclination, the robot is only able to move with the use of a trochanter joint.

Experiments have confirmed the improvements achieved in terms of energy efficiency. The power indicator energetic cost of transport (CoT) on flat terrain was 6.05 when using gait and 2.41 when using wheeled locomotion. In comparison, hexapod Weaver [24] has CoT 15.2 on flat terrain.

Table 6.7: The power indicator energetic cost of transport for both tripod gait and wheeled locomotion on different slopes.

Movement	Slope	Speed	Current [†]	Current T [‡]	CoT [†]	CoT T [‡]
tripod	0	0.12	5.22	-	6,05	-
tripod	14	0.12	7.87	6.30	9.12	7.30
tripod	23	0.10	7.83	7.16	10.88	9.95
tripod	32	0.07	-	8.04	-	15.97
wheels	0	0.20	3.47	-	2.41	-
wheels	14	0.20	5.37	4.52	3.73	3.14
wheels	23	0.20	6.29	4.59	4.37	3.19
wheels	32	0.20	7.35	4.80	5.11	3.34
wheels	40	0.15	-	4.72	-	4.37

[†] without the use of trochanter joint; [‡] with the use of trochanter joint.

Chapter 7

Conclusion

This thesis explores the field of walking robots, in particular hexapods, and the possible inspiration in nature for their design, construction and control. Suitable inspiration for six-legged robots can be found in insects. The basic characteristics of insects are discussed, focusing on their body and limb structure, nervous system, behaviour and movement. The second part of the thesis focuses on the aspects of walking robots, their body and leg structure, motion and stability, and controllers. Examples of existing robots are also presented. The following parts of the thesis describe the innovative hexapod robot WHexaR (Wheeled Hexapod Robot, see Figure 7.1) and its adaptive controller I designed and implemented. This robot has a total of 42 degrees of freedom. Each leg has seven joints. Five of them are used for positioning the leg and the remaining two form a wheeled chassis. One joint is used to adjust the direction of the wheel and the other drives the wheel itself. The segmentation of robot's leg and the architecture of its controller has found inspiration in nature. The number of joints and the length of the leg segments were chosen based on the researched insect characteristics. The proposed controller is capable of changing the movement pattern based on the current terrain conditions and the use of the implemented reflexes that mimic insect behaviour increases the stability and reliability of the robot's movement. The trochanter joint allows the entire leg to be rotated parallel to the acceleration of gravity, this feature is used especially when moving on sloping terrain. The rotation of the leg better distributes the weight of the robot over all legs and reduces the torque required for the servomotors to move, resulting in overall energy savings. Rotating the leg also increases the stability of the robot, allowing it to move across steeper terrain than robots that do not have this joint. The wheeled chassis increases the robot's movement speed on flat terrain and reduces its energy consumption.

The experiments confirmed that the combination of trochanter joint and the terrain controller allows my robot to walk up to an inclination of 32°, to ride inclined terrains up to 40° and remain statically stable on slopes up to 50°. This is an improvement compared to other relevant robots such as LAURON [148], which is able to walk at an inclination of 25° and stand stably up to 42° and Weaver [24], which is capable of walking up to 30° and remain stable until 50°. I've also achieved an improvement in terms of energy efficiency. The measured value of power indicator energetic cost of transport of my robot when walking on flat terrain was 6.05. When using wheeled locomotion, a value of 2.41 was achieved. In comparison, hexapod Weaver has cost of transport 15.2 on flat terrain.

I dealt with hexapod robots already during my bachelor and master studies. I have also participated in several exhibitions and conferences. With my first robot I built I have won first place in the EEICT student conference. Later, I improved this robot and won several

awards at the Excel@FIT student conference, including the first place in the Technological level category and the gold sponsor award.

I have published a paper about my robot WHexaR in the journal Open Computer Science (Q2), which has been cited several times [201]. My most recent manuscript deals with the energy efficiency of my robot. It was published in the journal Robotics (IF 3.7, Q1) [202].

Figure 7.1: WHexaR (Wheeled Hexapod Robot) is a six-legged robot designed and constructed as part of this work.

Bibliography

[1] ADAFRUIT. *LSM9DS1 Accelerometer + Gyro + Magnetometer 9-DOF Breakout Board* [https://learn.adafruit.com/adafruit-lsm9ds1-accelerometer-plus-gyro-plus-magnetometer-9-dof-breakout/]. 2017. [Online; visited 23-07-2023].

[2] ALEXANDER, R. M. The gaits of bipedal and quadrupedal animals. *The International Journal of Robotics Research.* Sage Publications Sage CA: Thousand Oaks, CA. 1984, vol. 3, no. 2, p. 49–59.

[3] ALEXANDER, R. *Exploring Biomechanics: Animals in Motion.* Scientific American Library, 1992. Library series. ISBN 9780716750352. Available at: https://books.google.cz/books?id=9lkuvgEACAAJ.

[4] ALLEGRO MICROSYSTEMS, INC.. *ACS712* [https://www.sparkfun.com/datasheets/BreakoutBoards/0712.pdf]. 2023. [Online; visited 10-08-2023].

[5] AMAR, F., BUDANOV, V., BIDAUD, P., PLUMET, F. and ANDRADE, G. A high mobility redundantly actuated mini-rover for self adaptation to terrain characteristics. In:. October 2000.

[6] ARDUINO. *Mega 2560 Rev3* [https://docs.arduino.cc/hardware/mega-2560]. 2023. [Online; visited 21-07-2023].

[7] ARENA, P., FORTUNA, L., FRASCA, M., PATANÉ, L. and PAVONE, M. Implementation and experimental validation of an autonomous hexapod robot. In: *Proceedings of the IEEE International Symposium on Circuits and Systems, Kos, Greece.* 2006, vol. 2124.

[8] ASARIAN, L., GLOY, V. and GEARY, N. Homeostasis. In: RAMACHANDRAN, V., ed. *Encyclopedia of Human Behavior (Second Edition).* Second Editionth ed. San Diego: Academic Press, 2012, p. 324–333. DOI: https://doi.org/10.1016/B978-0-12-375000-6.00191-9. ISBN 978-0-08-096180-4. Available at: https://www.sciencedirect.com/science/article/pii/B9780123750006001919.

[9] BAR COHEN, Y. Biomimetics: biologically inspired technology. january 2006.

[10] BAR COHEN, Y. Biomimetics—using nature to inspire human innovation. *Bioinspiration & biomimetics.* IOP Publishing. 2006, vol. 1, no. 1, p. P1.

[11] BARES, J., HEBERT, M., KANADE, T., KROTKOV, E., MITCHELL, T. et al. Ambler: an autonomous rover for planetary exploration. *Computer.* 1989, vol. 22, no. 6, p. 18–26. DOI: 10.1109/2.30717.

[12] BARES, J. and WETTERGREEN, D. Dante II: Technical Description, Results and Lessons Learned. *International Journal of Robotics Research.* July 1999, vol. 18, no. 7, p. 621 – 649.

[13] BARNES, R. D. *Arthropod* [https://www.britannica.com/animal/arthropod]. 2023. [Online; visited 2023-07-07].

[14] BÄSSLER, U. Sensory control of leg movement in the stick insect Carausius morosus. *Biological cybernetics.* Springer. 1977, vol. 25, no. 2, p. 61–72.

[15] BEER, R., CHIEL, H. and STERLING, L. S. Heterogeneous neural networks for adaptive behavior in dynamic environments. *Advances in neural information processing systems.* 1988, vol. 1.

[16] BEER, R. D. *Intelligence As Adaptive Behavior: An Experiment in Computational Neuroethology.* San Diego, CA, USA: Academic Press Professional, Inc., 1990. ISBN 0-12-084730-2.

[17] BEER, R. D., CHIEL, H. J., QUINN, R. D., ESPENSCHIED, K. S. and LARSSON, P. A distributed neural network architecture for hexapod robot locomotion. *Neural Computation.* MIT Press. 1992, vol. 4, no. 3, p. 356–365.

[18] BEER, R. D., QUINN, R. D., CHIEL, H. J. and RITZMANN, R. E. Biologically Inspired Approaches to Robotics: What Can We Learn from Insects? *Commun. ACM.* New York, NY, USA: Association for Computing Machinery. mar 1997, vol. 40, no. 3, p. 30–38. DOI: 10.1145/245108.245118. ISSN 0001-0782. Available at: https://doi.org/10.1145/245108.245118.

[19] BELTER, D. and SKRZYPCZYŃSKI, P. Integrated Motion Planning for a Hexapod Robot Walking on Rough Terrain. *IFAC Proceedings Volumes.* 2011, vol. 44, no. 1, p. 6918–6923. DOI: https://doi.org/10.3182/20110828-6-IT-1002.02234. ISSN 1474-6670. 18th IFAC World Congress. Available at: https://www.sciencedirect.com/science/article/pii/S1474667016447166.

[20] BELTER, D. and WALAS, K. A compact walking robot–flexible research and development platform. In: Springer. *Recent advances in automation, robotics and measuring techniques.* 2014, p. 343–352.

[21] BERNS, K., CORDES, S. and ILG, W. Adaptive, neural control architecture for the walking machine LAURON. In: *Proceedings of IEEE/RSJ International Conference on Intelligent Robots and Systems (IROS'94).* 1994, vol. 2, p. 1172–1177 vol.2. DOI: 10.1109/IROS.1994.407466.

[22] BESSONOV, A. P. and UMNOV, N. V. The Analysis of Gaits in Six-Legged Vehicles According to Their Static Stability. In: *On Theory and Practice of Robots and Manipulators: Volume I.* Vienna: Springer Vienna, 1974, p. 1–10. ISBN 978-3-7091-2993-7.

[23] BESTMANN, M., GÜLDENSTEIN, J. and ZHANG, J. High-frequency multi bus servo and sensor communication using the dynamixel protocol. In: Springer. *RoboCup 2019: Robot World Cup XXIII 23.* 2019, p. 16–29.

[24] Bjelonic, M., Kottege, N. and Beckerle, P. Proprioceptive control of an over-actuated hexapod robot in unstructured terrain. In: *2016 IEEE/RSJ International Conference on Intelligent Robots and Systems (IROS)*. 2016, p. 2042–2049. DOI: 10.1109/IROS.2016.7759321.

[25] Bjelonic, M., Sankar, P. K., Bellicoso, C. D., Vallery, H. and Hutter, M. Rolling in the deep–hybrid locomotion for wheeled-legged robots using online trajectory optimization. *IEEE Robotics and Automation Letters*. IEEE. 2020, vol. 5, no. 2, p. 3626–3633.

[26] Boston Dynamics. *Atlas* [https://www.bostondynamics.com/atlas]. 2023. [Online; visited 2023-07-06].

[27] Boston Dynamics. *Legacy Robots* [https://www.bostondynamics.com/legacy]. 2023. [Online; visited 2023-05-28].

[28] Boston Dynamics. *Spot - The Agile Mobile Robot* [https://www.bostondynamics.com/products/spot]. 2023. [Online; visited 2023-07-06].

[29] Brady Boettcher. *Force-sensitive Resistor (FSR) | SensorWiki* [https://sensorwiki.org/sensors/force-sensitive_resistor]. 2023. [Online; visited 23-07-2023].

[30] Brown, T. G. On the nature of the fundamental activity of the nervous centres; together with an analysis of the conditioning of rhythmic activity in progression, and a theory of the evolution of function in the nervous system. *The Journal of physiology*. Wiley-Blackwell. 1914, vol. 48, no. 1, p. 18.

[31] Brown, T. G. The intrinsic factors in the act of progression in the mammal. *Proceedings of the Royal Society of London. Series B, containing papers of a biological character*. The Royal Society London. 1911, vol. 84, no. 572, p. 308–319.

[32] Buchegger, A., Lassnig, K., Loigge, S., Mühlbacher, C. and Steinbauer, G. An Autonomous Vehicle for Parcel Delivery in Urban Areas. In: *2018 21st International Conference on Intelligent Transportation Systems (ITSC)*. 2018, p. 2961–2967. DOI: 10.1109/ITSC.2018.8569339.

[33] Butterfass, J., Grebenstein, M., Liu, H. and Hirzinger, G. DLR-Hand II: next generation of a dextrous robot hand. In: *Proceedings 2001 ICRA. IEEE International Conference on Robotics and Automation (Cat. No.01CH37164)*. 2001, vol. 1, p. 109–114 vol.1. DOI: 10.1109/ROBOT.2001.932538.

[34] Büschges, A. and DiCaprio, R. 4.26 - Somatosensation in Invertebrates. In: Fritzsch, B., ed. *The Senses: A Comprehensive Reference (Second Edition)*. Second Editionth ed. Oxford: Elsevier, 2020, p. 419–425. DOI: https://doi.org/10.1016/B978-0-12-805408-6.00362-6. ISBN 978-0-12-805409-3. Available at: https://www.sciencedirect.com/science/article/pii/B9780128054086003626.

[35] Carbone, G., Yatsun, A., Yatsun, S. and Ceccarelli, M. Design and simulation of cassino hexapod robot. In: *2009 13th WSEAS International Conference on SYSTEMS*. 2009, p. 301–307.

[36] CARBONE, G. and CECCARELLI, M. *Legged robotic systems.* INTECH Open Access Publisher, 2005.

[37] CHAPMAN, R., SIMPSON, S. and DOUGLAS, A. *The Insects: Structure and Function.* Cambridge University Press, 2013. The Insects: Structure and Function. ISBN 9780521113892. Available at: https://books.google.cz/books?id=NXJEi8fo7CkC.

[38] CHIEL, H. J., BEER, R. D., QUINN, R. D. and ESPENSCHIED, K. S. Robustness of a distributed neural network controller for locomotion in a hexapod robot. *Robotics and Automation, IEEE Transactions on.* IEEE. 1992, vol. 8, no. 3, p. 293–303.

[39] CHUNG, H.-Y., HOU, C.-C. and HSU, S.-Y. A CPG-inspired controller for a hexapod robot with adaptive walking. In: *Automatic Control Conference (CACS), 2014 CACS International.* Nov 2014, p. 117–121. DOI: 10.1109/CACS.2014.7097173.

[40] CHVÁTAL, A. Jiří Procháska (1749-1820): Part 1: A Significant Czech Anatomist, Physiologist and Neuroscientist of the Eighteenth Century. *Journal of the history of the neurosciences.* july 2014, vol. 23, p. 1–10. DOI: 10.1080/0964704X.2014.881310.

[41] CORDES, S., BERNS, K. and LEPPANEN, I. Sensor components of the six-legged walking machine LAURON II. In: *1997 8th International Conference on Advanced Robotics. Proceedings. ICAR'97.* 1997, p. 71–76. DOI: 10.1109/ICAR.1997.620164.

[42] CRESPI, A., BADERTSCHER, A., GUIGNARD, A. and IJSPEERT, A. J. AmphiBot I: an amphibious snake-like robot. *Robotics and Autonomous Systems.* Elsevier. 2005, vol. 50, no. 4, p. 163–175.

[43] CYBERNETICZOO.COM cyberne1. *1983 – Six-Legged Hydraulic Walker – Ivan Sutherland* [https://cyberneticzoo.com/walking-machines/1983-six-legged-hydraulic-walker-ivan-sutherland-american/]. 2010. [Online; visited 2023-07-16].

[44] DADAFSHAR, M. Accelerometer and gyroscopes sensors: operation, sensing, and applications. *Maxim Integrated [online].* 2014.

[45] DAVID BYRNE, D. W. *Insect biology materials* [https://ag.arizona.edu/classes/ento415/lecture2009.html]. 2009. [Online; visited 2023-07-13].

[46] DAVLIAKOS, I., RODITIS, I., LIKA, K., BREKI, C.-M. and PAPADOPOULOS, E. Design, development, and control of a tough electrohydraulic hexapod robot for subsea operations. *Advanced Robotics.* Taylor & Francis. 2018, vol. 32, no. 9, p. 477–499. DOI: 10.1080/01691864.2018.1461684. Available at: https://doi.org/10.1080/01691864.2018.1461684.

[47] DEANGELIS, B. D., ZAVATONE VETH, J. A. and CLARK, D. A. The manifold structure of limb coordination in walking *Drosophila. ELife.* eLife Sciences Publications, Ltd. jun 2019, vol. 8, p. e46409. DOI: 10.7554/eLife.46409. ISSN 2050-084X. Available at: https://doi.org/10.7554/eLife.46409.

[48] DI PRISCO, G. V., WALLE, P., GRILLNER, S. et al. Synaptic effects of intraspinal stretch receptor neurons mediating movement-related feedback during locomotion. *Brain research.* Elsevier. 1990, vol. 530, no. 1, p. 161–166.

[49] DING, X., WANG, Z., ROVETTA, A. and ZHU, J. Locomotion Analysis of Hexapod Robot. In:. March 2010. DOI: 10.5772/8822. ISBN 978-953-307-030-8.

[50] DRAHANSKÝ, M., LUŽA, R. and ZBOŘIL, V. F. RUDA - Robot for Search for Human Beings in Debris and Avalanches. In: *Proceedings of ISDA 2015*. Faculty of Information Technology, Czech Technical University, 2016, p. 1–6. DOI: 10.1109/ISDA.2015.7489264. ISBN 978-1-4673-8712-5. Available at: https://www.fit.vut.cz/research/publication/10989.

[51] DUAN, X., CHEN, W., YU, S. and LIU, J. Tripod gaits planning and kinematics analysis of a hexapod robot. In: IEEE. *2009 IEEE International Conference on Control and Automation*. 2009, p. 1850–1855.

[52] DUDEK, G., GIGUERE, P., PRAHACS, C., SAUNDERSON, S., SATTAR, J. et al. AQUA: An Amphibious Autonomous Robot. *Computer*. 2007, vol. 40, no. 1, p. 46–53. DOI: 10.1109/MC.2007.6.

[53] ELFES, A., STEINDL, R., TALBOT, F., KENDOUL, F., SIKKA, P. et al. The multilegged autonomous explorer (MAX). In: IEEE. *2017 IEEE International Conference on Robotics and Automation (ICRA)*. 2017, p. 1050–1057. DOI: 10.1109/ICRA.2017.7989126.

[54] ENDO, G. and HIROSE, S. Study on Roller-Walker (system integration and basic experiments). In: *Proceedings 1999 IEEE International Conference on Robotics and Automation (Cat. No.99CH36288C)*. 1999, vol. 3, p. 2032–2037 vol.3. DOI: 10.1109/ROBOT.1999.770406.

[55] EPPS, B. P., ALVARADO, P. Valdivia y, YOUCEF TOUMI, K. and TECHET, A. H. Swimming performance of a biomimetic compliant fish-like robot. *Experiments in fluids*. Springer. 2009, vol. 47, p. 927–939.

[56] ERDEN, M. S. and LEBLEBICIOĞLU, K. Free gait generation with reinforcement learning for a six-legged robot. *Robotics and Autonomous Systems*. 2008, vol. 56, no. 3, p. 199–212. DOI: https://doi.org/10.1016/j.robot.2007.08.001. ISSN 0921-8890. Available at: https://www.sciencedirect.com/science/article/pii/S0921889007000991.

[57] ESPENSCHIED, K. S., QUINN, R. D., BEER, R. D. and CHIEL, H. J. Biologically based distributed control and local reflexes improve rough terrain locomotion in a hexapod robot. *Robotics and autonomous systems*. Elsevier. 1996, vol. 18, no. 1, p. 59–64.

[58] FEDERLE, W., RIEHLE, M., CURTIS, A. S. and FULL, R. J. An integrative study of insect adhesion: mechanics and wet adhesion of pretarsal pads in ants. *Integrative and Comparative Biology*. Oxford University Press. 2002, vol. 42, no. 6, p. 1100–1106.

[59] FERRELL, C. A comparison of three insect-inspired locomotion controllers. *Robotics and autonomous systems*. Elsevier. 1995, vol. 16, 2-4, p. 135–159.

[60] FIELD, L. and MATHESON, T. Chordotonal Organs of Insects. *Advances in Insect Physiology - ADVAN INSECT PHYSIOL*. december 1998, vol. 27. DOI: 10.1016/S0065-2806(08)60013-2.

[61] FRANTSEVICH, L. and WANG, W. Gimbals in the insect leg. *Arthropod Structure & Development.* 2009, vol. 38, no. 1, p. 16–30. DOI: https://doi.org/10.1016/j.asd.2008.06.002. ISSN 1467-8039. Available at: https://www.sciencedirect.com/science/article/pii/S1467803908000650.

[62] GABRIELLI, G. What price speed? Specific power required for propulsion of vehicles. *Mechanical Engineering-CIME.* American Society of Mechanical Engineers. 2011, vol. 133, no. 10, p. 4–5.

[63] GALLOWAY, K., HAYNES, G., ILHAN, D., JOHNSON, A., KNOPF, R. et al. X-RHex: A Highly Mobile Hexapedal Robot for Sensorimotor Tasks. *Technical Reports (ESE).* november 2010.

[64] GASSMANN, B., SCHOLL, K.-U. and BERNS, K. Locomotion of LAURON III in rough terrain. In: *2001 IEEE/ASME International Conference on Advanced Intelligent Mechatronics. Proceedings (Cat. No.01TH8556).* 2001, vol. 2, p. 959–964 vol.2. DOI: 10.1109/AIM.2001.936810.

[65] GEBEHART, C., SCHMIDT, J. and BÜSCHGES, A. Distributed processing of load and movement feedback in the premotor network controlling an insect leg joint. *Journal of Neurophysiology.* 2021, vol. 125, no. 5, p. 1800–1813. DOI: 10.1152/jn.00090.2021. PMID: 33788591. Available at: https://doi.org/10.1152/jn.00090.2021.

[66] GOLDSCHMIDT, D., HESSE, F., WÖRGÖTTER, F. and MANOONPONG, P. Biologically Inspired Reactive Climbing Behavior of Hexapod Robots. In:. October 2012, p. 4632 –4637. DOI: 10.1109/IROS.2012.6386135.

[67] GOLDSCHMIDT, D., WÖRGÖTTER, F. and MANOONPONG, P. Biologically-inspired adaptive obstacle negotiation behavior of hexapod robots. *Frontiers in neurorobotics.* Frontiers Media SA. 2014, vol. 8, p. 3.

[68] GONZALEZ DE SANTOS, P., COBANO, J., GARCIA, E., ESTREMERA, J. and ARMADA, M. A six-legged robot-based system for humanitarian demining missions. *Mechatronics.* 2007, vol. 17, no. 8, p. 417–430. DOI: https://doi.org/10.1016/j.mechatronics.2007.04.014. ISSN 0957-4158. Available at: https://www.sciencedirect.com/science/article/pii/S0957415807000463.

[69] GORNER, M., WIMBOCK, T., BAUMANN, A., FUCHS, M., BAHLS, T. et al. The DLR-Crawler: A testbed for actively compliant hexapod walking based on the fingers of DLR-Hand II. In: IEEE. *2008 IEEE/RSJ International Conference on Intelligent Robots and Systems.* 2008, p. 1525–1531. DOI: 10.1109/IROS.2008.4650655.

[70] GRAND, C., BENAMAR, F., PLUMET, F. and BIDAUD, P. Decoupled control of posture and trajectory of the hybrid wheel-legged robot hylos. In: *IEEE International Conference on Robotics and Automation, 2004. Proceedings. ICRA '04. 2004.* 2004, vol. 5, p. 5111–5116. DOI: 10.1109/ROBOT.2004.1302528.

[71] HAMMOND, C. and ESCLAPEZ, M. Chapter 6 - The chemical synapses. In: HAMMOND, C., ed. *Cellular and Molecular Neurophysiology (Fourth Edition).* Fourth Editionth ed. Boston: Academic Press, 2015, p. 121–144. DOI: https://doi.org/10.1016/B978-0-12-397032-9.00006-6. ISBN 978-0-12-397032-9.

Available at:
https://www.sciencedirect.com/science/article/pii/B9780123970329000066.

[72] Harley, C., English, B. and Ritzmann, R. Characterization of obstacle negotiation behaviors in the cockroach, Blaberus discoidalis. *Journal of Experimental Biology.* Company of Biologists. 2009, vol. 212, no. 10, p. 1463–1476.

[73] Heaston, J. R. and Hong, D. W. Design optimization of a novel tripedal locomotion robot through simulation and experiments for a single step dynamic gait. In: *International Design Engineering Technical Conferences and Computers and Information in Engineering Conference.* 2007, vol. 48094, p. 715–724.

[74] Hegner, R. W. and Engemann, J. G. *Invertebrate zoology.* Macmillan, 1968.

[75] Henrey, M., Ahmed, A., Boscariol, P., Shannon, L. and Menon, C. Abigaille-III: A versatile, bioinspired hexapod for scaling smooth vertical surfaces. *Journal of Bionic Engineering.* Elsevier. 2014, vol. 11, no. 1, p. 1–17.

[76] Hodoshima, R., Doi, T., Fukuda, Y., Hirose, S., Okamoto, T. et al. Development of a quadruped walking robot titan xi for steep slope operation-step over gait to avoid concrete frames on steep slopes. *Journal of Robotics and Mechatronics.* Fuji Technology Press Ltd. 2007, vol. 19, no. 1, p. 13–26.

[77] Hoy, R. R. and Robert, D. Tympanal hearing in insects. *Annual review of entomology.* Annual Reviews 4139 El Camino Way, PO Box 10139, Palo Alto, CA 94303-0139, USA. 1996, vol. 41, no. 1, p. 433–450.

[78] Huang, H., He, W., Wang, J., Zhang, L. and Fu, Q. An All Servo-Driven Bird-Like Flapping-Wing Aerial Robot Capable of Autonomous Flight. *IEEE/ASME Transactions on Mechatronics.* 2022, vol. 27, no. 6, p. 5484–5494. DOI: 10.1109/TMECH.2022.3182418.

[79] Hughes, G. M. The Co-Ordination of Insect Movements: I The Walking Movements of Insects. *Journal of Experimental Biology.* june 1952, vol. 29, no. 2, p. 267–285. DOI: 10.1242/jeb.29.2.267. ISSN 0022-0949. Available at: https://doi.org/10.1242/jeb.29.2.267.

[80] Ijspeert, A. J. Central pattern generators for locomotion control in animals and robots: a review. *Neural networks.* Elsevier. 2008, vol. 21, no. 4, p. 642–653.

[81] Ijspeert, A. J., Crespi, A., Ryczko, D. and Cabelguen, J.-M. From swimming to walking with a salamander robot driven by a spinal cord model. *Science.* American Association for the Advancement of Science. 2007, vol. 315, no. 5817, p. 1416–1420. ISSN 1095-9203.

[82] Iouguina, A., Dawson, J., Hallgrimsson, B. and Smart, G. Biologically informed disciplines: A comparative analysis of bionics, biomimetics, biomimicry, and bio-inspiration among others. *International Journal of Design & Nature and Ecodynamics.* WIT Press. 2014, vol. 9, no. 3, p. 197–205.

[83] Irawan, A. and Nonami, K. Optimal impedance control based on body inertia for a hydraulically driven hexapod robot walking on uneven and extremely soft terrain.

Journal of Field Robotics. 2011, vol. 28, no. 5, p. 690–713. DOI: https://doi.org/10.1002/rob.20404. Available at: https://onlinelibrary.wiley.com/doi/abs/10.1002/rob.20404.

[84] JAKIMOVSKI, B. *Biologically inspired approaches for locomotion, anomaly detection and reconfiguration for walking robots.* Berlin: Springer, 2011. ISBN 978-3-642-22505-5.

[85] JEHANNO, J.-M., CULLY, A., GRAND, C. and MOURET, J.-B. Design of a wheel-legged hexapod robot for creative adaptation. In: *Mobile Service Robotics.* World Scientific, 2014, p. 267–276.

[86] KAJITA, S. and ESPIAU, B. Legged robot. In: *Springer handbook of robotics.* Springer Berlin/Heidelberg, Germany, 2008, p. 361–389.

[87] KANDHARI, A., MEHRINGER, A., CHIEL, H. J., QUINN, R. D. and DALTORIO, K. A. Design and Actuation of a Fabric-Based Worm-Like Robot. *Biomimetics.* MDPI AG. Feb 2019, vol. 4, no. 1, p. 13. DOI: 10.3390/biomimetics4010013. ISSN 2313-7673. Available at: http://dx.doi.org/10.3390/biomimetics4010013.

[88] KEIL, T. and STEINBRECHT, R. A. Mechanosensitive and Olfactory Sensilla of Insects. In:. January 1984, vol. 2, p. 477–516. ISBN 978-1-4612-9685-0.

[89] KENNEDY, B., OKON, A., AGHAZARIAN, H., GARRETT, M., HUNTSBERGER, T. et al. The Lemur II-Class Robots for Inspection and Maintenance of Orbital Structures: A System Description. In: TOKHI, M. O., VIRK, G. S. and HOSSAIN, M. A., ed. *Climbing and Walking Robots.* Berlin, Heidelberg: Springer Berlin Heidelberg, 2006, p. 1069–1076. ISBN 978-3-540-26415-6.

[90] KHAN, M. R., AHMED, M., BILLAH, M. and SOHELI, F. A Novel Navigation Algorithm for Hexagonal Hexapod Robot. *American Journal of Engineering and Applied Sciences.* january 2010, vol. 3.

[91] KINGSLEY, J. S. The classification of the Arthropoda. *The American Naturalist.* Edwards and Docker. 1894, vol. 28, no. 326, p. 118–135.

[92] KOTTEGE, N., PARKINSON, C., MOGHADAM, P., ELFES, A. and SINGH, S. P. Energetics-informed hexapod gait transitions across terrains. In: IEEE. *2015 IEEE International Conference on Robotics and Automation (ICRA).* 2015, p. 5140–5147.

[93] KROTKOV, E., SIMMONS, R. and WHITTAKER, W. Autonomous walking results with the Ambler hexapod planetary rover. In: *Proceedings of the International Conference on Intelligent Autonomous Systems IAS.* 1993, vol. 3, p. 46–53.

[94] LEE, T.-T., LIAO, C.-M. and CHEN, T. On the stability properties of hexapod tripod gait. *IEEE Journal on Robotics and Automation.* 1988, vol. 4, no. 4, p. 427–434. DOI: 10.1109/56.808.

[95] LELE, A. S., FANG, Y., TING, J. and RAYCHOWDHURY, A. Learning to Walk: Spike Based Reinforcement Learning for Hexapod Robot Central Pattern Generation. In: *2020 2nd IEEE International Conference on Artificial Intelligence Circuits and Systems (AICAS).* 2020, p. 208–212. DOI: 10.1109/AICAS48895.2020.9073987.

[96] LI, Y., AHMED, A., SAMEOTO, D. and MENON, C. Abigaille II: toward the development of a spider-inspired climbing robot. *Robotica*. Cambridge University Press. 2012, vol. 30, no. 1, p. 79–89. DOI: 10.1017/S0263574711000373.

[97] LIANG, C., CHEE, K., ZOU, Y., ZHU, H., CAUSO, A. et al. Automated robot picking system for e-commerce fulfillment warehouse application. In: *The 14th IFToMM World Congress*. 2015.

[98] LUCIANO, D. S. and SHERMAN, J. S. Human functions and structure. *McGraw-Hill*. 1978, p. 105–106.

[99] MA, K. Y., CHIRARATTANANON, P. and WOOD, R. J. Design and fabrication of an insect-scale flying robot for control autonomy. In: IEEE. *2015 IEEE/RSJ International Conference on Intelligent Robots and Systems (IROS)*. 2015, p. 1558–1564.

[100] MARDER, E. and BUCHER, D. Central pattern generators and the control of rhythmic movements. *Current biology*. Elsevier. 2001, vol. 11, no. 23, p. R986–R996.

[101] MARDER, E. and CALABRESE, R. L. Principles of rhythmic motor pattern generation. *Physiological reviews*. Am Physiological Soc. 1996, vol. 76, no. 3, p. 687–717.

[102] MATSUOKA, K. Sustained oscillations generated by mutually inhibiting neurons with adaptation. *Biological cybernetics*. Springer. 1985, vol. 52, no. 6, p. 367–376.

[103] MATSUOKA, K. Mechanisms of frequency and pattern control in the neural rhythm generators. *Biological cybernetics*. Springer. 1987, vol. 56, 5-6, p. 345–353.

[104] MCCLELLAN, A. D. and JANG, W. Mechanosensory inputs to the central pattern generators for locomotion in the lamprey spinal cord: resetting, entrainment, and computer modeling. *Journal of Neurophysiology*. 1993, vol. 70, no. 6, p. 2442–2454.

[105] MCGHEE, R. and FRANK, A. On the stability properties of quadruped creeping gaits. *Mathematical Biosciences*. 1968, vol. 3, p. 331–351. DOI: https://doi.org/10.1016/0025-5564(68)90090-4. ISSN 0025-5564. Available at: https://www.sciencedirect.com/science/article/pii/0025556468900904.

[106] MCGHEE, R. B. and ISWANDHI, G. I. Adaptive Locomotion of a Multilegged Robot over Rough Terrain. *IEEE Transactions on Systems, Man, and Cybernetics*. 1979, vol. 9, no. 4, p. 176–182. DOI: 10.1109/TSMC.1979.4310180.

[107] MENDES, C. S., BARTOS, I., AKAY, T., MÁRKA, S. and MANN, R. S. Quantification of gait parameters in freely walking wild type and sensory deprived *Drosophila melanogaster*. *ELife*. eLife Sciences Publications, Ltd. jan 2013, vol. 2, p. e00231. DOI: 10.7554/eLife.00231. ISSN 2050-084X. Available at: https://doi.org/10.7554/eLife.00231.

[108] MENON, C., LI, Y., SAMEOTO, D. and MARTENS, C. Abigaille-I: Towards the development of a spider-inspired climbing robot for space use. In: *2008 2nd IEEE RAS & EMBS International Conference on Biomedical Robotics and Biomechatronics*. 2008, p. 384–389. DOI: 10.1109/BIOROB.2008.4762903.

[109] Microchip Technology. *ATmega2560* [https://www.microchip.com/en-us/product/ATmega2560]. 2023. [Online; visited 21-07-2023].

[110] Minati, L., Frasca, M., Yoshimura, N. and Koike, Y. Versatile Locomotion Control of a Hexapod Robot Using a Hierarchical Network of Nonlinear Oscillator Circuits. *IEEE Access.* 2018, vol. 6, p. 8042–8065. DOI: 10.1109/ACCESS.2018.2799145.

[111] Morazzani, I., Hong, D., Lahr, D. and Ren, P. Novel tripedal mobile robot and considerations for gait planning strategies based on kinematics. In: Springer. *Recent Progress in Robotics: Viable Robotic Service to Human: An Edition of the Selected Papers from the 13th International Conference on Advanced Robotics.* 2008, p. 35–48.

[112] Motorola. *Octal Buffer 74LS241* [https://datasheetspdf.com/pdf/375524/Motorola/74LS241/1]. 2023. [Online; visited 21-07-2023].

[113] Museum, O. L. *Otto-Lilienthal-Museum Anklam* [http://www.lilienthal-museum.de/olma/eotto.htm]. 2023. [Online; visited 2023-05-27].

[114] Mǎnoiu Olaru, S., Nitulescu, M. and Stoian, V. Hexapod robot. Mathematical support for modeling and control. *15th International Conference on System Theory, Control and Computing.* 2011, p. 1–6.

[115] Nam, G. *BIO-INSPIRED CONTROL OF HEXAPOD FOR NAVIGATING CONFINED SPACES IN DISASTER RECOVERY.* Dissertation.

[116] Neil, T. R. and Holderied, M. W. Chapter Two - Sound production and hearing in insects. In: Jurenka, R., ed. *Sound Communication in Insects.* Academic Press, 2021, vol. 61, p. 101–139. Advances in Insect Physiology. DOI: https://doi.org/10.1016/bs.aiip.2021.10.001. ISSN 0065-2806. Available at: https://www.sciencedirect.com/science/article/pii/S0065280621000187.

[117] Nelson, G. and Quinn, R. Posture control of a cockroach-like robot. In: *Proceedings. 1998 IEEE International Conference on Robotics and Automation (Cat. No.98CH36146).* 1998, vol. 1, p. 157–162 vol.1. DOI: 10.1109/ROBOT.1998.676348.

[118] Nelson, G., Quinn, R., Bachmann, R., Flannigan, W., Ritzmann, R. et al. Design and simulation of a cockroach-like hexapod robot. In: *Proceedings of International Conference on Robotics and Automation.* 1997, vol. 2, p. 1106–1111 vol.2. DOI: 10.1109/ROBOT.1997.614284.

[119] Nishii, J. An analytical estimation of the energy cost for legged locomotion. *Journal of theoretical biology.* Elsevier. 2006, vol. 238, no. 3, p. 636–645.

[120] Nonami, K. Dynamics and Control of Six Legged Walking Robot for Mine Detection. In: *Proc. of the Fifth Int. Conf. on Motion and Vibration Control (MOVIC2000), December 4-8, Sydney.* 2000.

[121] NONAMI, K. Development of mine detection robot COMET-II and COMET-III. In: *Proceedings of the 41st SICE Annual Conference. SICE 2002.* 2002, vol. 1, p. 346–351 vol.1. DOI: 10.1109/SICE.2002.1195420.

[122] NONAMI, K., BARAI, R. K., IRAWAN, A., DAUD, M. R., NONAMI, K. et al. Design and Optimization of Hydraulically Actuated Hexapod Robot COMET-IV. *Hydraulically Actuated Hexapod Robots: Design, Implementation and Control.* Springer. 2014, p. 41–84.

[123] ODROID. *Odroid-h3* [https://wiki.odroid.com/odroid-h3/start]. 2023. [Online; visited 2023-07-21].

[124] OKHOTSIMSKI, D. and PLATONOV, A. *Control Algorithm of the Walking Climbing Over Obstacles Proceeding of the International Conference on Artificial Intelligence.* Stanford, 1973.

[125] OROZCO MAGDALENO, E., BRAVO, F., CASTILLO CASTANEDA, E. and CARBONE, G. Evaluation of Locomotion Performances for a Mecanum-Wheeled Hybrid Hexapod Robot. *IEEE/ASME Transactions on Mechatronics.* september 2020, PP, p. 1–1. DOI: 10.1109/TMECH.2020.3027259.

[126] PARKER, G. B. and LEE, Z. Evolving neural networks for hexapod leg controllers. In: IEEE. *Intelligent Robots and Systems, 2003.(IROS 2003). Proceedings. 2003 IEEE/RSJ International Conference on.* 2003, vol. 2, p. 1376–1381.

[127] PAVONE, M., ARENA, P. and PATANÉ, L. An innovative mechanical and control architecture for a biomimetic hexapod for planetary exploration. *International Astronautical Federation - 56th International Astronautical Congress 2005.* january 2005, vol. 2.

[128] PETTERNELLA, M. and SALINARI, S. Simulation by digital computer of walking machine control system. In: *IFAC, IIC, and ANIPLA, Symposium on Automatic Control in Space, 5 Th, Genoa, Italy.* 1973.

[129] PLAYTER, R., BUEHLER, M. and RAIBERT, M. BigDog. In: GERHART, G. R., SHOEMAKER, C. M. and GAGE, D. W., ed. *Unmanned Systems Technology VIII.* SPIE, 2006, vol. 6230, p. 62302O. DOI: 10.1117/12.684087. Available at: https://doi.org/10.1117/12.684087.

[130] PRAHACS, C., SAUDNERS, A., SMITH, M. K., MCMORDIE, D. and BUEHLER, M. Towards legged amphibious mobile robotics. *Journal of Engineering Design and Innovation.* 2005, 1P.

[131] PREUMONT, A., ALEXANDRE, P. and GHUYS, D. Gait analysis and implementation of a six leg walking machine. In: *Fifth International Conference on Advanced Robotics 'Robots in Unstructured Environments.* 1991, p. 941–945 vol.2. DOI: 10.1109/ICAR.1991.240551.

[132] PRINGLE, J. W. S. The Reflex Mechanism of the Insect Leg. *Journal of Experimental Biology.* january 1940, vol. 17, no. 1, p. 8–17. DOI: 10.1242/jeb.17.1.8. ISSN 0022-0949. Available at: https://doi.org/10.1242/jeb.17.1.8.

[133] PROCHAZKA, A., CLARAC, F., LOEB, G. E., ROTHWELL, J. C. and WOLPAW, J. R. What do reflex and voluntary mean? Modern views on an ancient debate. *Experimental brain research*. Springer. 2000, vol. 130, p. 417–432.

[134] RAHEEM, F. and KHALEEL, H. Static Stability Analysis of Hexagonal Hexapod Robot for the Periodic Gaits. september 2014, vol. 1414.

[135] RAIBERT, M., BLANKESPOOR, K., NELSON, G. and PLAYTER, R. BigDog, the Rough-Terrain Quadruped Robot. *IFAC Proceedings Volumes*. 2008, vol. 41, no. 2, p. 10822–10825. DOI: https://doi.org/10.3182/20080706-5-KR-1001.01833. ISSN 1474-6670. 17th IFAC World Congress. Available at: https://www.sciencedirect.com/science/article/pii/S1474667016407020.

[136] RAMDYA, P., THANDIACKAL, R., CHERNEY, R., ASSELBORN, T., BENTON, R. et al. Climbing favours the tripod gait over alternative faster insect gaits. *Nature communications*. Nature Publishing Group UK London. 2017, vol. 8, no. 1, p. 14494.

[137] RASPBERRY PI. *Raspberry Pi 4 Model B specifications* [https://www.raspberrypi.com/products/raspberry-pi-4-model-b/specifications/]. 2023. [Online; visited 21-07-2023].

[138] RASPBERRY PI FOUNDATION. *Raspberry Pi* [http://www.raspberrypi.org/]. 2023. [Online; visited 21-07-2023].

[139] ROBOTIS. *Dynamixel MX Series* [https://emanual.robotis.com/docs/en/dxl/mx/]. 2021. [Online; visited 2023-01-29].

[140] ROBOTIS. *DYNAMIXEL Protocol 1.0* [https://emanual.robotis.com/docs/en/dxl/protocol1/]. 2023. [Online; visited 31-07-2023].

[141] ROBOTIS. *DYNAMIXEL Protocol 2.0* [https://emanual.robotis.com/docs/en/dxl/protocol2/]. 2023. [Online; visited 31-07-2023].

[142] ROBOTIS. *DYNAMIXEL SDK* [https://emanual.robotis.com/docs/en/software/dynamixel/dynamixel_sdk/overview/]. 2023. [Online; visited 31-07-2023].

[143] ROBOTIS. *DYNAMIXEL Wizard 2.0* [https://emanual.robotis.com/docs/en/software/dynamixel/dynamixel_wizard2/#usb-latency-setting]. 2023. [Online; visited 31-07-2023].

[144] ROBOTIS. *MX-64T/R/AT/AR* [https://emanual.robotis.com/docs/en/dxl/mx/mx-64/#control-table]. 2023. [Online; visited 31-07-2023].

[145] ROBOTIS. *U2D2* [https://emanual.robotis.com/docs/en/parts/interface/u2d2/]. 2023. [Online; visited 31-07-2023].

[146] ROENNAU, A., HEPPNER, G., KERSCHER, T. and DILLMANN, R. Fault diagnosis and system status monitoring for a six-legged walking robot. In: *2011 IEEE/ASME International Conference on Advanced Intelligent Mechatronics (AIM)*. 2011, p. 874–879. DOI: 10.1109/AIM.2011.6027107.

[147] ROENNAU, A., HEPPNER, G., NOWICKI, M. and DILLMANN, R. LAURON V: A versatile six-legged walking robot with advanced maneuverability. In: *2014 IEEE/ASME International Conference on Advanced Intelligent Mechatronics*. 2014, p. 82–87. DOI: 10.1109/AIM.2014.6878051.

[148] ROENNAU, A., HEPPNER, G., NOWICKI, M., ZOELLNER, J. and DILLMANN, R. Reactive posture behaviors for stable legged locomotion over steep inclines and large obstacles. In: *2014 IEEE/RSJ International Conference on Intelligent Robots and Systems*. 2014, p. 4888–4894. DOI: 10.1109/IROS.2014.6943257.

[149] RUSSELL, M. Odex 1: The first functionoid. *Robotics Age*. 1983, vol. 5, no. 5, p. 12–18.

[150] SANTOS, P. González de, GARCIA, E. and ESTREMERA, J. Improving walking-robot performances by optimizing leg distribution. *Autonomous Robots*. Springer. 2007, vol. 23, no. 4, p. 247–258.

[151] SARANLI, U., BUEHLER, M. and KODITSCHEK, D. E. RHex: A simple and highly mobile hexapod robot. *The International Journal of Robotics Research*. SAGE Publications. 2001, vol. 20, no. 7, p. 616–631.

[152] SCHILLING, M., HOINVILLE, T., SCHMITZ, J. and CRUSE, H. Walknet, a bio-inspired controller for hexapod walking. *Biological cybernetics*. Springer. 2013, vol. 107, no. 4, p. 397–419.

[153] SCHNEIDER, A., PASKARBEIT, J., SCHAEFFERSMANN, M. and SCHMITZ, J. HECTOR, a New Hexapod Robot Platform with Increased Mobility - Control Approach, Design and Communication. In: RÜCKERT, U., JOAQUIN, S. and FELIX, W., ed. *Advances in Autonomous Mini Robots*. Berlin, Heidelberg: Springer Berlin Heidelberg, 2012, p. 249–264. ISBN 978-3-642-27482-4.

[154] SCHOTT, J. and ROSSOR, M. The grasp and other primitive reflexes. *Journal of Neurology, Neurosurgery & Psychiatry*. BMJ Publishing Group Ltd. 2003, vol. 74, no. 5, p. 558–560.

[155] SCHUE, C. Simulation of Tripod Gaits for a Hexapod Underwater Walking Machine. june 1993, p. 270.

[156] SCHÜTZ, C. and DÜRR, V. Active tactile exploration for adaptive locomotion in the stick insect. *Philosophical Transactions of the Royal Society B: Biological Sciences*. The Royal Society. 2011, vol. 366, no. 1581, p. 2996–3005.

[157] SELVERSTON, A. I. Are central pattern generators understandable? *Behavioral and Brain Sciences*. Cambridge Univ Press. 1980, vol. 3, no. 04, p. 535–540.

[158] SEMINI, C., BARASUOL, V., GOLDSMITH, J., FRIGERIO, M., FOCCHI, M. et al. Design of the Hydraulically-Actuated, Torque-Controlled Quadruped Robot

HyQ2Max. *IEEE/ASME Transactions on Mechatronics.* october 2016, PP, p. 1–1.
DOI: 10.1109/TMECH.2016.2616284.

[159] SEMINI, C., TSAGARAKIS, N. G., GUGLIELMINO, E., FOCCHI, M., CANNELLA, F.
et al. Design of HyQ–a hydraulically and electrically actuated quadruped robot.
*Proceedings of the Institution of Mechanical Engineers, Part I: Journal of Systems
and Control Engineering.* SAGE Publications Sage UK: London, England. 2011,
vol. 225, no. 6, p. 831–849.

[160] SEOK, S., WANG, A., CHUAH, M. Y., HYUN, D. J., LEE, J. et al. Design principles
for energy-efficient legged locomotion and implementation on the MIT cheetah
robot. *Ieee/asme transactions on mechatronics.* IEEE. 2014, vol. 20, no. 3,
p. 1117–1129.

[161] SMITH, T. B., BARREIRO, J., SMITH, D. E., SUNSPIRAL, V. and CHAVEZ
CLEMENTE, D. ATHLETE's Feet: Mu1ti-Resolution Planning for a Hexapod
Robot. In: *International Conference on Automated Planning and Scheduling.* 2008,
ARC-E-DAA-TN-144.

[162] SONG, S.-M. and CHOI, B. The optimally stable ranges of 2n-legged wave gaits.
IEEE Transactions on Systems, Man, and Cybernetics. 1990, vol. 20, no. 4,
p. 888–902. DOI: 10.1109/21.105087.

[163] SONG, S.-M. and CHOI, B. The optimally stable ranges of 2n-legged wave gaits.
IEEE Transactions on Systems, Man, and Cybernetics. 1990, vol. 20, no. 4,
p. 888–902. DOI: 10.1109/21.105087.

[164] SPONG, M. W., HUTCHINSON, S. and VIDYASAGAR, M. *Robot dynamics and control.*
2ndth ed. John Wiley & Sons, 2020.

[165] STMICROELECTRONICS. *LSM9DS1*
[https://www.st.com/resource/en/datasheet/lsm9ds1.pdf]. 2015. [Online; visited
23-07-2023].

[166] SUN, S.-S. *A Theoretical study of gaits for legged locomotion systems.* The Ohio
State University, 1974.

[167] TAKAHASHI, Y., ARAI, T., MAE, Y., INOUE, K. and KOYACHI, N. Development of
multi-limb robot with omnidirectional manipulability and mobility. In: *Proceedings.
2000 IEEE/RSJ International Conference on Intelligent Robots and Systems (IROS
2000) (Cat. No.00CH37113).* 2000, vol. 3, p. 2012–2017 vol.3. DOI:
10.1109/IROS.2000.895266.

[168] TAKUBO, T., ARAI, T., INOUE, K., OCHI, H., KONISHI, T. et al. Integrated limb
mechanism robot ASTERISK. *Journal of Robotics and Mechatronics.* Fuji
Technology Press Ltd. 2006, vol. 18, no. 2, p. 203–214.

[169] TEDESCHI, F., CAFOLLA, D. and CARBONE, G. Design and operation of Cassino
Hexapod II. *International journal of mechanics and control.* 2014, vol. 15, no. 1,
p. 19–25.

[170] TEDESCHI, F. and CARBONE, G. Design issues for hexapod walking robots.
Robotics. MDPI. 2014, vol. 3, no. 2, p. 181–206.

[171] TEDESCHI, F. and CARBONE, G. Design of a Novel Leg-Wheel Hexapod Walking Robot. *Robotics*. 2017, vol. 6, no. 4. DOI: 10.3390/robotics6040040. ISSN 2218-6581. Available at: https://www.mdpi.com/2218-6581/6/4/40.

[172] THORP, J. H. Chapter 14 - Arthropoda and Related Groups. In: RESH, V. H. and CARDÉ, R. T., ed. *Encyclopedia of Insects (Second Edition)*. Second Editionth ed. San Diego: Academic Press, 2009, p. 50–56. DOI: https://doi.org/10.1016/B978-0-12-374144-8.00014-X. ISBN 978-0-12-374144-8. Available at: https://www.sciencedirect.com/science/article/pii/B978012374144800014X.

[173] TONG, Z., YE, Z., GAO, H., HE, J. and DENG, Z. Electro-hydraulic control system and frequency analysis for a hydraulically driven six-legged robot. In: *2016 IEEE International Conference on Aircraft Utility Systems (AUS)*. 2016, p. 554–559. DOI: 10.1109/AUS.2016.7748112.

[174] UGURLU, B. and KAWAMURA, A. ZMP-Based Online Jumping Pattern Generation for a One-Legged Robot. *IEEE Transactions on Industrial Electronics*. 2010, vol. 57, no. 5, p. 1701–1709. DOI: 10.1109/TIE.2009.2032439.

[175] URWIN WRIGHT, S., SANDERS, D. and CHEN, S. Terrain prediction for an eight-legged robot. *Journal of Robotic Systems*. Wiley Online Library. 2002, vol. 19, no. 2, p. 91–98.

[176] VELCRO. *Our Story - Velcro Companies History* [https://www.velcro.com/original-thinking/our-story/]. 2022. [Online; visited 2023-05-27].

[177] WAARD, M. de, INJA, M. and VISSER, A. Analysis of flat terrain for the atlas robot. In: *2013 3rd Joint Conference of AI & Robotics and 5th RoboCup Iran Open International Symposium*. 2013, p. 1–6. DOI: 10.1109/RIOS.2013.6595324.

[178] WALAS, K. and BELTER, D. Messor – verstatile walking robot for serach and rescue missions. *Journal of Automation, Mobile Robotics and Intelligent Systems*. Jan. 2013, vol. 5, no. 2, p. 28–34. Available at: https://www.jamris.org/index.php/JAMRIS/article/view/161.

[179] WALAS, K., BELTER, D. and KASINSKI, A. Control and environment sensing system for a six-legged robot. *Journal of Automation, Mobile Robotics and Intelligent Systems*. Aug. 2013, vol. 2, no. 3, p. 26–32. Available at: https://www.jamris.org/index.php/JAMRIS/article/view/602.

[180] WALDRON, K. and MCGHEE, R. The adaptive suspension vehicle. *IEEE Control Systems Magazine*. 1986, vol. 6, no. 6, p. 7–12. DOI: 10.1109/MCS.1986.1105145.

[181] WEBB, J., LEONESSA, A. and HONG, D. Gait design and gain-scheduled balance controller of an under-actuated robotic platform. In: *2015 IEEE/RSJ International Conference on Intelligent Robots and Systems (IROS)*. 2015, p. 5148–5155. DOI: 10.1109/IROS.2015.7354102.

[182] WEINGARTEN, J., KODITSCHEK, D., KOMSUOGLU, H. and MASSEY, C. Robotics as the Delivery Vehicle: A contexualized, social, self paced, engineering education for

life-long learners. *Robotics Science and Systems Workshop on „Research in Robots for Education“*. january 2007.

[183] WETTERGREEN, D., PANGELS, H. and BARES, J. Behavior-based gait execution for the Dante II walking robot. In: IEEE. *Proceedings 1995 IEEE/RSJ International Conference on Intelligent Robots and Systems. Human Robot Interaction and Cooperative Robots*. 1995, vol. 3, p. 274–279.

[184] WILCOX, B. H. ATHLETE: A cargo and habitat transporter for the moon. In: *2009 IEEE Aerospace conference*. 2009, p. 1–7. DOI: 10.1109/AERO.2009.4839568.

[185] WILLIAMS, T. L., SIGVARDT, K. A., KOPELL, N., ERMENTROUT, G. B. and REMLER, M. P. Forcing of coupled nonlinear oscillators: studies of intersegmental coordination in the lamprey locomotor central pattern generator. *Journal of neurophysiology*. American Physiological Society Bethesda, MD. 1990, vol. 64, no. 3, p. 862–871.

[186] WILLY MCALLISTER. *Voltage divider | Khan Academy* [https://www.khanacademy.org/science/electrical-engineering/ee-circuit-analysis-topic/ee-resistor-circuits/a/ee-voltage-divider]. 2023. [Online; visited 23-07-2023].

[187] WILSON, D. and WYMAN, R. Motor output patterns during random and rhythmic stimulation of locust thoracic ganglia. *Biophysical Journal*. Elsevier. 1965, vol. 5, no. 2, p. 121–143.

[188] WILSON, D. M. The central nervous control of flight in a locust. *J. exp. Biol.* Citeseer. 1961, vol. 38, no. 47, p. l–490.

[189] WILSON, D. M. Insect Walking. *Annual Review of Entomology*. 1966, vol. 11, no. 1, p. 103–122. DOI: 10.1146/annurev.en.11.010166.000535. PMID: 5321575. Available at: https://doi.org/10.1146/annurev.en.11.010166.000535.

[190] WONG, R. and PEARSON, K. Properties of the trochanteral hair plate and its function in the control of walking. *The Journal of experimental biology*. march 1976, vol. 64, p. 233–49. DOI: 10.1242/jeb.64.1.233.

[191] WOSNITZA, A., BOCKEMÜHL, T., DÜBBERT, M., SCHOLZ, H. and BÜSCHGES, A. Inter-leg coordination in the control of walking speed in Drosophila. *Journal of experimental biology*. Company of Biologists. 2013, vol. 216, no. 3, p. 480–491.

[192] YOSHIOKA, T., TAKUBO, T., ARAI, T. and KENJI INOUE
and. Hybrid Locomotion of Leg-Wheel ASTERISK H. *Journal of Robotics and Mechatronics*. 2008, vol. 20, no. 3, p. 403–412. DOI: 10.20965/jrm.2008.p0403.

[193] YU, H., GUO, W., DENG, J., LI, M. and CAI, H. A CPG-based locomotion control architecture for hexapod robot. In: IEEE. *Intelligent Robots and Systems (IROS), 2013 IEEE/RSJ International Conference on*. 2013, p. 5615–5621.

[194] ZAK, M. and ROZMAN, J. Design, construction and control of hexapod walking robot. In: *2015 IEEE 13th International Scientific Conference on Informatics*. 2015, p. 302–307. DOI: 10.1109/Informatics.2015.7377851.

[195] ZHANG, C.-D. and SONG, S.-M. A study of the stability of generalized wave gaits. *Mathematical Biosciences.* 1993, vol. 115, no. 1, p. 1–32. DOI: https://doi.org/10.1016/0025-5564(93)90045-C. ISSN 0025-5564. Available at: https://www.sciencedirect.com/science/article/pii/002555649390045C.

[196] ZHANG, M., FENG, S., WANG, L. and ZHENG, Y. Lotus effect in wetting and self-cleaning. *Biotribology.* 2016, vol. 5, p. 31–43. DOI: https://doi.org/10.1016/j.biotri.2015.08.002. ISSN 2352-5738. Available at: https://www.sciencedirect.com/science/article/pii/S2352573815300020.

[197] ZHAO, J., ZHANG, H., LIU, Y., YAN, J., ZANG, X. et al. Development of the hexapod robot HITCR-II for walking on unstructured terrain. In: *2012 IEEE International Conference on Mechatronics and Automation.* 2012, p. 64–69. DOI: 10.1109/ICMA.2012.6282808.

[198] ZIELIŃSKA, T. Autonomous walking machines-discussion of the prototyping problems. *Bulletin of the Polish academy of sciences. Technical Sciences.* Polska Akademia Nauk. Czytelnia Czasopism PAN. 2010, vol. 58, no. 3, p. 443–451.

[199] ČÍŽEK, P., ZOULA, M. and FAIGL, J. Design, Construction, and Rough-Terrain Locomotion Control of Novel Hexapod Walking Robot With Four Degrees of Freedom Per Leg. *IEEE Access.* 2021, vol. 9, p. 17866–17881. DOI: 10.1109/ACCESS.2021.3053492.

[200] ŽÁK, M., ROZMAN, J. and ZBOŘIL, F. V. Overview of bio-inspired control mechanisms for hexapod robot. *International Journal of Computer Information Systems and Industrial Management Applications.* Machine Intelligence Research (MIR) Labs. 2016, vol. 8, p. 125 – 134. ISSN 21507988.

[201] ŽÁK, M., ROZMAN, J. and ZBOŘIL, F. V. Design and Control of 7-DOF Omni-directional Hexapod Robot. *Open Computer Science.* 2021, vol. 11, no. 1, p. 80–89. DOI: doi:10.1515/comp-2020-0189. Available at: https://doi.org/10.1515/comp-2020-0189.

[202] ŽÁK, M., ROZMAN, J. and ZBOŘIL, F. V. Energy Efficiency of a Wheeled Bio-Inspired Hexapod Walking Robot in Sloping Terrain. *Robotics.* MDPI AG. Mar 2023, vol. 12, no. 2, p. 42. DOI: 10.3390/robotics12020042. ISSN 2218-6581. Available at: http://dx.doi.org/10.3390/robotics12020042.